



Kent Academic Repository

Benlaouer, Ouafa (2020) *Studies of Latrophilin Signalling in Cancer Cells.*
Doctor of Philosophy (PhD) thesis, University of Kent,.

Downloaded from

<https://kar.kent.ac.uk/83614/> The University of Kent's Academic Repository KAR

The version of record is available from

This document version

UNSPECIFIED

DOI for this version

Licence for this version

CC BY (Attribution)

Additional information

Versions of research works

Versions of Record

If this version is the version of record, it is the same as the published version available on the publisher's web site. Cite as the published version.

Author Accepted Manuscripts

If this document is identified as the Author Accepted Manuscript it is the version after peer review but before type setting, copy editing or publisher branding. Cite as Surname, Initial. (Year) 'Title of article'. To be published in *Title of Journal*, Volume and issue numbers [peer-reviewed accepted version]. Available at: DOI or URL (Accessed: date).

Enquiries

If you have questions about this document contact ResearchSupport@kent.ac.uk. Please include the URL of the record in KAR. If you believe that your, or a third party's rights have been compromised through this document please see our [Take Down policy](https://www.kent.ac.uk/guides/kar-the-kent-academic-repository#policies) (available from <https://www.kent.ac.uk/guides/kar-the-kent-academic-repository#policies>).

Studies of Latrophilin Signalling in Cancer Cells

Ouafa Benlaouer

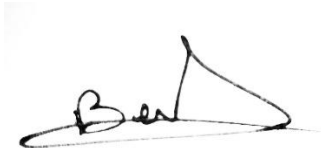
A thesis submitted in partial fulfilment of the requirements of
the University of Kent and the University of Greenwich for
the Degree of Doctor of Philosophy

July 2020

Declaration

I certify that this work has not been accepted in substance for any degree and is not concurrently being submitted for any degree other than that of Doctor of Philosophy being studied at the Universities of Greenwich and Kent. I also declare that this work is the result of my own investigations except where otherwise identified by references and that I have not plagiarized the work of others.

Signature of student:

A handwritten signature in black ink, appearing to be 'Ben', written on a light blue background.

Signature of supervisor:

A handwritten signature in black ink, written on a light blue background, consisting of a long horizontal line with a cursive signature above it.

Date: 30/06/2020

Acknowledgments

I would like to express my sincere gratitude to my supervisor Prof Yuri Ushkaryov for his support and guidance throughout my PhD and for his patience and for sharing with me his immense knowledge.

Beside my supervisor, I would also like to thank Dr Vadim Sumbayev for his continuous encouragement and friendly advice.

Many thanks to collaborators for permission to include some of their results in my thesis. These results are individually acknowledged in figure legends.

My sincere thanks also go to Dr Svetlana Sakhnevych and Danilo D'angela for being good friends, for all the fun we have had in the last few years and for helping me with my ups and downs during my writing up period.

Last but not least, I would like to thank my parents and siblings for their continuous support and incredible encouragements throughout my life.

Abstract

Cancer is one of the major causes of death worldwide. Acute myeloid leukaemia (AML), blood and bone marrow cancer, is usually characterised by rapid growth of malignant leukocytes that have developed several molecular mechanisms to escape immune system attack. Further studies suggest that the same immune escaping mechanism could be employed by solid cancers. However, the signalling mechanisms in cancer cells are poorly understood, and a better comprehension of these processes is vital for the development of biomarkers and potential anti-cancer treatments. Therefore, our aim was to study receptor expression and release of immune protective proteins in two types of cancer cells, AML and breast cancer cells.

Here, I report that an aGPCR, LPHN1, is expressed in AML cells and can be used as their biomarker. Our findings demonstrate that stimulation of LPHN1 expressed in AML cells by soluble FLRT3, an endogenous ligand of LPHN1/LPHN2/LPHN3, releases Tim-3 and Gal-9 complex, which helps AML cells to escape immune attack. By contrast, breast cancer cells, which express LPHN2, react to FLRT3 stimulation by trafficking Tim3 and Gal-9 complex to the cell surface rather than releasing it. I also developed a fluorescence-based versatile system for detecting cytosolic Ca^{2+} changes in adherent or suspension cells, which I used to investigate the LPHNs-mediated signalling in the AML and breast cancer cells. I have found that all cells expressing LPHN1 can be activated by α -LTX, an exogenous ligand of LPHN1, which induces Ca^{2+} signalling, while FLRT3 causes its signalling without increasing cytosolic Ca^{2+} . Taken together, our work led to the identification of LPHN1 as an absolute biomarker of AML cells and important new insights into intracellular signalling in cancer cells.

Abbreviations

aGPCR	Adhesion G protein-coupled receptor
AML	Acute myeloid leukaemia
CD	Circular dichroism
CICR	Ca ²⁺ induced Ca ²⁺ release
CTF	C-terminal fragment of LPHN
CTRH	Corticotropin-releasing hormone
DAG	Diacyl glycerol
dbcAMP	Dibutyryl cyclic AMP
EDTA	Ethylenediaminetetraacetic acid
FLRT3	Fibronectin-like domain-containing leucine-rich transmembrane protein 3
Gal-9	Galectin-9
GBL	Galactose-binding lectin
GPCRs	G protein-coupled receptors
GPS	GPCR proteolysis site
HRM	Hormone receptor motif
HRP	Horseradish peroxidase
ICRAC	Calcium-Release Activated Current
IL-6	Interleukin-6
IFN-γ	Interferon-gamma
IP₃	Inositol 1,4,5-triphosphate
IP₃R	Inositol 1,4,5-triphosphate receptor
K_d	Dissociation constant
kDa	kilodalton
Lasso	Latrophilin-associated synaptic surface organiser
LPHN	Latrophilin
α-LTX	α -Latrotoxin
LTX^{N4C}	Non-pore forming mutant recombinant latrotoxin
MCF-7	Breast cancer cell line

MCU	Mitochondrial Ca ²⁺ uniporter
NB2a	Murine neuroblastoma cell line
NCX	Na ⁺ Ca ²⁺ exchanger
NRXN	Neurexin I α
NTC	No-template control
NTF	N-terminal fragment of LPHN
PD-1	Programmed cell death protein 1
PDL	Poly-d-lysine
PFA	Paraformaldehyde
PIP₂	Phosphatidyl 4, 5 biphosphate
PKC	Protein kinase C
PLC	Phospholipase C
PM	Plasma membrane
PMCA	Plasma membrane Ca ²⁺ ATPase
PTPσ	Protein tyrosine phosphatase σ
PVDF	Polyvinylidene fluoride
ROCC	Receptor-operated calcium channels
RPTPσ	Receptor protein tyrosine phosphatase σ
RRP	Readily releasable pool
RYR	Ryanodine-sensitive receptors
SDS-PAGE	Sodium dodecyl sulphate-polyacrylamide gel electrophoresis
SERCA	Sarco/endoplasmic reticulum Ca ²⁺ ATPase
SFM	Serum free medium
SNARE	SNAP receptor
SOCC	Store operated calcium channel
SOCE	Store-operated Ca ²⁺ entry
SRCD	Synchrotron radiation circular dichroism
STIM1	Stromal interaction molecule 1
STP	Threonine, serine and proline-rich domain
TG	Thapsigargin
THP-1	Acute monocytic myeloid leukaemia cell line

Tim3	T cell immunoglobulin and mucin domain-containing protein 3
TMR	Transmembrane region
TRPC	Canonical transient receptor potential
VEGF	Vascular endothelial growth factor
VGCC	Voltage-gated calcium channels
Unc5	Netrin receptor C

Table of Contents

Declaration	I
Acknowledgments	II
Table of Contents.....	VII
Table of Figures.....	XI
Table of Tables.....	XIII
1. Introduction	1
1.1. The Discovery of Latrophilin	2
1.2. Latrophilin Structure	3
1.2.1. N-terminal Fragment	4
1.2.2. C-terminal Fragment.....	5
1.2.3. Autoproteolysis of LPHN Fragments	6
1.3. Tissue Distribution of Latrophilins	8
1.3.1. Latrophilins and Cancer	9
1.3.2. The role of Latrophilin 1 in Acute Myeloid Leukaemia	9
1.3.3. Latrophilin 2 and Breast Cancer	11
1.4. Latrophilins as GPCR.....	12
1.5. Latrophilin Signalling	13
1.6. Latrophilin Ligands	14
1.6.1. α -Latrotoxin.....	14
1.6.2. Teneurins, or Lasso	19
1.6.3. FLRT3.....	20
1.6.4. Contactin 6	22
1.7. Ca^{2+} Signalling.....	22
1.7.1. Calcium as a Universal Signalling Molecule	22
1.7.2. Intracellular Calcium Stores	24
1.7.3. Modulation of Voltage Gated Ca^{2+} Channels.....	27
1.7.4. Store-Operated Ca^{2+} Entry	27
1.8. Research Gap	29
1.9. Cytosolic Ca^{2+} Measurements.....	31
1.10. Aims and Objectives	36

2. Materials and Methods	37
2.1. Materials	38
2.2. Cell Culture	39
2.2.1. Cell lines	39
2.2.2. Primary human cells	40
2.2.3. Primary human blood plasma samples	40
2.2.4. Human breast tissue samples	41
2.2.5. Bone marrow extracts	41
2.3. Cell and Tissue lysis	42
2.3.1. Cells	42
2.3.2. Tissues	42
2.4. Determination of protein concentration	43
2.5. Latrotoxin	43
2.6. Latrotoxin binding assay	43
2.6.1. Sample preparation	43
2.6.2. Chloroform-methanol protein precipitation	44
2.7. Western blotting	45
2.7.1. SDS-polyacrylamide gel electrophoresis	45
2.7.2. Transfer	46
2.8. Immunodetection	46
2.9. Cytosolic Ca ²⁺ measurement	48
2.10. Synchrotron radiation circular dichroism spectroscopy	50
2.11. Enzyme-linked immunosorbent assay	52
2.11.1. Determination of released galectin-9 and soluble Tim-3	52
2.11.2. Determination of phospho-S2448 mTOR in cells	53
2.11.3. Detection of Tim-3-galectin-9 complex in cells and tissues	53
2.11.4. Detection of Tim-3-galectin-9 complex in culture medium	54
2.12. Determination of LPHN1 in human blood plasma	54
2.13. Quantitative real-time PCR	55
2.14. Determination of PKC- α activity	56
2.15. Measurement of PLC activity	56
2.16. Immunocytochemistry	57

2.17. Confocal microscopy and imaging flow cytometry.....	57
2.18. Fluorescence-activated cell sorting (FACS).....	59
2.19. Isolation of soluble NTF of LPHN1.....	60
2.20. Data analysis	60
3. LPHN1 interaction with FLRT3	61
3.1. Introduction	62
3.2. Purification of soluble NTF of LPHN1	62
3.3. FLRT3 causes a conformational change in LPHN1	65
3.4. Discussion	67
4. LPHN1 and regulation of cytosolic Ca ²⁺	69
4.1. Introduction	70
4.2. Ca ²⁺ homeostasis in NB2A cells expressing full size and truncated LPHN1	75
4.3. Store operated Ca ²⁺ channels	78
4.4. α-LTX signalling via LPHN1.....	81
4.5. FLRT3 does not induce fast signalling via LPHN1.....	83
4.6. FLRT3 binding to LPHN1-expressing NB2A cells	85
4.7. Possible LPHN1 ligands in the blood plasma	86
4.8. Discussion	88
5. The role of LPHN1 in AML cells.....	93
5.1. Introduction	94
5.2. Identification of LPHN1 in THP-1 cells.....	94
5.3. Presence of soluble LPHN1 fragments in AML blood plasma	95
5.4. Upregulation of LPHN1 expression in AML cells and haematopoietic stem cells.....	97
5.5. Upregulation of Gal-9 in AML cells by FLRT3 and LPHN1 interaction.....	100
5.6. Fast Ca ²⁺ signalling in THP-1 cells.....	103
5.7. Discussion	106
6. Signalling pathways in human breast cancer cells	111
6.1. Autocrine loop proteins in human tissues.....	112
6.2. Ca ²⁺ dynamics in MCF-7 cells	121
6.3. FLRT3 binding to LPHN2	122
6.4. α-LTX does not activate Ca ²⁺ signalling in MCF-7 cells.....	123

6.5. Discussion	124
7. General Discussion and Conclusions.....	127
8. References	133

Table of Figures

Figure 1. The structure of LPHNs.	4
Figure 2: Interactions between the NTF and CTF.	7
Figure 3: LPHN1-mediated signal transduction after stimulation with α -LTX.	19
Figure 4: LPHN1 and its ligands.	21
Figure 5: Intracellular calcium signalling pathways.	24
Figure 6: A scheme of Fluo-4 AM dye use and action.	33
Figure 7: Protein precipitation using the chloroform/methanol method.	44
Figure 8: A scheme of the Western blotting method.	47
Figure 9: The structures of full-size LPHN1 (LPH-42) and its soluble ectodomain LPH-51.	63
Figure 10: Isolation of LPH-51.	64
Figure 11: Quantification of purified LPH-51.	65
Figure 12: Interaction of FLRT3 with LPHN1 detected by CD spectroscopy.	66
Figure 13: Scatchard plot displaying FLRT3 binding to LPH-52. $K_d= 48.8$	67
Figure 14: The structure of LPHN1 constructs: full-size LPH-42 and truncated LPH-71.	71
Figure 15: Measurement of cytosolic Ca^{2+} dynamics in live cells.	74
Figure 16: The effect of TG on cytosolic Ca^{2+} in cells expressing full-size or mutant LPHN1.	76
Figure 17: Increased Ca^{2+} stores and SOCE in cells expressing full-size LPHN1.	77
Figure 18: Features of the SOCCs in NB2A cells.	80
Figure 19: α -LTX binding to different LPHN1 constructs in NB2a cells.	82
Figure 20: Ca^{2+} signalling induced by α -LTX in NB2a cells expressing full size or mutant LPHN1.	84
Figure 21: Sensitivity of FLRT3 detection.	86
Figure 22: FLRT3 interaction with NB2a cells expressing full-size or mutant LPHN1.	87
Figure 23: Intracellular Ca^{2+} dynamics in NB2a cells stimulated with human serum.	88
Figure 24: LPHN1 protein expression in human primary AML cells, THP-1 cells, and primary healthy leukocytes.	95
Figure 25: Soluble LPHN1 fragments in the blood plasma of AML patients.	96

Figure 26: Cortisol induces LPHN1 expression in human hematopoietic stem cells (HSC), AML cells and THP-1 cells, but not in healthy primary leukocytes.	98
Figure 27: Cortisol and Gal-9 levels in the blood plasma of AML patients and healthy donors.	99
Figure 28: Detection of LPHN1 on the surface of THP-1 cells.....	100
Figure 29: FLRT3 circulating in blood plasma induces Gal-9 secretion in AML cells in a LPHN1-dependent manner.....	102
Figure 30: Intracellular Ca ²⁺ stores and SOCE in THP-1 cells.....	104
Figure 31: Stimulation of LPHN1 by α-LTX in THP-1 cells.....	105
Figure 32: FLRT3 does not induce fast release of stored Ca ²⁺ in THP-1 cells.	106
Figure 33: A proposed mechanism of cortisol-induced increase in LPHN1 expression in AML cells followed by increased Gal-9 secretion.	110
Figure 34: Expression of LPHN2, FLRT3, Gal-9 and Tim3 in primary human breast cancer tissues.	113
Figure 35: Gal-9 expression in primary human breast cancer and healthy tissues.	114
Figure 36: PLC, PKCα and mTOR activity in human breast cancer primary tissues..	116
Figure 37: The presence of Tim3-Gal9 complex in primary human breast cancer.	117
Figure 38: Gal-9, Tim-3 and IL-2 blood plasma levels in human healthy donors, primary breast cancer patients and metastatic breast cancer patients.....	118
Figure 39: Expression of LPHN2, Gal-9, Tim3 and Tim3-Gal-9 complex in a breast cancer cell line.	119
Figure 40: FLRT3 causes translocation of Gal-9 to the cell surface in breast cancer MCF-7 cells.	120
Figure 41: Intracellular Ca ²⁺ dynamics in breast cancer cells.....	122
Figure 42: An interaction between the extracellular domain of FLRT3 and the olfactomedin-like domain of LPHN2.....	123
Figure 43: α-LTX does not stimulate fast Ca ²⁺ mobilisation in MCF-7 cells.	124
Figure 44: Schematic representation of LPHN1 induced translocation of Tim-3 and Galectin-9 onto cell surface in Acute myeloid leukaemia cells.....	129
Figure 45: Schematic representation of LPHN2 induced translocation of Tim-3-Gal-9 complex to the plasma membrane in breast cancer cells.	131

Table of Tables

Table 1. Acrylamide percentage in SDS-gels used for separating indicated protein ranges.....	46
Table 2. Antibodies used in this project.....	48

1. Introduction

1.1. The Discovery of Latrophilin

At the beginning of 1970s, Longenecker and his group discovered the effect of black widow spider venom component, *Latrodectus mactans*, on the frog neuromuscular junction (Birks *et al.*, 1960). They wanted to further study which neurotoxin component was responsible for the massive neurotransmitter release. α -latrotoxin (α -LTX) was then isolated and shown to form a Ca^{2+} permeable pore in a lipid bilayer membrane (Finkelstein *et al.*, 1976). Yet, this effect was observed only when α -LTX binds high affinity receptor in neuronal cells. Strangely, α -LTX was shown to act also in the absence of extracellular Ca^{2+} (Longenecker *et al.*, 1970) which suggested the presence of a high affinity presynaptic receptor that doesn't require extracellular Ca^{2+} for its exocytosis regulation. Due to the vital function of α -LTX in exocytosis, several groups were trying to identify the functional receptor of α -LTX using the toxin as an affinity adsorbent (Sheer and Meldolesi, 1985; Petrenko *et al.*, 1990).

As a result of these efforts, in 1990, Neurexin I α (NRXN) was identified as a high-affinity α -LTX receptor that can only bind the toxin in the presence of Ca^{2+} (Petrenko *et al.*, 1990; Ushkaryov *et al.*, 1992). Therefore, this result has led to a continued interest in the search for a Ca^{2+} -independent receptor. The extended search eventually resulted in the discovery of latrophilin by two laboratories, which was later classified as one of the first members of the adhesion G protein-coupled receptors (aGPCRs) (Davletov *et al.*, 1996; Krasnoperov *et al.*, 1997). This receptor was named as latrophilin (LPHN) by Ushkaryov and his group (Lelianova *et al.*, 1997), and as a Calcium Independent receptor for α -LTX (CIRL) by Petrenko and his group (Krasnoperov *et al.*, 1997), whereas the group of Sudhof combined both names to

reach the abbreviation of CL (Sugita *et al.*, 1998). Recently it has been renamed by the International Union of Basic & Clinical Pharmacology (IUPHAR) as an Adhesion G-protein-coupled Receptor of the Latrophilin group (ADGRL) (Hamann *et al.*, 2015). In this thesis, the more conventional abbreviation, LPHN, will be used.

Later, three homologues were identified for LPHNs in mammals (Ichtchenko *et al.*, 1999; Matsushita *et al.*, 1999), when rat and bovine LPHN cDNA were isolated. The first LPHN discovered, was named LPHN1, while the other two LPHN2 and LPHN3 were named based on their sequence homology to, and evolutionary distance from, LPHN1. Despite the high similarity between LPHN2 and LPHN1, LPHN2 binds to α -LTX with lower affinity compared to LPHN1 (Ichtchenko *et al.*, 1999). Due to its high affinity for α -LTX, LPHN1 is undoubtedly the most studied among the LPHN proteins.

1.2. Latrophilin Structure

LPHNs were classified as aGPCR for their unique adhesion receptor motifs linked to a GPCR core, comprising the following domains: long extracellular N-terminal domain, with ~850 residues, 7 transmembrane domains (7TRM) connected by intra- and extracellular loops, with ~240 residues; and long C-terminal cytoplasmic tail of ~370 amino acids (**Figure 1**). As a typical aGPCR LPHNs undergo constitutive proteolysis at a conserved GPCR proteolysis site (GPS), located just 19 amino acids upstream of the first transmembrane domain (Krasnoperov *et al.*, 1997; K. . Volynski *et al.*, 2004; Silva and Ushkaryov, 2010). This cleavage results in two LPHN fragments: the N-terminal fragment (NTF) and the C-terminal fragment (CTF). The NTF encompasses almost the entire extracellular N-terminal domain and contains no transmembrane domains,

while the CTF contains a short N-terminal extracellular sequence, the seven transmembrane domains and the cytosolic tail. Both fragments appear to function independently of each other, as they have been found in distinct membrane locations and can be internalised at different rates (Silva and Ushkaryov, 2010; Huang *et al.*, 2012). Structure similarity between the three LPHNs are 48-63% identical, and the following structural description applies to all LPHNs.

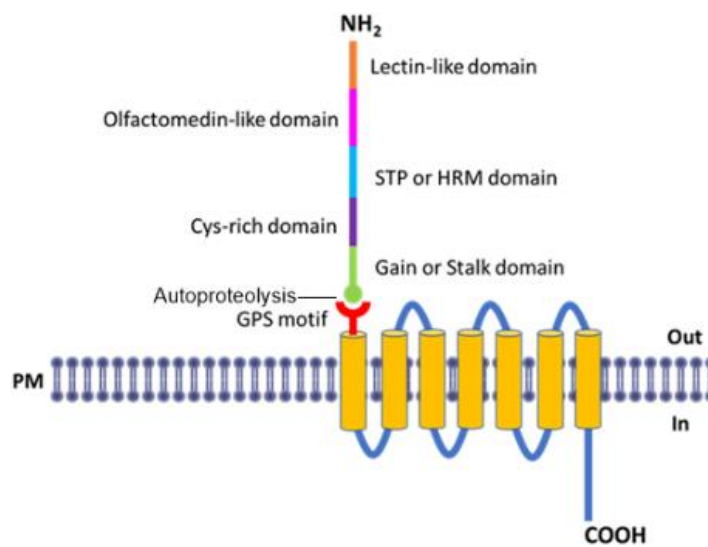


Figure 1. The structure of LPHNs.

Schematic representation of the LPHN domain structure, consisting of the long NTF, 7 TMRs and the CTF, which is a typical α GPCR structure. The NTF contains the lectin-like domain, olfactomedin domain, HRM domain, cysteine rich domain and GAIN domain, where LPHNs undergo proteolysis. G-proteins usually interact with LPHNs at the third intracellular loop of the 7 TMRs.

1.2.1. N-terminal Fragment

NTF (**Figure 1**) is heavily glycosylated which is important for its trafficking to the plasma membrane and begins with a hydrophobic signal peptide (Krasnoperov *et al.*, 1997; K. Volynski *et al.*, 2004). Immediately after a long cysteine-rich domain homologous to galactose-binding lectin (GBL) also named as lectin-like domain (Krasnoperov *et al.*, 1997; Lelianova *et al.*, 1997). Following the lectin-like domain, an

Olfactomedin domain is found; it is essential for neurogenesis and cell cycle regulation. Mutations in this domain have been linked to several neurological and psychiatric diseases. Following the olfactomedin domain, a sequence of 79 amino acid-rich of serines, threonines and prolines presents (Krasnoperov *et al.*, 1999) (STP domain). The STP domain in LPHN is highly homologous to the domain found in GPCRs that belong to the secretin family (Harmar, 2001). It is also known as "hormone-binding domain" (Harmar, 2001), "signature domain" (Matsushita *et al.*, 1999) or "hormone receptor motif" (HRM) (Rohou *et al.*, 2007). The HRM domain has two conserved tryptophan and three to four conserved cysteine residues, which may create internal disulphide bridges. Just after the HRM domain, a "stalk" domain is found; this region is essential for the cleavage of LPHN and other aGPCR (Stacey *et al.*, 2001).

Truncations of the stalk domain prevent α -LTX from binding to LPHN, which may suggest that α -LTX binds LPHN at this position (Sugita *et al.*, 1998) this was also confirmed a year later by Krasnoperov and her group (Krasnoperov *et al.*, 1999). The stalk domain is attached to GPCR proteolysis site (GPS), a short sequence containing four cysteine residues (Krasnoperov *et al.*, 1997) making it the most C-terminal NTF domain. Most importantly, this is the site where posttranslational cleavage occurs, resulting in the two fragments, NTF and CTF.

1.2.2. C-terminal Fragment

The CTF (**Figure 1**) begins immediately after the cleavage site within GPS motif (Volynski *et al.*, 2004). The most outstanding property of the CTF is the presence of 7 TMRs that are very similar to those of the secretin family GPCRs. Within the 7 TMR

region, the CTF has two cysteine residues which can form an intramolecular disulphide bridge. One other prominent feature of the CTF as an aGPCR is the presence of a negative charge within the third TMR, which is linked to the region in which a G protein binds GPCRs (Röthe *et al.*, 2019). In addition, the CTF contains other features, including multiple palmitoylation and phosphorylation sites (Krasnoperov *et al.*, 1997; Rahman *et al.*, 2019). Interestingly, the CTF phosphorylation plays an important role in the interaction of LPHN fragments, as it has been shown by Rahman and his group that the phosphorylated CTF has a higher affinity for the NTF compared to the non-phosphorylated CTF and that the binding of α -LTX to the NTF induces the coupling of these fragments. Ligand binding to the NTF-CTF complex leads to the recruitment of the receptor-like protein tyrosine phosphatase σ (RPTP σ) to the complex, resulting in the CTF dephosphorylation and complex dissociation (Rahman *et al.*, 2019). These findings may have important implications for the regulation of LPHNs fragments function.

1.2.3. Autoproteolysis of LPHN Fragments

LPHN was the first aGPCR for which GPS motif was directly recognised by CTF sequencing (Krasnoperov *et al.*, 1997). Since then, many studies have been conducted to examine the autoproteolysis cleavage of other aGPCRs (Lin *et al.*, 2004; Araç *et al.*, 2012). Autoproteolysis of LPHN (**Figure 1**) usually happens in the endoplasmic reticulum (ER) and is vital for its trafficking to the cell surface (Krasnoperov *et al.*, 2002; Volynski *et al.*, 2004). Apparently, full-size LPHN and other full size aGPCRs are not generally present in live tissues due to their short life presence on the cell surface or complete cleavage in the ER. Few evidences show

some enzymatic activity involvement in the creation of these fragments (Krasnoperov *et al.*, 2002). As previously described, the NTF does not include any TMR; yet, it is not released into the medium and remains non-covalently bound to the membrane by forming a complex with CTF or by an unknown membrane anchor (K. . Volynski *et al.*, 2004) (**Figure 2**). This was also supported by the fact that proteolysis at a different site located between the GPS and the first TMR, releases a small amount of the NTF into the medium (Krasnoperov *et al.*, 2009). On the other hand, studies showed that only 7-8 residues within the CTF part of the GPS are responsible for the interaction between both fragments (Krasnoperov *et al.*, 2002; Volynski *et al.*, 2004). Despite the short sequence of these residues holding both fragments together, even extremely harsh conditions are not

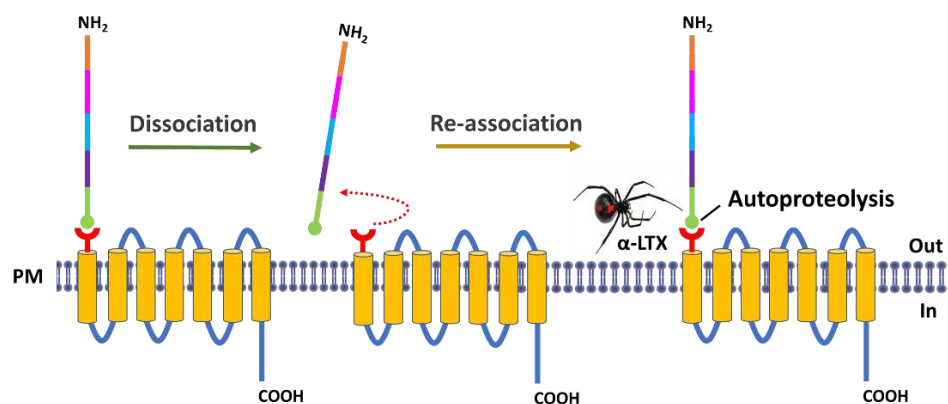


Figure 2: Interactions between the NTF and CTF.

Both fragments can exist as independent proteins in the plasma membrane (PM), but when a ligand, like α-LTX, binds to the NTF, it induces fragments association and signalling transduction via G protein coupling.

able to dissociate the NTF-CTF complex, such as pH 2.4, pH 12, 4 M Mg²⁺ or 8 M urea

(Silva and Ushkaryov, 2010; Rahman *et al.*, 2019). However, a weak detergent (perfluoro-octanoic acid) that does not fully solubilise the plasma membrane, breaks the NTF-CTF complex (Silva *et al.*, 2009). Taken together, these data indicate that NTF is bound somehow to the plasma membrane differently from the interaction with the CTF. Under certain conditions, stimulation with α -LTX or LTX^{N4C}, solubilisation of plasma membrane with detergent and phosphorylation of the CTF, the free NTF and CTF can re-associate (K. . Volynski *et al.*, 2004; Rahman *et al.*, 2019)

1.3. Tissue Distribution of Latrophilins

Despite the high sequence homology between LPHNs, each receptor subtype has a different expression pattern. Several groups tried to study these expression differences; one of the first investigations was done on different rat tissues, including brain, liver, heart, lung, kidney, spleen, and muscle. Northern blot analysis of several rat RNA tissues was used and probed specifically for LPHN1, 2 and 3 (Matsushita *et al.*, 1999). Results showed that LPHN1 and 3 were mostly expressed in the brain. LPHN1 was also expressed in low amounts in the kidney, lung, and spleen, while LPHN3 was also expressed in the lung and spleen. On the other hand, LPHN2 was expressed ubiquitously. Another study was done by the Petrenko group investigating the distribution of LPHN2 and LPHN3 in different human tissue samples. The results showed that LPHN3 mRNA was found in the heart, placenta, pancreas, kidneys, and testes, whereas LPHN2 mRNA was everywhere, in agreement with the previous investigation (Ichtchenko *et al.*, 1999). It is important that in both studies α -LTX agarose was used to identify LPHN in different tissues. This means that only those forms of LPHN that bind α -LTX were isolated, in this case LPHN1 and LPHN2 only. A

more recent study showed that LPHN2 and LPHN3 were highly expressed in foetal and adult adrenal glands (Xing *et al.*, 2009). Therefore, these studies suggest that LPHNs may have widespread physiological functions, that need to be investigated.

1.3.1. Latrophilins and Cancer

Nowadays, cancer is one of the top reasons of human death worldwide. Usually it starts with a dysregulation in cell cycle, which results in the abnormal growth of cells and their spreading through other body tissues. Therefore, the importance of identifying new biomarkers or discovering new tumour-suppressor genes and continuously developing effective cancer treatments has a huge impact on increasing cancer survival rates. GPCRs are considered one of the largest families of drug targets, yet they are rarely used as a target for cancer treatment (Nieto Gutierrez and McDonald, 2018). Moreover, many studies showed the involvement of several aGPCRs in cancer, with important cellular functions in cancer development; this includes: cell adhesion, migration and guidance (Tang *et al.*, 2013; Aust *et al.*, 2016). LPHNs are one of the aGPCRs that have been linked to several cancers. Studies showed the involvement of LPHN1 gene in low invasion lung cell lines (Hsu *et al.*, 2009) and mutations in LPHN3 gene has been linked to cancers in lung, ovarian, breast and prostate (Kan *et al.*, 2010). The exact role of LPHNs in cancer development has not been investigated in depth; therefore, further studies must be done.

1.3.2. The role of Latrophilin 1 in Acute Myeloid Leukaemia

Acute myeloid leukaemia is blood cancer with abnormally differentiated blasts of myeloid lineage, which results in the rapid growth of immature myeloid cells and

reduction in the normal hemopoiesis causing severe anaemia, increased rise of infections and in some cases haemorrhage (Short *et al.*, 2018). Acute myeloid leukaemia remains a major medical global burden and the determination of proteins expressed in malignant cells and absent in healthy cells is essential. Recently, Sumbayev in collaboration with Ushkaryov discovered that LPHN1 is expressed in acute myeloid leukaemia (AML) cell lines and in primary leukemic cells, but absent in healthy leukocytes (Sumbayev *et al.*, 2016). Thus, LPHN1 is a unique, absolute biomarker of leukaemia, and it may be a promising diagnostic marker or even a target for drugs to treat AML. Therefore, the characterisation of its function in AML cells is essential. Stimulation of LPHN1 in the brain by its ligand leads to Ca²⁺ mobilisation, which in return causes neurotransmitter release and maintenance of several neuronal functions. However, the role of LPHN1 in non-neuronal cells remains unclear and should be thoroughly investigated. It has been shown previously that exocytotic activity in cancer cells is essential for the release of cytokines and growth factors, which are both required by myeloid cells during their development (Civini *et al.*, 2013). Myeloid leukocytes need a source of energy and oxygen in order to transform into malignant cells. With uncontrolled proliferation of malignant leukocytes, energy and oxygen are in short supply and malignant cells must fight healthy cells for the supplies. Therefore, malignant cells have developed a way to survive and proliferate in this harsh environment by aerobic glycolysis to generate ATP, which is known as the Warburg effect (Vander Heiden *et al.*, 2009) (Behrmann *et al.*, 2018).

Malignant cells induce the expression of vascular endothelial growth factor (VEGF),

leading to the induction of angiogenesis. In addition to VEGF and other pro-angiogenic factors, leukemic cells induce the release of interleukin-6 (IL-6), which is another crucial factor that promotes their survival. The release of these cytokines and growth factors can be especially supported by proteins that can stimulate exocytosis. LPHN1 is known to induce exocytosis when stimulated by its ligand. However, an endogenous ligand of LPHN1 in leukaemia is still unknown. Therefore, one of the objectives of this thesis is to approach the identification of an endogenous ligand of LPHN1 in AML cells and to understand the physiological role of LPHN1 in these cells.

1.3.3. *Latrophilin 2 and Breast Cancer*

Breast cancer is considered one of the most common cancers in women and there is a need for new biomarkers and treatments of breast cancer. It has been discovered that human LPHN2 gene overexpression may be involved in breast cancer (White *et al.*, 1998). Indeed, in a different study done by the same group, 12 breast cancer cell lines were shown to overexpress the LPHN2 gene (White *et al.*, 2000), confirming the previous findings. Mutations in LPHN2 were also associated with urothelial carcinoma of the bladder (Zhang *et al.*, 2014). Moreover, galectin-9 (Gal-9), a member of the β -galactoside-binding lectin family, plays a major role in several cellular biological mechanisms, such as apoptosis, immune response, and cell aggregation. Interestingly, Gal-9 was found to be expressed in breast cancer cells and its expression was involved in preventing cancer cells from metastasis by inducing aggregation of breast cancer cells and reducing adhesion to the extracellular matrices which is an essential step in tumor cell invasion (Yamauchi *et al.*, 2006).

1.4. Latrophilins as GPCR

GPCRs are a group of cell-surface molecules that consists of five main families in mammals, the largest family member being the Rhodopsin family (class A), with about 284 members, followed by the Adhesion GPCR family with 33 members, and then 22 members of the Glutamate family (class C), 15 members of the Secretin family (class B) and 11 members of the Frizzled family (Schiöth and Fredriksson, 2005; Civelli *et al.*, 2013). At the beginning, aGPCRs were classified as class B, but then several observations allowed the researchers to distinguish between aGPCRs and secretin family, including the special autocatalytic processing of aGPCRs, their long N termini and functional roles in cell-cell and cell-matrix interactions (Harmar, 2001).

In contrast to secretin family members, which normally mediate hormonal signalling and are not autocatalytically processed (Hamann *et al.*, 2015), aGPCRs are the second largest GPCR family, yet the least studied and understood (Fredriksson *et al.*, 2003).

LPHN was initially classified as a member of the secretin family, based on its high sequence homology with the TMRs of that family group in addition to its ability to bind G proteins within its CTF. However, this was not a strong reason to classify it as a GPCR, therefore, many groups investigated the function of this receptor in details.

As a result, LPHN was reclassified as the first member of aGPCRs and was explicitly shown to bind $G\alpha_0$ and $G\alpha_{q/11}$ (Lelianova *et al.*, 1997; Rahman *et al.*, 1999; Serova *et al.*, 2008). Moreover, the binding between CTF and G proteins depends on the ability of G proteins to cleave GTP (Rahman *et al.*, 1999). Therefore, isolation of the LPHN-G protein complex increases when GDP and EGTA are added to the solubilising buffer, which leads to the inhibition of GTPase activity. When GTP and Mg^{2+} were added to

purification buffer, it reinforces the activity of GTPase, which result in the dissociation of G proteins and their loss from the column eluate (Rahman *et al.*, 1999). However, the addition of extra GTP reinstates the binding of LPHN1 with its G protein, implying that this binding is functional and not only physical.

1.5. Latrophilin Signalling

The LPHN signalling pathway has been studied using mainly the exogenous ligand, α -LTX, and its mutant form LTX^{N4C} (Volynski *et al.*, 2003). The signalling induced by this ligand is based on the activation of G protein pathways. Particularly, in neuronal and non-neuronal cells expressing LPHN1, LTX^{N4C} caused activation of phospholipase C (PLC), IP₃-dependent effects (possibly depletion of IP₃ stores) and an increase in cytosolic Ca²⁺ (Lelianova *et al.*, 1997; Davletov *et al.*, 1998) (**Figure 3**).

However, the challenge in the study of the LPHN signalling pathway was due to the fact that α -LTX binds to two different receptors in addition to its ability to form Ca²⁺ permeable pore (Südhof and Starke, 2008; Silva *et al.*, 2009). As scientists were trying to solve this obstacle, Südhof and his group made a step forward into LPHN research area by creating the mutant α -LTX, LTX^{N4C} (Ichtchenko *et al.*, 1998).

This mutant LTX does not have the ability to form transmembrane pores, yet it stimulates neurotransmitter release in neuronal tissues (Ashton *et al.*, 2001; Silva *et al.*, 2009). This indicates that the α -LTX effect was at least partially due to receptor stimulation and not only pore formation. However, LTX^{N4C} can bind other neuronal receptors: NRXN and RPTP σ , which made it possible that the effect did not depend on G protein signalling. In addition, LTX^{N4C} required extracellular Ca²⁺ for its action in

the nerve terminals (Capogna *et al.*, 2003; Volynski *et al.*, 2003), which might suggest that the toxin induces influx of Ca^{2+} rather than release of Ca^{2+} from intracellular stores. Therefore, to confirm which receptor is involved in this signalling transduction, neuroblastoma cells (NB2a) expressing NRXN or LPHN were stimulated by LTX^{N4C}. Stimulation of cells expressing LPHN resulted in PLC activation and release of intracellular Ca^{2+} , while this did not happen in cells expressing NRXN or mutant LPHN (possessing one TMR and unable to signal, LPHN 71) (K. Volynski *et al.*, 2004) (**Figure 3**). These results indicate that LPHN1 via its CTF is able to activate PLC and release of Ca^{2+} from intracellular stores.

Several signalling studies showed that stimulation of neuronal LPHN1 showed an exocytotic effect via G protein pathway, and that they are fast and reach a maximum within seconds or minutes. Moreover, this signalling capability has the same properties even in synaptosomes and neuromuscular junctions. This leads us to an important conclusion that LPHN1 actions are local within presynaptic terminals and does not need to send signals to the cell body and nucleus (Ashton *et al.*, 2001; Silva *et al.*, 2011). On the other hand, LPHN1 can relate to other signalling pathways, particularly considering the ability of free NTF to bind to CTFs from different adhesion GPCRs.

1.6. Latrophilin Ligands

1.6.1. α -Latrotoxin

Acute pain, paralysis and sometimes death are the symptoms you would have experienced if a black widow spider bit you. This effect is mainly due to one

component of black widow spider venom called α -LTX. α -LTX is considered the main exogenous ligand of LPHN1. Several studies were performed to study the effect of this toxin on different vertebrate neurotransmitters (Gorio *et al.*, 1978; Tzeng and Siekevitz, 1978), and the toxin stimulated the release of all neurotransmitters tested.

α -LTX is a propeller-shaped tetramer that has a hydrophobic base that allows its insertion into the cell membrane. At the base of the channel, the central pore is 25 Å in diameter, but then widens to a diameter of 36 Å in the middle of the channel and narrows to 10 Å at the top. It has been described that α -LTX monomer structure is shaped as letter L and consists of three domains: the wing, body and head (Orlova *et al.*, 2000). The binding of α -LTX to LPHN1's NTF does not depend on the presence of Ca^{2+} or any other divalent cations; however, the absence of divalent cations leads to the breakdown of α -LTX tetramers, which still allows the binding of the toxin dimers to and activation of LPHN1, but also eliminates pore formation (Davletov *et al.*, 1998; Sugita *et al.*, 1998; Orlova *et al.*, 2000).

Therefore, having an α -LTX version that can solely form dimers was essential for studying LPHN1 function. This mutant toxin, LTX^{N4C}, was produced by the insertion of four amino acids between the N-terminal and the ankyrin repeats. In this way, the new sequence prevents pore formation through interference with its oligomerisation (Capogna *et al.*, 2003; Volynski *et al.*, 2003). Several studies were conducted in order to study the interaction between α -LTX with different forms of mutant LPHN1 (Krasnoperov *et al.*, 1999). This experiment showed that full size NTF with HRM, Stalk and GPS domain was necessary for α -LTX binding. This may suggest that α -LTX binds to LPHN1 at multiple points, with a low affinity at each point of contact. Specifically,

the HRM domain which was presumed to be the binding region for hormone receptors, but α -LTX could not bind this region alone. The binding of α -LTX to NTF at multiple sites may create enough binding force, leading to receptor activation. α -LTX activity suggested that its receptor would be highly present in the nervous system, more specifically the brain.

Furthermore, as previously mentioned α -LTX binds to NRXN and RPTP σ , which allows pore formation in the cell membrane, yet does not show massive neurotransmitter release as seen with LPHN1. The main difference between LPHN1 and NRXN is that the latter needs extracellular Ca^{2+} for the binding to occur, but does not show any signalling capabilities (Ushkaryov *et al.*, 1992; Davletov *et al.*, 1998) Although RPTP σ binds to α -LTX independently of Ca^{2+} presence and has signalling capabilities (Aicher *et al.*, 1997; Bittner *et al.*, 2002), it is not expressed only in the brain and therefore cannot explain the specifically neuronal effect of α -LTX.

The first study in which α -LTX showed a massive neurotransmitter release was done on a frog neuromuscular junction using electrophysiological recordings (Longenecker *et al.*, 1970; Gorio *et al.*, 1978). When the buffer used was without extracellular Ca^{2+} , a slow rise in the exocytotic release was shown, after a few seconds to minutes, the frequency of exocytosis reached a broad peak, then gradually decreased back to resting state (Lelyanova *et al.*, 2009); then at some point the release of neurotransmitter stopped. This can be explained by the fact that the presence of extracellular Ca^{2+} is essential for recycling synaptic vesicles (Wu and Wu, 2014). When extracellular Ca^{2+} was added, a high frequency of bursts of exocytosis appeared, which was most likely due to LPHN1 signalling, Ca^{2+} stores depletion and subsequent

influx of extracellular Ca^{2+} (Lelyanova *et al.*, 2009). This effect slows down as well, probably due to α -LTX overwhelming the release apparatus (Silva *et al.*, 2009). Therefore, α -LTX has several mechanisms of action including Ca^{2+} dependent/independent effects and pore formation, as opposed to LPHN1 signalling effect. In the presence of Ca^{2+} , exocytosis of synaptic vesicles stimulated by α -LTX pore formation is different from release triggered by LPHN1 signalling (Davletov *et al.*, 1998; Rahman *et al.*, 1999; Ashton *et al.*, 2001). Pore mediated release was observed after LPHN1 stimulated release of readily releasable pool (RRP) vesicles, which acts on unprimed vesicles (Ashton *et al.*, 2001).

Interestingly, another group in 2019 stated that LPHN1 signalling mechanism in the absence of Ca^{2+} depends on the classical SNARE proteins, such as synaptobrevin, SNAP-25 and partially the active zone protein Munc13-1 (Deák *et al.*, 2009). Exocytosis stimulated by the influx of Ca^{2+} through the pore did not require any SNARE proteins, which may suggest that neuronal exocytosis can be stimulated by a different pathway that involves the presence of high concentration of Ca^{2+} . Since α -LTX pore lacks ion selectivity (Mironov *et al.*, 1986) other cations can stimulate neurotransmitter release. For example, sodium (Na^+) has been claimed as one of these ions that is able to support some of α -LTX signalling in the absence of extracellular Ca^{2+} . Deri *et al.* (Deri and Adam-Vizi, 1993) found that the lack of extracellular Na^+ reduced the release of ACh release stimulated by Ca^{2+} influx in synaptosomes. The same observation was seen in the frog neurotransmitter junction, where the absence of extracellular Na^+ reduced Ca^{2+} and neurotransmitter release (Deri and Adam-Vizi, 1993). These observations led the scientist to hypothesize that

Na⁺ influx through the α-LTX pore stimulated Ca²⁺ release from mitochondria. Using proton gradient uncoupler carbonyl cyanide 3-chlorophenylhydrazone (CCCP), which depletes mitochondria of its Ca²⁺, showed a relatively similar increase in the cytosolic Ca²⁺ concentration as was produced by α-LTX. However, since some Ca²⁺ and neurotransmitter release was still observed in the absence of Na⁺ and the use of CCCP did not increase neurotransmitter release, these data may indicate that α-LTX has Na⁺-independent actions, which remain to be identified.

Which specific Ca²⁺ stores are stimulated by α-LTX is not yet clear. It has been claimed by (Tsang *et al.*, 2000) that α-LTX is not inducing Ca²⁺ release from ER stores, on the other hand several other studies showed that release of Ca²⁺ from ER stores was crucial for exocytosis of vesicles in RRP mediated by the stimulation of LPHN1 (Davletov *et al.*, 1998; Ashton *et al.*, 2001). Furthermore, release of Ca²⁺ from mitochondria did not fully mimic the complete α-LTX's effects on release, which indicates that the increase of cytosolic Ca²⁺ concentration does not represent the full action of α-LTX, and that LPHN1 plays an important role in mediating α-LTX effects on neurotransmitter release.

Due to the large size of the α-LTX pore, it may allow small molecules, such as fluorescein isothiocyanate (FITC) (Rahman *et al.*, 1999) and neurotransmitters (Davletov *et al.*, 1998) to pass, therefore, non-vesicular efflux of neurotransmitter is another α-LTX mode of action on synaptic terminals. This was detected by observing some of neurotransmitter release even after: 1) the removal of extracellular Ca²⁺, 2) inhibiting neuronal exocytosis using the potent inhibitor clostridial neurotoxins, 3) emptying of synaptic vesicles by bafilomycin (Davletov *et al.*, 1998; Rahman *et al.*,

1999; Ashton *et al.*, 2001).

The studies done so far were focused on the action of α -LTX on LPHN1 at synaptic terminals. Yet, many questions remain to be answered about the signalling pathway of LPHN1 when stimulated by α -LTX in malignant cells. The aim of this thesis is to investigate this mechanism using neuronal cancer cells neuroblastoma cells (NB2a cells) as a model compared with acute myeloid leukaemia cells (THP-1 cells) and breast cancer cells (MCF-7 cells).

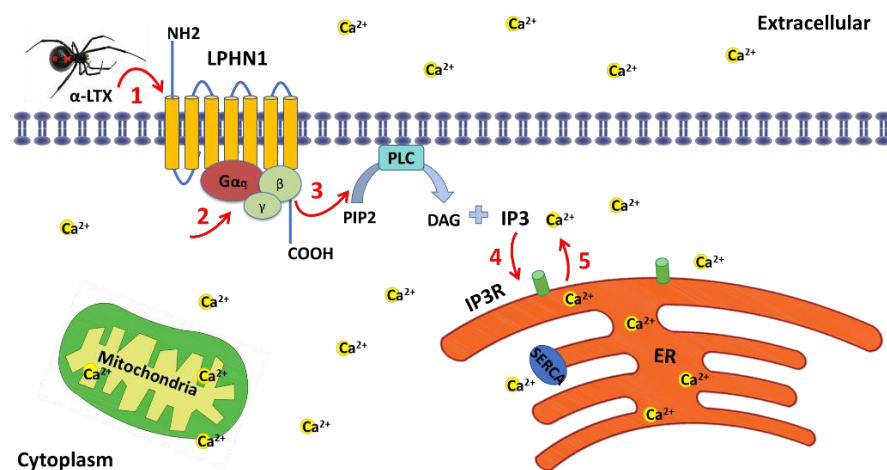


Figure 3: LPHN1-mediated signal transduction after stimulation with α -LTX.

Stimulation of LPHN1 by α -LTX leads to G proteins coupling, activation of PLC and production of IP3. IP3 will then bind IP₃R located in the membrane of the ER. This binding leads to the release of Ca²⁺ into the cytosol.

1.6.2. Teneurins, or Lasso

Teneurin-2 (Ten-2) or Lasso (latrophilin-associated synaptic surface organiser), is a large glycoprotein expressed on the postsynaptic membrane (**Figure 4**) and was the first discovered endogenous ligand for LPHN1, consisting of four subfamily members: teneurin-1, -2, -3 and -4 (Silva and Ushkaryov, 2011; Ushkaryov *et al.*, 2019). Of the

four teneurin members, ten-2 was the only high-affinity ligand to be isolated by LPHN1 affinity chromatography (Silva and Ushkaryov, 2011; Ushkaryov *et al.*, 2019).

The interaction between ten-2 and LPHN1 usually occurs between the C-terminus of Ten-2 and NTF of LPHN specifically at the lectin-like domain and olfactomedin domain. This interaction results in stabilising intercellular adhesion and stimulates Ca²⁺ mobilisation and activation of cAMP pathway (Silva *et al.*, 2011; Li *et al.*, 2018). In addition to alternative splicing, Ten-2 can also produce C-terminally cleaved products, known as teneurin C-terminal associated proteins (TCAP), which has an effect on metabolism, reproduction and neuronal morphology (Al Chawaf *et al.*, 2007; Boucard *et al.*, 2014). Recent studies suggest that TCAP may interact directly with LPHN1 due to the sequence overlap between TCAP and lectin domain in LPHN1 (Husić *et al.*, 2019).

1.6.3. FLRT3

Fibronectin Leucine Rich Transmembrane gene (FLRT) was firstly discovered by Lacy and his group in 1999 when they were screening a human adult skeletal muscle library in order to identify a novel extracellular matrix protein (Lacy *et al.*, 1999). FLRT proteins (**Figure 4**) are a family of three proteins with a secondary structure comprised of 10 leucine rich repeats surrounded by C-terminal and N-terminal cysteine regions, a fibronectin-like domain, a transmembrane domain and a short intracellular tail (Haines *et al.*, 2006). Protein secondary structure and glycosylation of membrane proteins expressed at the cell surface, suggests that they may function as cell adhesion or signalling molecules. FLRT family in vertebrates are present in three isoforms (FLRT1-3). All of them are expressed in the brain, FLRT1 in the kidney,

FLRT2 in skeletal muscle, pancreas and heart, whereas FLRT3 in many tissues (Lacy *et al.*, 1999).

In an attempt to identify a ligand for LPHN3, O'Sullivan and his group used a recombinant protein, consisting of the extracellular domain of LPHN3 fused to the IgG Fc domain, to find probe rat synaptosomal extracts using affinity chromatography and mass spectrometry. FLRT3 was detected, along with Ten, as one of the proteins co-purifying with LPHN3 (O'Sullivan *et al.*, 2012). In the same study, O'Sullivan and his group found that FLRT3 binds LPHN3 with high-affinity binding generated by trans cross-linking of the receptor ligand-binding sites. This interaction has a role in the development of synaptic circuits. In addition, FLRTs have been reported to function in cell migration and axon guidance through their binding with Unc5 proteins (Yamagishi *et al.*, 2011).

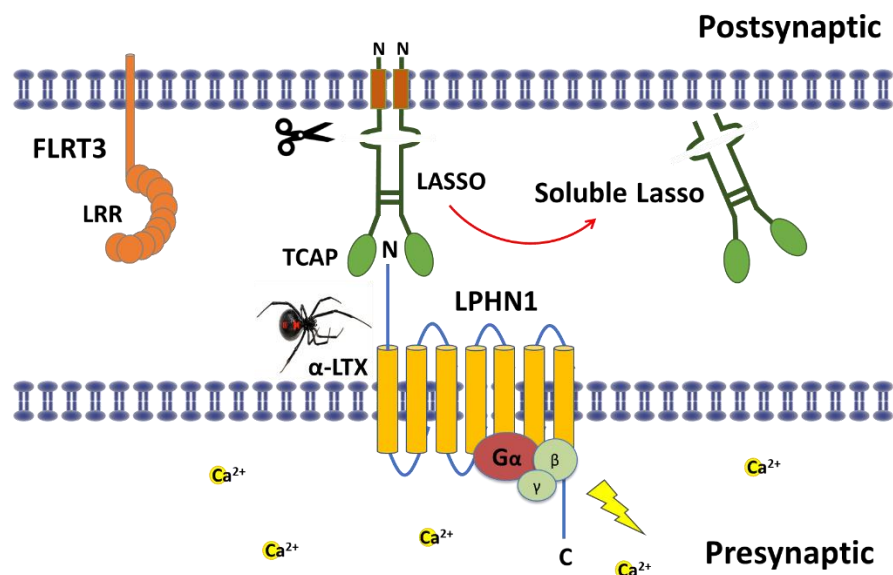


Figure 4: LPHN1 and its ligands.

Schematic of trans-synaptic ligand-receptor complex of Lasso and LPHN1, with its other LPHN1-binding ligands, fibronectin leucine-rich transmembrane protein3 (FLRT3) and α -LTX. Lasso is cleaved within the ectodomain and partially released into the medium.

1.6.4. Contactin 6

Contactins are part of immunoglobulin subfamily that is expressed mainly in the central nervous system. It consists of immunoglobulin-like and fibronectin repeats in the extracellular region and GPI anchor that help contactin to stay attached to the cell membrane and control the autonomous intracellular signalling. In vertebrates, the subgroup comprises of 6 members (contactin-1, -2, -3, -4, -5, -6), of which only contactin-6 (NB-3) was able to bind LPHN1 (Zuko *et al.*, 2016)

1.7. Ca²⁺ Signalling

1.7.1. Calcium as a Universal Signalling Molecule

Ca²⁺ is commonly mentioned as the universal signalling molecule. Indeed, it plays a crucial role in regulating a vast range of cellular functions, including neurotransmitter release, proliferation, cell cycle progression, apoptosis and gene transcription (Bootman, 2012)(Munaron *et al.*, 2004). Due to the vast involvement of Ca²⁺ in different biological processes, a range of proteins are devoted to its release, chelation, and sequestration, resulting in an extraordinarily precise biological system with different temporal and spatial dynamics (Berridge *et al.*, 2003). Usually, the cytoplasmic Ca²⁺ concentration at rest is tightly kept approximately at 100 nM. The fundamental biological question here is how cells control and maintain the concentration of cellular Ca²⁺?

Cells maintain a tight control over intracellular Ca²⁺ levels (**Figure 5**), by removing

excessive cytosolic Ca^{2+} out of the cells using different pumps, such as Plasma Membrane Ca^{2+} ATPase (PMCA) and the $\text{Na}^+/\text{Ca}^{2+}$ exchanger (NCX) (Brini and Carafoli, 2011). In addition, calcium-binding proteins such as calmodulin plays an important role in the regulation of intracellular calcium concentration by indirectly regulating gene transcription through phosphorylation and dephosphorylation of transcription factors (Saimi and Kung, 2002). Alternatively, sarco/endoplasmic reticulum Ca^{2+} ATPase (SERCA) and the mitochondrial Ca^{2+} uniporter (MCU) are used to sequester Ca^{2+} inside the intracellular stores (ER or mitochondria, respectively) (Pathak and Trebak, 2018). Subsequently, the cytoplasmic Ca^{2+} concentration is lower than the extracellular Ca^{2+} concentration, where it is usually about 1.8 to 2 mM. The extracellular calcium and calcium found in intracellular compartments serves as the main sources of free Ca^{2+} ions or its bound form (Bygravel and Benedetti, 1996). When a receptor is stimulated, Ca^{2+} signalling occurs (**Figure 5**). This may involve the influx of Ca^{2+} ions from the extracellular space, through the voltage-gated calcium channels (VGCC) and/or store-operated calcium channels (SOCC), which permit the influx of Ca^{2+} ions down its 20,000-fold concentration gradient. Receptor stimulation can also result in activation of a different biological mechanism, which will trigger the release of Ca^{2+} ions from intracellular stores through inositol 1,4,5-triphosphate receptors (IP_3R) or ryanodine receptors (RyR), resulting in a significant increase in Ca^{2+} concentration. Therefore, the overall cytoplasmic Ca^{2+} concentration can increase several folds above the resting levels due to signalling events.

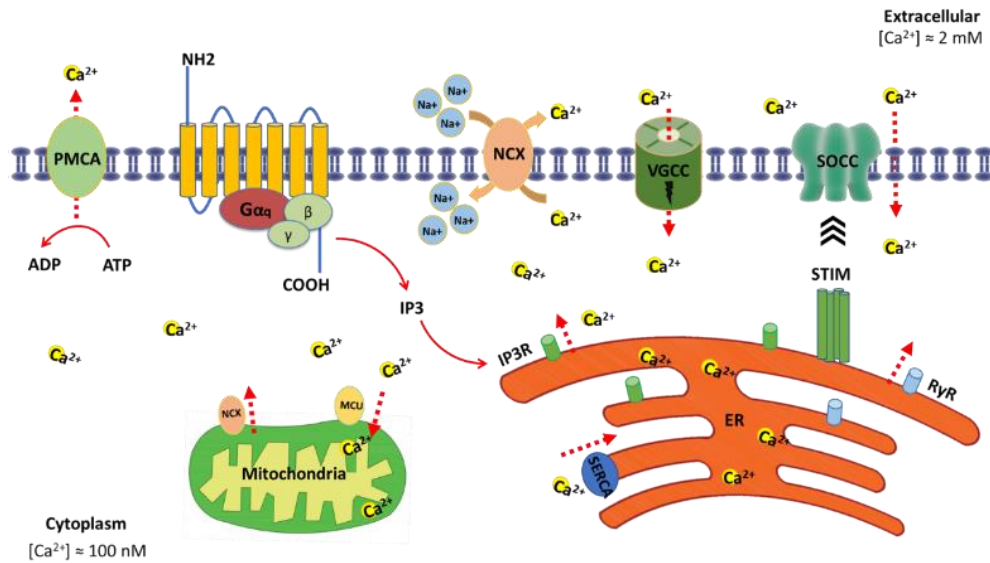


Figure 5: Intracellular calcium signalling pathways.

Ca^{2+} enters the cytosol through VGCC and SOCCs, GPCRs activate IP₃ production by PLC, resulting in the opening of IP₃R in the ER membrane and subsequent release of Ca^{2+} . Ca^{2+} activates calcium-induced calcium release (CICR) via RyRs. Depletion of ER Ca^{2+} leads to oligomerisation of stromal interaction molecules (STIM) and activation of SOCCs. The SERCA pump in the ER membrane and the mitochondrial uniporter in the mitochondria (MCU) take up Ca^{2+} from the cytosol. The PMCA and the NCX remove Ca^{2+} across the plasma membrane. Mitochondrial NCX slowly leaks Ca^{2+} from the mitochondria when the cell is at rest.

1.7.2. Intracellular Calcium Stores

As previously stated, stimulation of cell membrane receptor leads to activation of intracellular Ca^{2+} stores that lead to an increase in cytoplasmic Ca^{2+} concentration. A continuous increase in cytoplasmic Ca^{2+} concentration can lead to cytotoxicity; therefore, cells must have an intracellular compartment that controls the release of Ca^{2+} ion into cytosol. One of the major intracellular compartments that regulate such effect is the ER (**Figure 5**). The function of the ER as a Ca^{2+} store is to accumulate or release Ca^{2+} ions against its electrochemical gradient.

1.7.2.1. SERCA Pump

SERCA is an ATPase pump that transports two Ca^{2+} ions from the cytoplasm into the ER (**Figure 5**) (Periasamy and Kalyanasundaram, 2007; Periasamy *et al.*, 2017). This transportation uses ATP which will cause SERCA phosphorylation and eventually conformational changes that will allow Ca^{2+} to be pumped into the ER lumen, against the gradient of Ca^{2+} concentration, in exchange for protons. After each cycle, the enzyme is dephosphorylated to restart a new catalytic cycle (Toyoshima and Inesi, 2004; Toyoshima *et al.*, 2004; Periasamy *et al.*, 2008). In order to study better the activity of the SERCA pump, several scientists used a large variety of SERCA pump inhibitors. One of the most popular SERCA pump inhibitor used was thapsigargin (TG), a plant-derived sesquiterpene lactone (Lyttonsg *et al.*, 1991). By using SERCA pump inhibitors and other experimental methods, scientists concluded that the SERCA pump contributes to the regulation of the overall cytoplasmic Ca^{2+} concentration, but also other regulatory proteins must be also present.

1.7.2.2. ER Calcium Release Channels

ER possesses two main Ca^{2+} release channels (**Figure 5**) including Ryanodine Receptor (RyR) and IP_3R (Lanner *et al.*, 2010) (Mikoshiha, 2015). Both channels are tetramers that become activated by lower cytoplasmic Ca^{2+} concentration and inhibited by high cytoplasmic Ca^{2+} concentration (Meissner, 2004; Foskett *et al.*, 2007). There are three RyR isoforms, all are expressed in the brain (Abu-Omar *et al.*, 2018; Islam, 2011). While RyR is localised in the ER, its regulation can involve the cell membrane: where the plasma membrane and ER come close together, VGCCs in the plasma membrane can directly contact RyR1 in the ER. When the cell membrane is depolarised, this

induces the opening of VGCCs. This transmits a conformational change to RyR1 and results in its opening and a fast spark of Ca^{2+} release into the cytosol (1-2 ms time to peak). It has been shown that one subunit of RyR contacts one VGCC, which means that one RyR channel may connect with four VGCCs. However, not all RyRs are connected to all VGCCs and usually the free RyRs may be stimulated as a result of CICR (Fill and Copello, 2002). Similarly, IP_3R become activated by cytosolic Ca^{2+} ions or by IP_3 (Foskett *et al.*, 2007); even at low IP_3 concentration, IP_3R is still able to be activated, irrespective of the amount of IP_3 produced by receptor stimulation (Van der Wal *et al.*, 2001; Dickson *et al.*, 2013).

1.7.3. Modulation of Voltage Gated Ca²⁺ Channels

The electrical activity of neurons relies highly on the activity of various voltage gated ion channels that are permeable to different ions, including sodium, calcium, and potassium. While Na⁺ and K⁺ play an important role in the generation of action potentials in nervous and cardiac tissues, calcium ions are different, not only being able to alter membrane potential, but also can serve as a signalling entity (Clapham, 2007; Catterall, 2011). Under normal resting conditions, cytoplasmic Ca²⁺ concentration is maintained around 100 nM due to the intermittent release of Ca²⁺ from intracellular stores and the activity of calcium-buffering molecules and Ca²⁺ pumps (Albrecht *et al.*, 2002). Small or large changes in membrane voltage result in opening of VGCC, which results in Ca²⁺ influx across the plasma membrane, consequently the average cytosolic Ca²⁺ concentration rise to micromolar ranges (Wadel ., 2007). This will trigger a wide range of physiological mechanisms including neurite outgrowth, gene transduction, neurotransmitter release and activation of Ca²⁺ dependent enzymes such as calmodulin-dependent enzymes and protein kinase C (PKC) (Wheeler *et al.*, 1995)(Wheeler and Brownlee, 2008). However, continuous Ca²⁺ influx will lead to cytotoxicity (Stanika *et al.*, 2012); as a result the activity of VGCC should be regulated somehow in order to avoid cell toxicity. Several mechanisms are responsible for regulating the activation of these channels, including intrinsic gating processes and cell signalling pathways (Simms and Zamponi, 2012).

1.7.4. Store-Operated Ca²⁺ Entry

Reciprocally, calcium stores can regulate the influx of Ca²⁺ from the extracellular space (**Figure 5**). Store-operated Ca²⁺ entry (SOCE) is a universal calcium influx

mechanism in eukaryotic cells. In the last few years, many scientists were trying to reveal the mechanism behind the accumulation of Ca^{2+} in the ER stores or influx of Ca^{2+} into the cytoplasm, and the nature of these channels has been the subject of interest for many researchers. One of the first channels implicated as a component of SOCE were the transient receptor potential canonical (TRPC) channels, which consist of seven members (TRPC 1-7) (Minke and Cook, 2002; Venkatachalam and Montell, 2007). TRPC channels contain N-terminal ankyrin repeats, six transmembrane domains with a pore-forming loop between the fifth and sixth domains, and a highly conserved C-terminus domain (Minke and Cook, 2002; Venkatachalam and Montell, 2007). None of the TRPC family of Ca^{2+} permeable cation channels produced upon stimulation currents similar to calcium release activated current (I_{crac}) as they are non-cation selective and weakly permeable to Ca^{2+} (Venkatachalam and Montell, 2007). Therefore, several groups were trying to identify the components of TRPC channels and the regulatory proteins in SOCE.

Shortly after, they found that depletion of the ER stores leads to accumulation of stromal interaction molecule 1 (STIM1) proteins and activation of SOCCs in the plasma membrane, which in turn opens and allows Ca^{2+} influx to the cytosol. Stimulation of receptor such as LPHN activates indirectly IP_3Rs , which leads at the end to store depletion; this will trigger SOCE in the proximal plasma membrane, causing highly restricted Ca^{2+} entry for local signalling (Lopez *et al.*, 2020).

Store-operated or "capacitative" Ca^{2+} entry was firstly discovered by Putney in 1986 (Putney, 1986). SOCE refers to a mechanism that is induced when Ca^{2+} concentration drops in the ER stores as a result of Ca^{2+} release, and a signalling mechanism is

activated in order to replenish Ca^{2+} in the ER. This signalling causes the activation of certain plasma membrane channels and influx of Ca^{2+} into the cytosol (Putney, 2005). The role of SOCE was firstly thought to be limited to refiling Ca^{2+} intracellular stores after agonist stimulation. However, later Kwan and co-workers showed that stores refiling is not solely connected to SOCE, but also to the uptake of Ca^{2+} into the stores by the SERCA (Kwan *et al.*, 1990). This was demonstrated by using Lanthanum, a trivalent cation that can block capacitative Ca^{2+} influx through SOCCs. Since the discovery of SOCE, many studies were conducted to understand the physiological function of Ca^{2+} channels in the PM and the mechanism of their activation. In early studies regarding the mechanisms of such an activation, several hypotheses were made, including 1) conformational coupling between Ca^{2+} sensor in the ER and the PM; 2) an indirect coupling between the ER and the Ca^{2+} channels in the PM via diffusible messengers. In an attempt to understand the secret behind the connection of calcium channels in the plasma membrane and the elements in the ER/SR, STIM1 (**Figure 5**) was discovered as the ER Ca^{2+} sensor (Roos *et al.*, 2005). Additionally, it was found that STIM1 sends the information regarding the stores filling to SOCCs (Zhang *et al.*, 2005).

1.8. Research Gap

Cellular Ca^{2+} signalling is known to be tissue specific, which means that the cells in a specific tissue produce Ca^{2+} signalling differently from another cell in another tissue (Aust, *et al.*, 2016). Excitable cells, such as cardiomyocytes, require rapid Ca^{2+} mobilisation within milliseconds (Bers, 2002), whereas non-electrically excitable cells require slow Ca^{2+} mobilisation within 10 sec and sometimes even longer, especially if

this signal is used to control gene expression and metabolism (Dupont *et al.*, 2011). Usually the rapid Ca^{2+} mobilisation is due to the opening of VGCCs in the plasma membrane, which then stimulate RyRs to release Ca^{2+} from ER stores. On the other hand, slow Ca^{2+} mobilisation is usually triggered by IP_3 which binds to IP_3Rs leading to release of Ca^{2+} from stores (Galione, 2011).

To study these mechanisms researchers, need a standardised and highly specific system, consisting of a plasma membrane receptor which can be activated by a specific agonist and which is linked to a characteristic cellular response that can be easily detected. In fact, LPHN1 and its downstream mechanisms represent an almost ideal system for dissecting intracellular Ca^{2+} signalling that connects an extracellular stimulus to a strong cellular reaction. Indeed, (1) this aGPCR is linked to the stimulation of cytosolic Ca^{2+} signals; (2) an increase in cytosolic calcium can be easily detected; (3) LPHN1 is specifically activated by $\text{LTX}^{\text{N}4\text{C}}$ and endogenous ligands that have been recently discovered; (4) LPHN1 is known to be linked to exocytosis of neurotransmitters and hormones and it can therefore be used to study the mechanisms and physiological role of exocytosis in different cells. Therefore, we used LPHN1 expressed naturally or exogenously in cells of different type and measured changes in cytosolic Ca^{2+} and release of several physiologically important substances.

When NB2a cells expressing full-size LPHN1 are stimulated by $\alpha\text{-LTX}$ in Ca^{2+} free solution, a slow increase in the cytosolic Ca^{2+} concentration is observed while when extracellular Ca^{2+} is added to the cells, a rapid increase in cytosolic concentration is achieved.** The mechanism behind these observations is poorly understood. Therefore, one part of this work was to study the cytosolic Ca^{2+} mobilisation

mechanisms in NB2a cells expressing full size LPHN1 or mutant LPHN1, which is unable to send intracellular signals. This allowed us to compare LPHN1-mediated signalling with any off-target effects of the agonist. On the other hand, it has been shown that AML cells express LPHN1, while healthy leukocytes do not. Much is still unknown regarding the physiological role of LPHN1 in these cells, the ligand that stimulates LPHN1 in these cells and much more. Thus, AML cells in comparison with healthy leukocytes represent another complementary system for deciphering LPHN1-mediated signalling. Similarly, nothing is known about the role of other LPHN proteins in breast cancer, except that LPHN2 expression is increased in these cells, raising a possibility that LPHN2 may be linked to the characteristics of cancer cells. To summarise, we used several types of malignant cells to understand the functions of LPHN1, both when it is naturally expressed and when it is introduced artificially. In particular, NB2a cells were used primarily to investigate the Ca^{2+} mobilisation mechanism used by excitable malignant cells, while the knowledge of this mechanism was then applied to reveal the role of LPHN1 in AML cells (THP-1) and breast cancer cells (MCF-7).

1.9. Cytosolic Ca^{2+} Measurements

Detection of cytosolic calcium can be carried out using different means, but the most reliable and convenient approach is based on the use of fluorescent dyes. They can be loaded into cells through an electrode or expressed in the form of fluorescent proteins. However, small molecular weight dyes, such as fura-2, Fluo-3 and calcium green, can be loaded into cells by diffusion across the membrane in a membrane permeant form. These dyes change fluorescent intensity upon binding calcium ions

in a concentration-dependent manner. Advantages of these dyes include: response time of milliseconds, possibility of continuous measurements, high specificity towards the target ion, ability to load both adhesion and suspension cells. While small fluorescent dyes also have some disadvantages (such as the possibility of dye entry into organelles, relative difficulty of calibration, high cost, possibility of photo-toxicity and photo-bleaching), their advantages outweigh these drawbacks.

In this project, the measurement of intracellular Ca^{2+} levels was investigated using the Ca^{2+} indicator, called Fluo-4-AM, which is Fluo-4 modified by acetoxymethyl esterification (**Figure 6**). The acetoxymethyl groups do not only confer an amphiphilic character on the hydrophilic Fluo-4 dye and allow it to penetrate the plasma membrane, but they also permit Ca^{2+} detection only after the dye enters the cell. The reason behind this is the cleavage of the acetoxymethyl ester groups inside the cell by intracellular esterases, after which Fluo-4 becomes active and able to bind Ca^{2+} with its exposed carboxylic acid moieties (**Figure 6**). When Ca^{2+} binds to Fluo-4, this results in a strong increase in fluorescent signal.

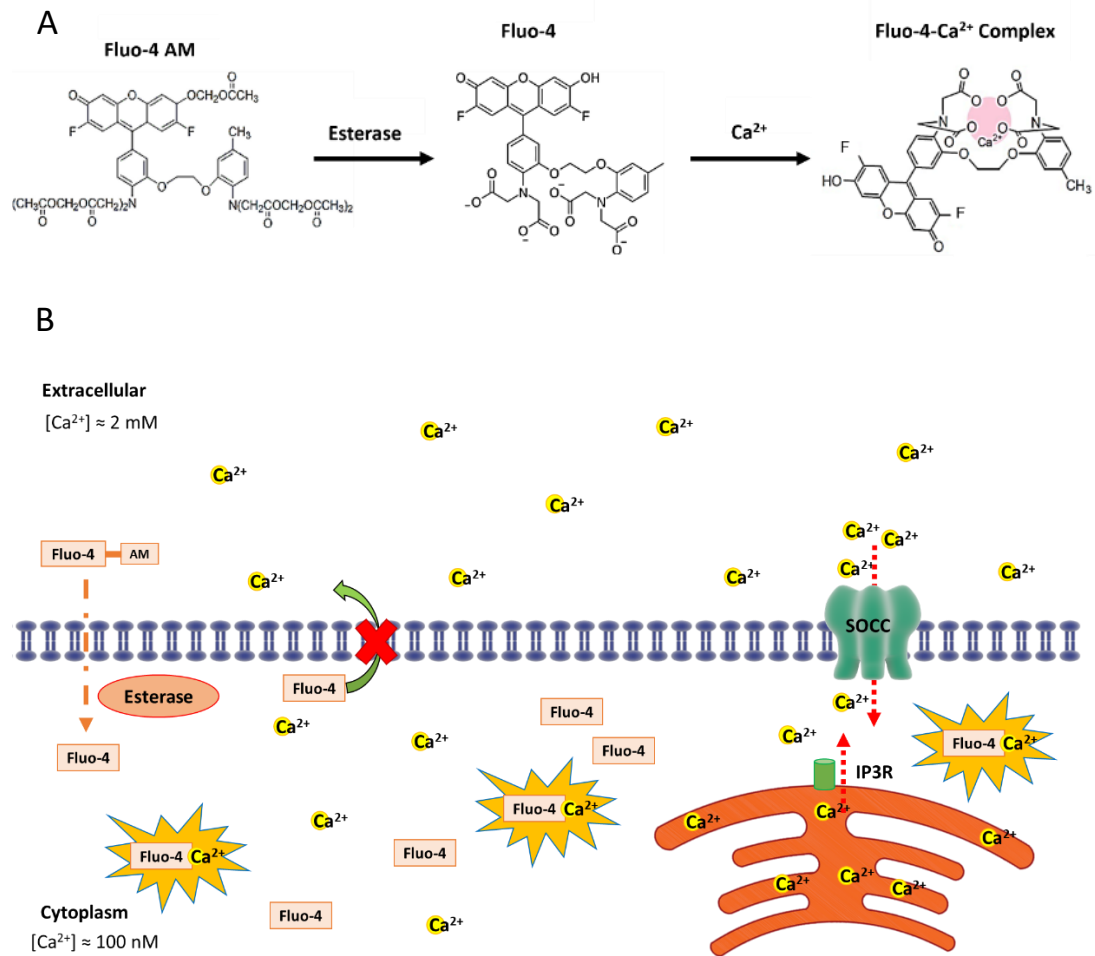


Figure 6: A scheme of Fluo-4 AM dye use and action.

A) Structure of Fluo-4 AM. Esterases break down the ester bonds in Fluo-4 AM, revealing carboxylic acid moieties that can bind Ca²⁺. B) Schematic representation of cytosolic Ca²⁺ measurement using Fluo-4 AM dye. Fluo-4 binds to cytosolic Ca²⁺ after it crosses the PM and is cleaved by esterases. Activation of a GPCR, like LPHN1, leads to intracellular Ca²⁺ changes. The emission of fluorescent Ca²⁺ sensitive dye, like Fluo-4, relatively increases when binding to Ca²⁺.

It has been reported that Fluo-4 has excellent properties reflecting the low and rapid changes in intracellular free Ca²⁺: it has a K_d of 345 nM and is excited by 488 nm light, i.e. operates within the visible light spectrum which is less harmful to cells. Single wavelength indicator was used in this study, as indicators characterized by single

peaks in the excitation and emission spectra have a higher temporal resolution of local Ca^{2+} signals compared to ratiometric indicators. Importantly, prior to my project, the kinetic properties of SOCE in THP-1 and MCF-7 cells were completely unknown and in the first instance required temporal optimisation of the experimental approach.

The resting level of intracellular Ca^{2+} changes was evaluated by normalising the change in fluorescence intensity, which was perfectly adequate for the purpose of this project. The aim of the thesis was to characterise LPHN1-mediated cytosolic Ca^{2+} change in NB2a cells, THP-1 and MCF-7 cells. The estimation of the cytosolic Ca^{2+} concentration is possible by monitoring the fluorescence intensity for single-wavelength dye, as fluorescence intensities at maximum (F_{max}) and minimum (F_{min}) that represent the states of the fluorophore when it is saturated with Ca^{2+} or is virtually free of Ca^{2+} , respectively. The K_d is the dissociation constant which approximately represents the fluorescence half-way between F_{min} and F_{max} and provides the highest sensitivity, an estimate K_d value is known (Maravall *et al.*, 2000). The following equation represents the relationship between intracellular Ca^{2+} concentration $[\text{Ca}^{2+}]_i$ and the intensity of fluorescence signal (F) for a non-ratiometric indicator (Eq. 1.1):

$$[\text{Ca}^{2+}]_i = K_d * (F - F_{\text{min}}) / (F_{\text{max}} - F) \quad (1.1)$$

This equation is derived from (Eq. 1.2), which shows the relationship between Ca^{2+} indicator fluorescence and $[\text{Ca}^{2+}]_i$, is given by the law of mass action, which states that the rate of any chemical reaction is proportional to the product of the masses of the reacting substances. Eq. 1.3 describes the sources of fluorescence in a Ca^{2+}

recording system. The detected fluorescence consists of the fluorescence of free fluorophores [F] and fluorophores bound to Ca²⁺ [FCa], and S_F and S_{FCa} are coefficients describing the brightness of indicator in bound and unbound forms. This can be rearranged as the fluorescence from all Ca²⁺-free fluorophores (S_F[F]_T) and the additional fluorescence from Ca²⁺- bound fluorophores (S_{FCa} - S_F) [FCa] (Maravall *et al.*, 2000).

$$[FCa^{2+}] = [F]_T [Ca^{2+}] / K_d + [Ca^{2+}] \quad (1.2)$$

$$(1.3)$$

$$F = S_F[F] + S_{FCa} [FCa^{2+}] = S_F[F]_T + (S_{FCa} - S_F) [FCa^{2+}]$$

S_{FCa}[F]_T is given by F_{max}, which can be measured by permeabilizing cells in the presence of 2 mM Ca²⁺, and S_F[F]_T is given by F_{min(abs)} which can be measured by chelating all Ca²⁺ following permeabilisation. The fluorescence of a Ca²⁺ indicator depends on the ratio of free indicator [F] to Ca²⁺-bound indicator [FCa]; thus, (Eq.1.1) follows.

1.10. Aims and Objectives

The aim of this project was to study LPHN1 signalling pathways in human malignant cells. The following objectives were addressed to achieve this aim:

- 1) To characterize murine neuroblastoma cells (NB2a) as a model cancer system, featuring neuron-like excitability, for investigating Ca^{2+} regulation using LPHN1 ligands and other pharmacological agents.
- 2) To study Ca^{2+} regulation in the acute myeloid leukaemia cell line (THP-1)
- 3) To isolate and test potential endogenous ligands of LPHN1 in leukemic cells
- 4) To study Ca^{2+} regulation in the breast cancer cell line (MCF-7)

2. Materials and Methods

2.1. Materials

All basic laboratory chemicals were purchased from Sigma-Aldrich (Sigma-Aldrich Company Ltd, Dorset, UK), unless otherwise stated. Dulbecco's modified Eagle's medium (DMEM), foetal bovine serum (FBS) were from Gibco. Mouse monoclonal antibodies against mTOR and β -actin, and rabbit polyclonal antibodies against phospho-S2448 mTOR, galectin-9, and an HRP-labelled rabbit anti-mouse secondary antibody were purchased from Abcam (Cambridge, UK). Human recombinant FLRT3, a mouse monoclonal antibody against LPHN1 and a rabbit antibody against FLRT3 were purchased from R&D systems and Santa Cruz Biotechnology (Dallas, Texas, USA) respectively. PAL1 and RL1 rabbit polyclonal antibodies against LPHN1 were described before (Volynski *et al.*, 2000; Davydov *et al.*, 2009). A rabbit antibody against native LPHN1 was obtained from Abcam (Cambridge, UK). Goat anti-mouse and goat anti-rabbit fluorescent dye-labelled antibodies were obtained from LI-COR (Lincoln, Nebraska USA). ELISA-based assay kit for the detection of galectin-9 was purchased from Bio-Techne (R&D Systems, Abingdon, UK). An anti-Tim-3 mouse monoclonal antibody, its single chain variant, human Ig-like V-type domain of Tim-3 (amino acid residues 22–124). All other chemicals purchased were of the highest grade of purity commercially available.

2.2. Cell Culture

2.2.1. Cell lines

NB2a mouse neuroblastoma cells were maintained in DMEM supplemented with GlutaMAX™, 10% (v/v) FBS, and 1% penicillin/streptomycin. Stable-transfected NB2a cell lines were also maintained in 300 µg/ml G418 sulphate. Cells were kept at 37°C in a humidified atmosphere of 5% CO₂ in air. Cells were passaged after 2 to 3 days when approximately 70-80% confluency was reached. 0.05 %Trypsin-EDTA was used to detach cells. Differentiation of NB2a cells was induced 24 h after plating by serum deprivation and/or addition of dibutyryl-cAMP (dbcAMP). The cells were washed once with phosphate buffered saline (PBS) and medium was replaced with Neurobasal-A medium supplemented with 2% B-27 and 0.5 mM GlutaMAX™ (serum free, SF) or in SF medium with/without 1.0 mM dbcAMP. Cells were differentiated for another 24-48 h and until 70-80% confluent. The generation of recombinant receptors was described in (Volynski *et al.*, 2000) and the generation of stably-transfected cell lines was described in (K. . Volynski *et al.*, 2004).

THP-1 human myeloid leukaemia monocytes, MCF-7 human epithelial breast cancer, and K562 human immortalised myelogenous leukaemia cells were cultured in RPMI 1640 medium with L-glutamine and sodium bicarbonate and supplemented with 10% FBS, 1% (v/v) penicillin/streptomycin sulphate. Differentiation was induced 24 h after plating cells, by serum deprivation. Cells were washed once with phosphate buffered saline (PBS) and medium was replaced with SF medium. Cell lines were accompanied by test certificates and were cultured according to manufacturer's protocols. The

cells were cultured for a maximum of 30-35 passages.

2.2.2. Primary human cells

Primary human AML mononuclear blasts (AML-PB001F, newly diagnosed/untreated) were bought from AllCells (Alameda, CA, USA) and handled in accordance with the manufacturer's instructions following ethical approval (REC reference: 16-SS-033). Other primary human AML cells were obtained from the sample bank of the University Medical Centre Hamburg-Eppendorf (Ethik-Kommission der Ärztekammer Hamburg, reference: PV3469). Cells were incubated in IMDM medium containing 15% BIT 9500 serum substitute, 100 μ M mercaptoethanol, 100 ng/ml stem cell factor (SCF), 50 ng/ml FLT3, 20 ng/ml G-CSF, 20 ng/ml IL-3, 1 μ M UM729 and 500 nM stemregenin 1 (SR1). Primary human healthy leukocytes and primary human NK cells were purified from buffy coats obtained from the National Health Blood and Transfusion Service (NHSBT, UK) following ethical approval (REC reference: 16-SS-033).

2.2.3. Primary human blood plasma samples

Blood plasma from healthy donors was provided by the National Health Blood and Transfusion Service (NHSBT, UK) following ethical approval (REC reference: 16-SS-033). Primary human AML plasma samples were obtained from the sample bank of University Medical Centre Hamburg-Eppendorf (Ethik-Kommission der Ärztekammer Hamburg, reference: PV3469). Primary cells were cultured for 2-3 passages maximum, before being used for the experiments.

2.2.4. Human breast tissue samples

Primary human tumour tissue samples paired together with peripheral tissues (from the same patient) were collected surgically from breast cancer patients treated at the Colchester General Hospital, following written consent taken before surgery. Paired normal (healthy) peripheral tissues were removed during macroscopic examination of a tumour by pathologists. Blood samples were collected before breast surgery from patients with primary breast cancer and before treatment from patients with metastatic breast cancer. Samples were also collected from healthy donors (individuals with no diagnosed pathology), which were used as control samples. Blood separation was performed using a buoyant density method employing Histopaque 1119-1 (Sigma, St. Louis, MO) according to the manufacturer's protocol. Ethical approval documentation for these studies was obtained from the NRES Essex Research Ethics Committee and the Research & Innovation Department of the Colchester Hospitals University, NHS Foundation Trust [MH 363 (AM03) and 09/H0301/37]

2.2.5. Bone marrow extracts

Bone marrow was extracted from femur bones of six-week-old, C57/BL16 mice, kindly provided by Dr. Gurprit Lall, School of Pharmacy, University of Kent. The average weight of the mice was 25 ± 2.5 g and they were used, following the approval by the Institutional Animal Welfare and Ethics Review Body. Animals were handled by authorized personnel in accordance with the Declaration of Helsinki protocols. Bone marrow was isolated from femur bone heads as described before (Sakhnevych, 2019) Cells were maintained in RPMI 1640 medium supplemented with 10% FBS,

penicillin (50 IU/ml) and streptomycin sulphate (50 µg/ml). Homogenised extracts were produced from extracted bone marrow with final protein concentration 1 mg/ml.

2.3. Cell and Tissue lysis

2.3.1. Cells

Cell pellets obtained after the centrifugation were washed first with ice-cold PBS, then resuspended in ice-cold lysis buffer (PBS, 1% Triton X-100, 2 mM Ethylenediaminetetraacetic acid (EDTA), 1% mix of protease phosphatase inhibitors, pH 7.4) and kept at 4 °C for 60-90 min with constant agitation. Samples were then centrifuged at 10,000 *g*, and the supernatants containing protein extracts were used immediately after the isolation or stored at -20°C until future use.

2.3.2. Tissues

Frozen tissue (100 mg) was initially ground into a powder and then, homogenised in 100 µL ice-cold lysis buffer (20mM Tris/HEPES pH 8.0, 2 mM EDTA, 0.5 M NaCl, 0.5% sodium deoxycholate, 0.5% Triton X-100, 0.25 M sucrose, supplemented with 50 mM 2-mercaptoethanol, 50 µM of protease inhibitor (PMSF), 1 µM pepstatin just before use). Tissues were homogenised using Polytron Homogenizer (Capitol Scientific, USA), tissue homogenates were then filtered through medical gauzes and centrifuged at +4 °C at 10,000 *g* for 15 min. After the centrifugation, proteins present in the supernatants were precipitated by adding equal volumes of ice-cold acetone and incubating on ice for 30 min. Protein pellets were obtained by centrifugation (4 °C, 10,000 *g*, 15 min) followed by air drying at room temperature and then dissolved in

the SDS-lysis buffer described in (D'Arcy *et al.*, 2008).

2.4. Determination of protein concentration

The protein concentration of the samples was measured in triplicates using the Bradford assay. Briefly, 5 μ l of cell lysate were mixed with 150 μ l of Bradford reagent (0.01% (w/v) Coomassie Brilliant Blue G-250, 4.7% (w/v) ethanol and 8.5% (w/v) phosphoric acid) in a microwell plate. After 5 min incubation, the optical density at 620 nm was determined in a plate reader.

2.5. Latrotoxin

Production of recombinant latrotoxins, α -LTX and LTX^{N4C}, used in this study was previously described in (Ashton *et al.*, 2001; Volynski *et al.*, 2003), respectively.

2.6. Latrotoxin binding assay

2.6.1. Sample preparation

Cells expressing full-size LPHN1 or mutant LPH-71 were seeded in T-150 flasks for 24 h, as described previously in Section 2.2.1. Then, cells were differentiated in a SF medium for another 24 h, medium was then removed, followed by addition of PBS, pH 7.4, supplemented with 1 mg/mL bovine serum albumin (BSA) and 2 mM EDTA, then incubated for 5 min at 37 °C. Cells were detached by tapping the flask, centrifuged at 10,000 *g* for 5 min and resuspended at 25×10^6 cells per mL. Cells were treated with 5 nM α -LTX for 30 min with constant gentle rotation, at 4°C, then centrifuged at 10,000 *g* for 2 min. The supernatant, which contained free α -LTX, was

transferred to a fresh tube. The cell pellet was washed twice with ice-cold PBS, centrifuged for 30 s and then lysed in ice-cold PBS containing 1% Triton X-100, 1% protease inhibitor mix and 2 mM EDTA for 2 h, with constant gentle rotation, at 4°C. Sample buffer (6x) was added to lysed samples, vortexed and heated at 50 °C for 30 min.

2.6.2. Chloroform-methanol protein precipitation

The supernatant which contained unbound α -LTX was transferred to a 50 ml centrifuge tube. One volume of methanol, followed by one volume of chloroform was added to one volume of the protein sample, the mixture was vigorously vortexed for 2 min (**Figure 7**). The mixture was centrifuged at $10,000 \times g$ for 5-10 min. The methanol layer was removed from the top of the sample, followed by removing the chloroform layer without disturbing the pellet. Protein pellet was then washed with acetone (ratio 1:5), which was added to remove any traces of chloroform. Acetone was removed and the pellet was air dried. The pellet was then dissolved in sample buffer (1x). Samples were boiled for 5 min at 95°C.

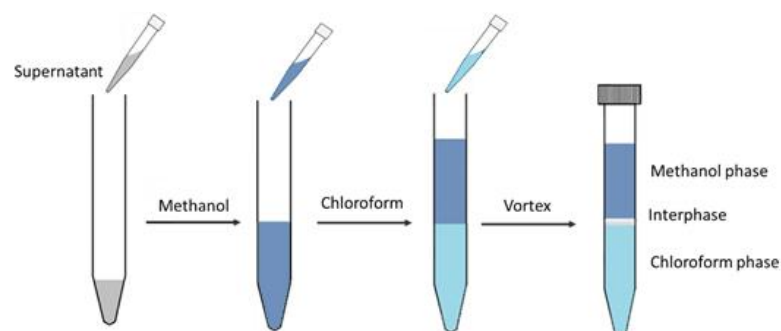


Figure 7: Protein precipitation using the chloroform/methanol method.

A sample was mixed with an equal volume of methanol, 2 volumes of chloroform, vortexed and centrifuged, as described in the text. Denatured proteins concentrated at the interphase.

2.7. Western blotting

2.7.1. SDS-polyacrylamide gel electrophoresis

Tissue, cell lysates and supernatants were first mixed with 2X, 4X or 6X sample buffer (final 1X concentrations were: 125 mM Tris-HCL, 2% sodium dodecyl sulphate (SDS), 10% glycerol, 1 mM dithiothreitol (DTT), 0.02% bromophenol blue, pH 6.8) and boiled for 5 min, at 95 °C, or heated for 20 min at 50 °C, then stored at -20 °C or used directly. The proteins were then separated based on their molecular mass by SDS-polyacrylamide gel electrophoresis (SDS-PAGE). National Diagnostics reagents were used to prepare gels, following the manufacturer's protocol. Resolving gel was prepared using ProtoGel 40% (w/v) acrylamide/methylene bis-acrylamide solution (37.5:1 ratio), 4X ProtoGel Resolving Buffer (1.5 M Tris-HCl, 0.4% SDS, pH 8.8). Stacking gel was prepared using ProtoGel 40%, ProtoGel Stacking Buffer (0.5 M Tris-HCl, 0.4% SDS, pH 6.8). 0.001% (v/v) TEMED and 0.001% (w/v) ammonium persulfate were added to initiate polymerisation. Gels were placed into an electrophoresis tank (Bio-Rad) and the inner and outer chambers were filled with running buffer consisting of 0.25 M Tris-base, 1.92 M glycine, and 1% (w/v) SDS. Wells were flushed with running buffer, before loading samples. Protein samples (20-50 µL) and molecular weight markers (5 µL, PageRuler, Fermentas) were loaded into wells. Polyacrylamide gel percentage was determined according to the molecular mass of the target protein, as shown in **Table 1**. Samples were separated initially at a voltage of 80 V, for 10 mins, then at 160 V, for 1.10 h.

Table 1. Acrylamide percentage in SDS-gels used for separating indicated protein ranges.

Mass Range (kDa)	≥250	80-200	50-80	25-50	<25
Gel percentage (%)	5	8	10	12	15

2.7.2. Transfer

After electrophoresis, the separated proteins were transferred onto polyvinylidene fluoride (PVDF) membranes (0.45 µm pore) in a wet electrophoretic transfer system (Invitrogen). PVDF membranes were activated by submerging in methanol prior to use. The transfer tank was filled with transfer buffer consisting of 0.025 M Tris, 0.192 M Glycine, 20% (v/v) methanol, pH 8.5, and the transfer carried out at a constant current of 120 mA for 1.5 h. The buffer was chilled to 5 °C using a circulating thermostat (Grant) and constantly mixed with magnetic stirrer. Alternatively, separated proteins were transferred from gels onto nitrocellulose membrane in a semi-dry system (BioRad). Filter pads, filter paper and nitrocellulose membrane were soaked in transfer buffer and assembled with the obtained gel as a blotting sandwich, as shown in **Figure 8**.

2.8. Immunodetection

Membranes were blocked immediately after transfer in a blocking buffer, consisting of 5% BSA dissolved in 20 mM Tris-HCL, 500 mM NaCl, 0.05% Tween-20, for 1 h at room temperature, with gentle agitation. Membranes were placed in 50 mL centrifuge tubes and exposed to primary antibodies diluted in 5 mL of blocking buffer (**Table 2**), with constant rotation for at least 1h.

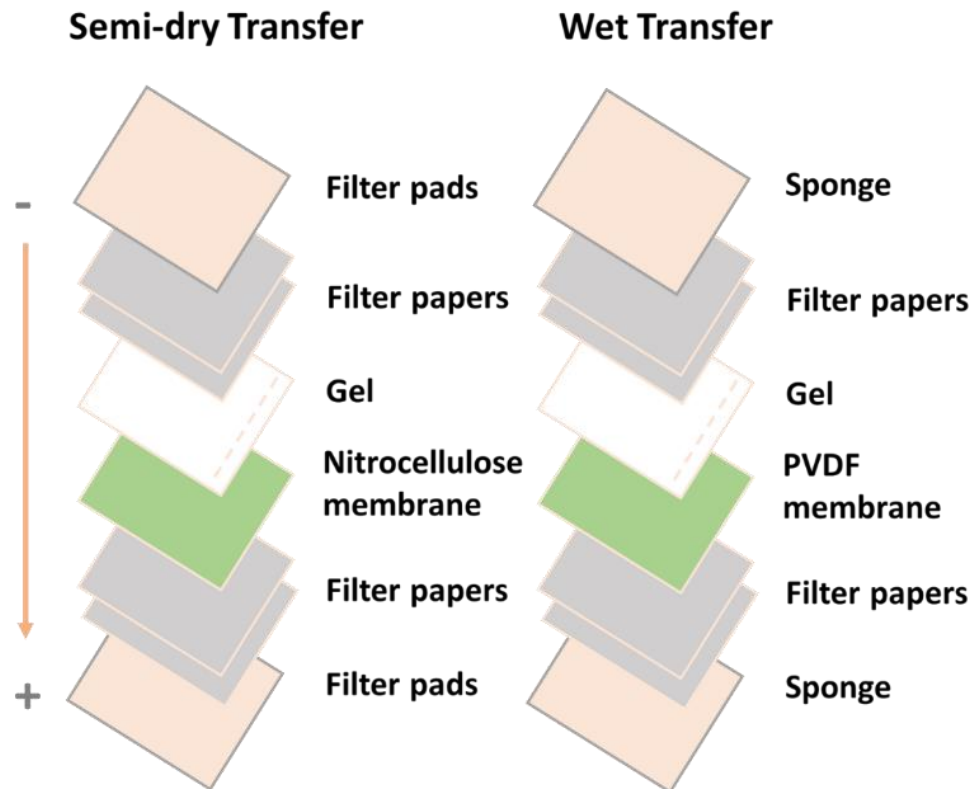


Figure 8: A scheme of the Western blotting method.

Diagrams represent the setup of a blotting sandwich for semi-dry or wet transfer. Membranes were placed nearest to the anode while the gel was oriented towards the cathode. The SDS-bound proteins (negative charge) migrate out of the gel towards the positive electrode and bind to the membrane.

Following the incubation with primary antibodies, membranes were washed in TBST 3 times for 10-20 min each, under constant rotation. After this, membranes were incubated with secondary antibodies for another 1 h in the dark and then washed in the same manner. Fluorescent images of labelled membranes were visualised using an Odyssey imaging system (LI-COR) and were quantitatively analysed in ImageJ or Odyssey software and values were subsequently normalized against those of β -actin or total protein loaded. Western blot analysis was employed to detect the LPHN1-2,

α -LTX, FLRT3, Tim-3, galectin-9, G α q in cell or tissue lysates.

Table 2. Antibodies used in this project.

Target	Species	Dilution	Supplier	Additional info
V5 polyclonal	Rabbit	1:2000	Sigma Aldrich	ab3792
LTX serum	Rabbit	1:1000	Produced in the lab	(Y.Ushkaryov Lab)
FLRT3	Human/Mouse	1:1000	R&D system/Santa Cruz Biotechnology	2795-FL-050/sc-514482
Tim3	Mouse	1:000	Produced in the lab	(Prokhorov <i>et al.</i> , 2015)
Gal-9	Rabbit	1:000	Abcam	ab227046
LPHN1 (PAL1)	Rabbit	1:500	Produced in the lab	(Davydov <i>et al.</i> , 2009)
LPHN1 (RL1)	Rabbit	1:500	Produced in the lab	(Davletov <i>et al.</i> , 1998)
LPHN1	Rabbit/Mouse	1:1000	Abcam/Santa Cruz Biotechnology	ab140825/sc-514562
LPHN2 (PAL2)	Rabbit	1:500	Produced in the lab	(Davydov <i>et al.</i> , 2009)
LPHN2	Rabbit	1:1000	Abcam	ab139498

2.9. Cytosolic Ca²⁺ measurement

Cells were seeded onto a 96 well plate, clear-bottom, with black walls (Corning®), at a density of 4,000-5,000 cells per well and cultured in DMEM with GlutaMax™ and 10% (v/v) FBS, and 1% (v/v) Penicillin-Streptomycin. After 24 h, the medium was removed and replaced with SF medium to differentiate cells for another 24 h until reaching 70-80% confluency (Section 2.2.1). For non-adherent cells, the plate was coated first with Poly-D-lysine (PDL) (Sigma-Aldrich) to enable cell adherence, then cells were seeded directly in SF medium (RPMI) at a density of 8,000-9,000 cells per well for 24 h. After differentiation, cells were loaded with the cell-permeant Ca²⁺ indicator Fluo-4 AM diluted in SF medium. 50 μ g Fluo-4 AM was initially dissolved in

10 μ l DMSO, containing Pluronic F-127 (10%), then diluted in SF medium to reach a final dye concentration of 2 μ M, and less than 0.01% for Pluronic F-127TM. Cells were incubated with 2 μ M Fluo-4 AM, for 30 min, at room temperature, in the dark. Cells were then washed twice with recording buffer consisting of (in mM) NaCl 145, KCl 5.6, glucose 5.6, MgCl₂ 1, HEPES 15, BSA 0.5 mg/ml, sulfinpyrazone 0.25, pH 7.4. Cells were washed twice and incubated for a further 20 min to allow for de-esterification of AM esters. Fluoroskan Ascent FL microplate fluorometer (Labsystems) was used to measure the fluorescence intensities with 485/538 nm excitation/emission filters with 3 mm diameter of excitation beam. Fluorescence intensity was measured every 15 s, with 100 ms integration time for each well. After de-esterification of AM ester, the plate was transferred into the fluorometer to measure the baseline fluorescence for 3-5 min in Ca²⁺-free recording buffer (stage 1). Cells were then treated with different pharmacological compounds and toxins added rapidly to individual wells by pipette (stage 2). As a negative control, cells were treated with recording buffer only in addition to using WT cells when available. Cells were then exposed to 2 mM Ca²⁺ diluted in recording buffer, which was added automatically using an internal mechanical dispenser (stage 3), and Ca²⁺ influx was recorded for 15 min.

Maximum fluorescence was determined after the addition of 0.1% Triton X-100 to permeabilize the cells (stage 4). Initial volume in each well was 25-75 μ L and compounds were added in 25-50 μ L. Total volume at end of experiment ranged from 110 to 139 μ L. Experiments were done in replicates (3 wells per plate) and repeated independently at least three times. Fluorescence measurements were normalized to the average baseline value (F_{\min}) and the average maximal value achieved with Triton X-100 (F_{\max}). Changes in cytosolic Ca²⁺ concentration was measured by calculating the

changes in normalised fluorescence ΔF_n (equation 2.1).

$$\Delta F_n = (F - F_{\min}) / (F_{\max} - F_{\min}) \quad (2.1)$$

Ca^{2+} release (the size of intracellular stores) was measured as a maximum ΔF_n amplitude above baseline achieved upon the addition of 3-10 μM thapsigargin (TG) or a different pharmacological compound. SOCE was measured as the maximum ΔF_n amplitude reached after the addition of 2 mM extracellular Ca^{2+} . Stimulation of LPHN1 with $\alpha\text{-LTX}$ triggered the activation of Ca^{2+} signalling pathway in which Ca^{2+} release, SOCE were quantified as in TG experiments. Ca^{2+} release was measured as a change in ΔF_n over the last 300 s of exposure to $\alpha\text{-LTX}$.

2.10. Synchrotron radiation circular dichroism spectroscopy

The interaction of LPHN1 and LPHN2 with FLRT3 were studied with synchrotron radiation circular dichroism (SRCD) spectroscopy at beamline B23, Diamond Light Source (Didcot, UK). This technique was used in order to study the binding between LPHN receptors and ligand (FLRT3) in free solutions. The extracellular fragment of LPHN1, LPH-51, and commercially available human recombinant FLRT3 were analysed, either alone or in combination with each other, with stoichiometry of 1:1 molar ratio and pure water was used as a negative control. SRCD measurements were carried out using 15 nM soluble LPH-51, in a 1 cm path length cell of 3 mm aperture diameter, using a Module B instrument with 1 nm increment, 1 s integration time and 1.2 nm bandwidth, at 23 °C. The cuvette capacity was 60 μl . Likewise, human recombinant LPHN2 (olfactomedin-like domain, MyBioSource, San Diego, Ca, USA)

was analysed alone or with FLRT3 by SRCD. In this case, SRCD measurements were performed using 0.7 μ M samples. The obtained results were analysed using CDApps (Hussain *et al.*, 2015) and OriginLAB™.

2.11. Enzyme-linked immunosorbent assay

Enzyme-linked immunosorbent assay (ELISA) was used for the detection and measurement of target proteins in the cell culture media, human plasma, and cell and tissue lysates.

2.11.1. Determination of released galectin-9 and soluble Tim-3

Solid phase sandwich ELISA (R&D Systems assay kits) was used to measure the levels of galectin-9 and soluble Tim-3 (sTim-3) in cell culture media or in human blood plasma, according to the manufacturer's protocol. Briefly, 96 well microplate coated with PDL was treated with 100 μ L of capture antibody for the targeted protein for overnight (16 h), at room temperature. Capture antibody was diluted in PBS buffer just before well loading, as recommended by manufacturer's protocol. Next day, the wells were blocked with blocking buffer consisting of PBS with 1% BSA for at least 1 h, at room temperature, under constant agitation. Wells were then incubated with either culture media or human blood plasma (100 μ L) for another 2 h, under the same conditions. The wells were washed with TBST buffer and incubated with 100 μ L of specific biotinylated detection antibody diluted in PBS with 1% BSA, for at least two hours. After incubation with biotinylated detection antibody, wells were washed again with TBST buffer and incubated with 100 μ L of streptavidin conjugated with horseradish peroxidase (HRP) diluted in PBS with 1% BSA for at least 30 min, at room temperature. After incubation with streptavidin-HRP, wells were washed with TBST and then incubated with 100 μ L of substrate solution consisting of 0.2% H_2O_2 , 56 mM o-phenylenediamine (OPD), for maximum 10 min, at room temperature, in the dark. To stop the reaction, 100 μ L of 1.8 M H_2SO_4 was added and after 2-5 min colour

change was observed. HRP catalyses the oxidation of OPD by H₂O₂ to 2,3-diaminophenazine (DAP), whose maximum absorbance wavelength is linked to the pH of solution. Addition of H₂SO₄ decreases pH, which leads to irreversible inactivation of HRP and the formation of protonated form of DAP, whose absorbance can be measured between 450-500 nm. Acquired absorbance values were directly proportional to the concentration of targeted protein (Fornera and Walde, 2010; Hinterberger *et al.*, 2018).

2.11.2. Determination of phospho-S2448 mTOR in cells

Phosphorylation of mTOR was analysed by ELISA as previously described in (Yasinska *et al.*, 2014). Briefly, Plates were coated with mouse anti-mTOR antibody, then blocked with blocking solution, as mentioned earlier. Then wells were incubated with samples (cell lysates) for at least 2 h, at room temperature. Plates were washed with TBST, then incubated with anti-phospho-S2448 mTOR antibody for another 2 h, at room temperature. Plates were washed again and incubated with HRP-labelled goat anti-rabbit IgG (Abcam) for at least 30 min, at room temperature. Next, secondary antibodies were detected by peroxidase reaction, as mentioned in section 2.11.1.

2.11.3. Detection of Tim-3-galectin-9 complex in cells and tissues

To detect Tim-3-Galectin-9 complex Elisa was used (Gonçalves Silva *et al.*, 2016). Mouse single-chain antibody was used as a capture antibody for Tim3. Wells were incubated with cell or tissue lysates for 2 h, at room temperature. Wells were washed with TBST and then incubated with biotinylated goat antibody against galectin-9 (detection antibody of R&D Systems ELISA kit) for another 2 h, at room temperature.

Plates were washed and incubated with HRP-Streptavidin for 30 min, at room temperature, followed by the previously mentioned step in section 2.11.1.

2.11.4. Detection of Tim-3-galectin-9 complex in culture medium

Firstly, mouse single-chain antibody was used as a capture antibody for Tim-3, plates were blocked with blocking buffer (PBS and 2% BSA). Culture medium (RPMI-1640) of THP-1 cells was added to the wells of the plate and incubated for 4 h, at room temperature. After incubation period, plates were washed with TBST and 0.2 M glycine-HCL (pH 2) was used to extract proteins. Extracted proteins were then neutralised and lysed with lysis buffer, followed by Western blot analysis, as described above. Both, anti-Tim3 and galectin-9 antibodies were used to visualise Tim-3-galectin-9 complex.

2.12. Determination of LPHN1 in human blood plasma

Mouse monoclonal LPHN1 antibody was used as a capture antibody for LPHN1 in human blood plasma, followed by addition of blocking buffer (2% BSA/TBST). Human blood plasma samples were then added to each well and incubated for 4 h, at room temperature. Plates were then washed thrice, and bound proteins were eluted from the wells with glycine-HCL buffer, at pH 2.0. Isolated proteins were lysed with lysis buffer (pH 7.5) and mixed with sample buffer (4×) heated for 5 min at 95 °C. Two different techniques were then used with three different LPHN1 antibodies in order to detect LPHN1 in human blood plasma. The first technique was western blot analysis which was performed using rabbit PAL1 anti-LPHN1 antibody or rabbit Abcam anti-LPHN1 antibody, as described in section 2.8. The second technique was

ELISA; in this case, mouse monoclonal LPHN1 antibody was used as a capture antibody and PAL1 as a detection antibody. The plate was incubated then with HRP-labelled anti-rabbit secondary antibody, followed by the steps mentioned in section 2.11.1.

2.13. Quantitative real-time PCR

Quantitative real-time PCR (qRT-PCR) was performed to measure mRNA levels corresponding to target proteins. Total RNA was isolated from the cells using a GenElute mammalian total RNA preparation kit (Sigma-Aldrich). mRNA was then converted into complementary DNA, using a reverse-transcription cDNA synthesis kit (Roche, Burgess Hill, UK), according to manufacturer's protocol, and amplified by qRT-PCR, as described below. For Galectin-9, the following primers were used: 5'-CTTTCATCACCACCATTCTG-3' and 5'-ATGTGGAACCTCTGAGCACTG-3'. for actin, the following pair of primers were employed: 5'-TGACGGGGTCACCCACACTGTGCCCATCTA-3' and 5'-CTAGAAGCATTGCGGTGCGATGGAGGG-3'. For LPHN1, the following primers were used: 5'-AGCCGCCCCGAGGCCGGAACCTA-3' and 5'-AGGTTGGCCCCGCTGGCATAGAGGGAGTC-3'. qRT-PCR was performed on a LightCycler® 480 (Roche), using SYBR Green I Master kit (Roche). PCR reactions started with incubation at 95 °C for 3 min 30s, followed by 45 cycles 10 s 95 °C, 20 s 60 °C and 10 s 72 °C, and a melting curve analysis to verify the amplified products. Amplification of the correct products was also confirmed by agarose gel electrophoresis. To show that the measured fluorescence was from amplification of cDNA template only, a no-template control (NTC) was included for LPHN1 and Gal-9 whereby cDNA was replaced with nuclease-

free water in the reaction master mix. Values representing LPHN1 and galectin-9 mRNA levels were normalised against the level of β -actin, as a housekeeping gene. Analysis was performed according to the manufacturer's protocol.

2.14. Determination of PKC- α activity

PKC- α activity in samples was quantified based on its ability to phosphorylate a specific substrate (Micol *et al.*, 1999). ELISA plates were initially coated with 0.2 mg/ml histone III_S. Samples were then mixed with reaction buffer consisting of 20 mM Tris-HCl, 200 μ M CaCl₂, 5 mM MgCl₂ and 20 μ M ATP (pH 7.5), at a ratio of 1:5, added to the wells and incubated for 30 min, at 37°C. After incubation, plates were washed with TBST, and phosphorylation of histone III_S was detected using spectrophotometry employing molybdenum blue reaction (Nagul *et al.*, 2015). Data obtained were then normalised against total amount of protein present in each sample.

2.15. Measurement of PLC activity

PLC activity was measured based on its ability to catalyse hydrolysis of PIP₂, with formation of DAG and IP₃. Initially, 30 μ L of cell or tissue lysates were mixed with 70 μ L of PIP₂ assay buffer containing 20 mM Tris-HCl, 0.1% sodium deoxycholate, 300 μ M CaCl₂, 100 μ M EDTA, 100 mM NaCl (pH 7.2) and incubated for 60 min, at 37°C. After incubation with assay buffer, 100 μ L of an organic extraction mixture (heptane/isopropanol at a ratio of 13:7) was added to 100 μ L of a sample. The resulted emulsions were then left to form a biphasic system. The organic phase was then extracted with lysis buffer, and combined with sample buffer, followed by SDS-

PAGE on 33%gels. PIP₂, DAG and IP₃ were visualised in the gels, using Toluidine Blue staining (Sigma-Aldrich) (Prokhorov *et al.*, 2015; Li *et al.*, 2017).

2.16. Immunocytochemistry

Immunocytochemistry without cell permeabilisation was performed to characterise cell-surface expression of Tim-3, galectin-9 and CD8. Briefly, cells were mixed with RPMI medium containing primary antibodies against one of the target proteins and incubated for at least 3 h under constant agitation, at 4°C. Cells were then washed with PBS or tissue culture medium, then re-suspended in the fresh medium containing fluorescently labelled goat secondary antibodies (Li-Cor) and incubated for another 2 h under constant agitation, in the dark. Cells were then washed, placed in the wells of a microtiter plate and scanned with an Odyssey imaging system (Li-Cor). Cells incubated with secondary antibodies only were used as a negative control. A similar approach was also used to study the interaction of the RL-1 antibody with the surface of THP-1 cells.

2.17. Confocal microscopy and imaging flow cytometry

THP-1 cells were cultured over 12 mm coverslips in 24-well plates. Cells were treated overnight with phorbol 12-myristate 13-acetate (PMA), to activate PKC, and then permeabilised with ice-cold methanol (MeOH) or MeOH/acetone for 20 min. Otherwise, cells were fixed using 2% paraformaldehyde solution for 10-20 min, at room temperature, followed by washing cells 3 times with PBS and addition of 0.1% Triton X-100 to permeabilise cells. After permeabilisation, coverslips were blocked with 10% goat serum in PBS, for 1 h, at room temperature. Primary antibodies against

Tim3 and galectin-9 were added (1 µg/ml for both) and incubated overnight, at 4°C. Goat-anti-mouse Alexa Fluor 488 and goat-anti-rabbit Alexa Fluor 555 were used as secondary antibodies and incubated for 45 min, at room temperature, in the dark. Coverslips were observed under Olympus laser scanning confocal microscope, as described (Fasler-Kan *et al.*, 2010; Prokhorov *et al.*, 2015). The images obtained were analysed by proprietary image acquisition software (Olympus). Imaging flow cytometry was done according to a previously described protocol (Fasler-Kan *et al.*, 2016). In brief, mouse anti-Tim-3 and rabbit anti-galectin-9 antibodies were incubated with permeabilised cells for about 1 h, at room temperature. Goat anti-mouse Alexa Fluor 647 and goat-anti-rabbit Alexa Fluor 488 were used as secondary antibodies. Obtained images were analysed using IDEAS analytical software on ImageStream X mark II (Amnis-EMD-Millipore, USA). This method described in more detail in (Gonçalves Silva *et al.*, 2017).

For Tim-3-galectin-9 co-localisation imaging in breast tissue slices, a Nikon A1si laser scanning confocal microscope was used, equipped with a Plan Fluor DIC 40x, 1.3-N.A., oil-immersion objective. NIS Elements software (version 3.21.03, Nikon, Tokyo, Japan) was utilized to analyse the data. Cell images were acquired in three channels for DAPI (excitation at 399 nm and 10% laser power, emission at 450 nm; nuclei labelling), Alexa Fluor 488 (excitation at 488 nm and 10% laser power, emission at 525 nm, green channel; galectin-9), Alexa Fluor 555 (excitation at 561 nm and 10% laser power, emission at 595nm, red channel; Tim-3), with a photomultiplier tube gain of 100 arbitrary units. This method is described in (Yasinska *et al.*, 2019).

2.18. Fluorescence-activated cell sorting (FACS)

Cell surface presence of Tim-3 and galectin-9 were determined using FACS. The cells were initially fixed with 2% paraformaldehyde solution, washed 3 times with PBS and permeabilised with 0.1% Triton-100. Cells were then incubated with mouse anti-Tim-3 and rabbit anti-galectin-9 antibodies overnight, at 4°C. Goat anti-mouse Alexa Fluor 647 and goat-anti-rabbit Alexa Fluor 488 were used as secondary antibodies. The distribution of target proteins was analysed using FACS Calibur cytometer and CellQuestPro software (Becton Dickinson, USA).

2.19. Isolation of soluble NTF of LPHN1

Cells stably expressing LPH-51 were cultured in SF DMEM medium for 48 h. 30 ml of this medium was then collected, centrifuged at 10,000 *g* for 5 min, and the supernatant was incubated overnight with 500 μ L of anti-V5 antibody Agarose (Sigma-Aldrich), with constant shaking, at 4 C. After incubation, medium was removed, the column was washed with 10 volumes of PBS, and then the absorbed protein was eluted with 5 volumes of 50 mM triethylamine (TEA) in 150 mM NaCl (pH \sim 12), on ice. Any residual protein was further eluted with 3 volumes of 0.1 M NaOH and neutralized with 150 mM NaCl, 1 M HEPES (pH 7.4). The fractions were then collected and combined. Protein analysis was done by western blotting, as described in section 2.7. The protein was then concentrated by ultrafiltration using Amicon[®] Ultra-15 centrifugal filter units (Merck).

2.20. Data analysis

Data were analysed using Excel (Microsoft). Data are generally presented as the mean \pm SEM of *n* determinations. Statistical analysis was performed in the Prism software (GraphPad). Unless otherwise stated, two-tailed Student's *t*-test was performed for comparisons between two groups of data. One-way analysis of variance (ANOVA) was used to compare three or more groups of data. Statistically significant difference was accepted at $p < 0.05$. The level of significance was also indicated on graphs using asterisks: $p < 0.05$: *, $p < 0.01$: **, $p < 0.001$: ***.

3. LPHN1 interaction with FLRT3

3.1. Introduction

Several proteins binding to LPHN1 have been discovered: teneurin, FLRT and contactin (see section 1.6). While the interaction between Ten2 and LPHN1 has been studied very well (Silva *et al.*, 2011; Boucard *et al.*, 2014) and the role of contactin is currently unclear, it was necessary to investigate the interaction between LPHN1 and FLRT3. Indeed, as will be shown below, FLRT3 is hypothesised to be the main functional agonist of LPHN1 ectopically expressed in AML cells. This was consistent with other publications which detected an interaction of LPHN1 with FLRT3 (O'Sullivan *et al.*, 2012; Boucard *et al.*, 2014). However, these data contradicted those from our lab: in particular, FLRT3 binding to LPHN1 was not detectable in LPHN1-affinity chromatography experiments which led to abundant isolation of Ten2 (Silva *et al.*, 2011). Because of this controversy, it was necessary to find under which conditions, if at all, LPHN1 could interact with FLRT3. Thus, the aim of this part of the project was to purify LPHN1 and use it in direct binding assays with FLRT3.

3.2. Purification of soluble NTF of LPHN1

A special construct for the expression and purification of a soluble NTF of LPHN1 was created in the lab, LPH-51 (K.Volynski *et al.*, 2004) (**Figure 9**). This construct contained the whole extracellular domain of LPHN1, including the GAIN domain and the autoproteolysis site, but only 15 amino acids downstream of it, because a stop codon was placed at this position into the cDNA encoding this construct. NB2A cells were stably transfected with LPH-51 and grown in SF medium, which cause the differentiation of NB2A cells and the correct (neuronal-type) glycosylation of the NTF

of LPHN1. LPH-51 was isolated from the conditioned medium by affinity chromatography on immobilised V5 antibody. Fractions collected after mild alkaline elution were tested for the presence of LPH-51 protein using Western blot analysis (**Figure 10**). The analysis showed that the first five elution fractions contained large amounts of LPH-51. The column was also eluted by strong alkali treatment to elute any remaining LPH-51. The results (**Figure 10**) show that both the column washes and alkaline eluates were free of any LPH-51. Fractions containing LPH-51 were combined and concentrated. During concentration by ultrafiltration, the LPH-51 sample was periodically diluted and concentrated again, to remove as much TEA and NaCl as possible, as these substances could interfere with CD spectroscopy.

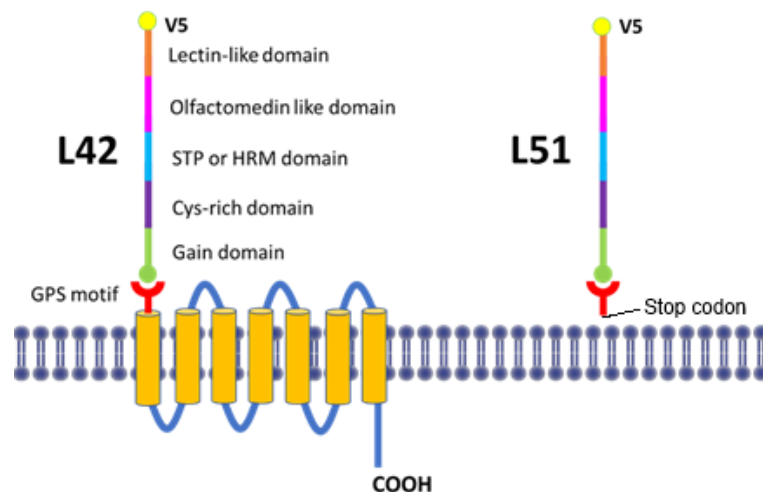


Figure 9: The structures of full-size LPHN1 (LPH-42) and its soluble ectodomain LPH-51.

LPH-51 was created in the lab: it consists of the NTF with an N-terminal V5 tag, the natural cleavage site in the GPS domain and contains a stop codon after the first 15 residues of the CTF.

To quantify the amount of LPH-51 present in the final sample, it was subjected to SDS-PAGE in parallel with different amounts of BSA, followed by Coomassie staining (**Figure 11**). It is important to understand that BSA and glycosylated proteins do not

bind the Coomassie dye equally: BSA is usually stained better, which means that the amount of LPH-51 could be underestimated. However, previous experiments on LPH-51 quantification in comparison with BSA, conducted in the laboratory and followed by sequence analysis, have allowed us to produce a correlation coefficient, where ImageJ was used to measure the integrated density of the serial BSA amounts (**Figure 11B**) and LPH-51. Computer aided densitometry of the gel, corrected for the difference in staining, indicated that the LPH-51 sample contained approximately 20 ng protein. Notably, LPH-51 was essentially undegraded (**Figure 11A**). Obtained LPH-51 was then used in a FLRT3 binding assay.

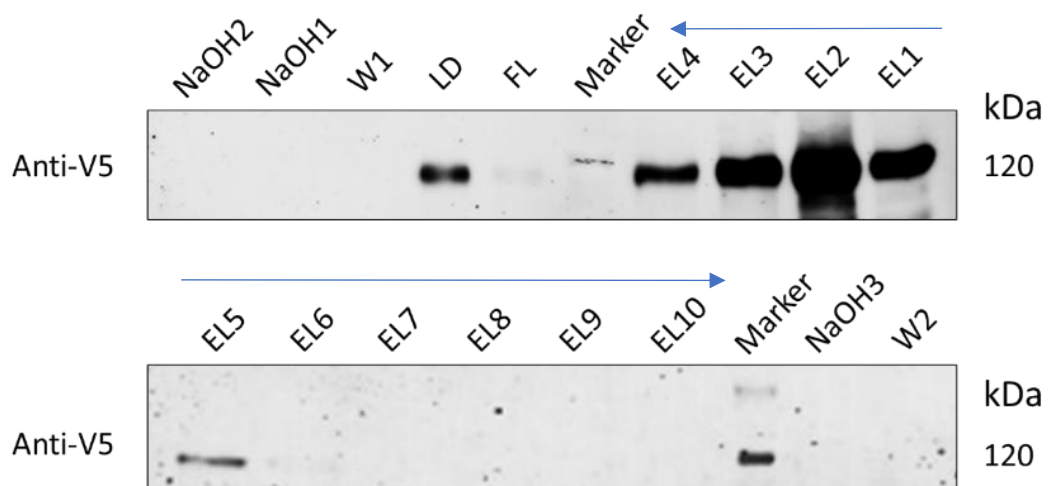


Figure 10: Isolation of LPH-51.

NB2A cells expressing LPH-51 were cultured in SF medium for 48 h at 37 °C. Medium was then collected and incubated with Anti-V5 antibody immobilised on Agarose, washed and eluted with 50 mM TEA and 150 mM NaCl (pH 10), followed by elution with 50 mM NaOH (pH 12) and then neutralised with 1 M HEPES, pH7.0. Eluates were analysed by Western blotting. EL: eluates, FL: flow through fractions, LD: loaded medium, W: wash fractions; arrows: the loading order of sequentially eluted samples.

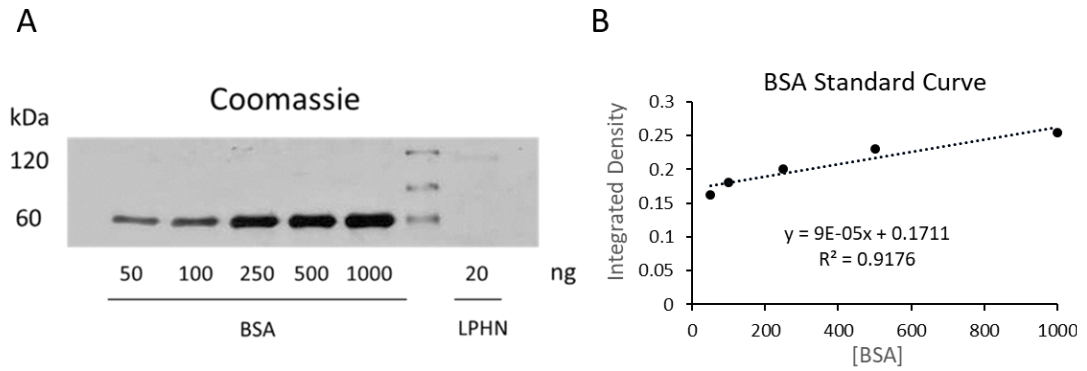


Figure 11: Quantification of purified LPH-51.

A) The affinity chromatography eluates 1-6 containing LPH-51 were combined and concentrated by ultrafiltration, followed by SDS-PAGE in 8% SDS gel and Coomassie Blue R250 staining. Indicated amounts of BSA were loaded on the gel as protein staining standards for LPH-51 quantification. B) BSA standard curve demonstrate a linear correlation of integrated density with BSA concentration (ng/ml).

3.3. FLRT3 causes a conformational change in LPHN1

A sample of commercially available soluble extracellular domain of FLRT3 and LPH-51 were mixed in a cuvette for circular dichroism (CD) spectroscopy and allowed binding was also assessed by synchrotron radiation circular dichroism (SRCD) spectroscopy. High-purity NTF of LPHN1 was isolated by V5-antibody affinity chromatography, as described above. A CD spectrum obtained after mixing LPHN1 and FLRT3 was significantly different from the simulated spectrum (see **Figure 12a**). This indicates that the two proteins interacted in solution, which led to a conformational change in both proteins. Interestingly, the calculated binding curve had a non-monotonous shape, suggesting that the binding was not uniform and that there were two types of binding interactions: with apparent dissociation constants, K_d , of 2 nM and 48.8 nM (see **Figure 12b**).

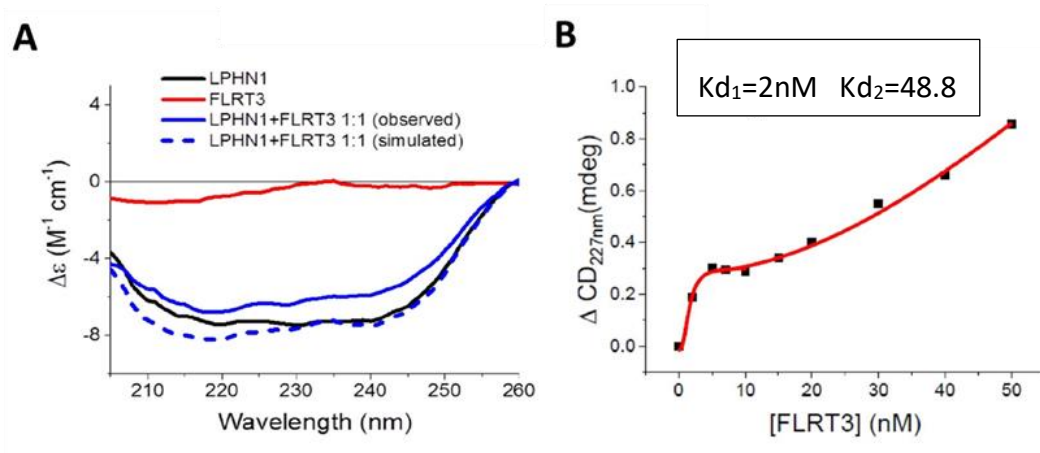


Figure 12: Interaction of FLRT3 with LPHN1 detected by CD spectroscopy.

A) SRCD spectroscopy of FLRT3, LPHN1 and FLRT3-LPHN1 interaction (both simulated and real curves are shown). B) LPHN1 CD spectrum changes as a function of FLRT3 concentration in the binding interaction between FLRT3 and LPHN1. There are two modes of interaction detectable, with two apparent K_d : 2 nM and 45 nM.

The hump in the beginning of the graph (see Figure 12B) does not represent the amount used in our experiment as 20 nM of LPH-52 was used. This indicate that FLRT3 must have reached saturation at 2 nM which cannot be true as 20 nM of LPH-52 was used for the binding experiment. Therefore, the last 5 data points were used to build a scatchardplot to predict the second K_d (see Figure 13).

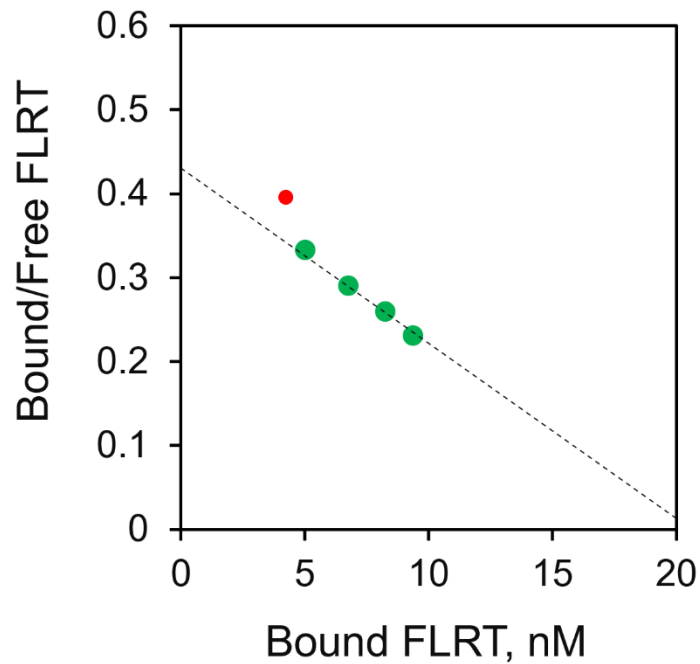


Figure 13: Scatchard plot displaying FLRT3 binding to LPH-52. $K_d = 48.8$.

3.4. Discussion

While controversial accounts of LPHN1-FLRT3 interaction have been published, reporting no interaction (Silva *et al.*, 2011), low affinity interaction (O’Sullivan *et al.*, 2012) or high affinity interaction (Boucard *et al.*, 2014), our experiments with purified soluble extracellular domains of the two proteins indicate that there must be an interaction. However, the binding is complex and includes at least 2 types, with different affinities (2 and 45 nM) (**Figure 12**). It is not currently clear what causes this complex interaction. It is unlikely to be due to heterogeneity of the samples, because they were synthesised in respective monospecific cell cultures and highly purified. We know, however, that Full-length LPHN1 can dimerise. This dimerisation could lead to heterogeneous interactions because monomers and dimers of LPHN1 could

interact with FLRT3 with different affinities (personal communication, Yuri Ushkaryov).

In addition, structural studies of LPHN3 (a distant homologue of LPHN1) and FLRT3 (Jackson *et al.*, 2015; Lu *et al.*, 2015) suggest that association of FLRT3 with LPHN can occur in two stages: the interaction includes a single pair of charged residues and multiple low affinity bonds (hydrogen and Van Der Waals). Obviously, if equilibrium was achieved in our binding experiments (higher affinity binding site), the kinetics of interaction would not have affected the final binding curve and apparent affinity. However, it is interesting to note that in all experiments where a high affinity of FLRT3 for LPHN1 was demonstrated (Boucard *et al.*, 2014), the interaction was allowed to continue overnight. This could suggest that the interaction of these two proteins involves a slow change in the conformation of one or both, allowing them to adjust (bend/twist) and thus increase the area of interaction. As a result, with a very long incubation time a very high affinity could be achieved. Because our solution binding experiments only involved a 30 min co-incubation of the two proteins, it is possible that the true equilibrium was not achieved, and therefore only the lower affinity interaction was observed (**Figure 12**).

Nevertheless, our experiments clearly demonstrated that in short period of time lower affinity interaction between FLRT3 and LPHN1 can be easily shown by using a high purity proteins and optimal solution conditions, where there are no constraints imposed by cell-surface attachment of one or both proteins.

4. LPHN1 and regulation of cytosolic Ca²⁺

4.1. Introduction

In this chapter, I addressed Objective 1 to dissect the intracellular mechanisms of Ca^{2+} regulation mediated by LPHN1. This task required development of an adequate cellular system. The choice of cells was dictated by the (1) requirement for easy propagation in culture; (2) possibility of transient or stable transfection with plasmid-based cDNA expression vectors; (3) lack of endogenous LPHN1 expression; and (4) ability to differentiate into neuron-like excitable cells. Mouse neuroblastoma cells, NB2A, possess all these features and therefore, this cell line was selected as the basal cell system for this part of the project.

The next task was to make it possible to distinguish the intracellular mechanisms specifically linked to LPHN1 downstream signalling from any other effects of LPHN1 ligands. Indeed, some of the LPHN1 ligands could bind to this receptor, but act on the cells without inducing LPHN1-mediated signals. One prominent example of such a ligand is α -LTX, which can both activate LPHN1 and also form Ca^{2+} -permeable membrane pores; obviously pore-dependent effects have to be determined and compensated for. Alternatively, LPHN1 ligands could also bind to other cell-surface receptors and cause LPHN1-independent effects. Examples of this type of ligands are α -LTX (which binds also to NRXNs and RPTP σ), Ten2 and FLRT (which have been shown to interact with other proteins). To solve this problem, I used NB2A cells stably expressing full-size LPHN1 (**Figure 14**) as the main experimental model, and included two important controls. One control was NB2A cells stably expressing a truncated LPHN1, LPH-71 (**Figure 14**). This recombinant protein contained the NTF of LPHN1 (and therefore was able to bind all LPHN1 ligands), but only had one TMR from NRX

(and therefore lacked any ability to interact with G-proteins and send intracellular signals characteristic of LPHN1 with 7TMRs). The second control used was wild-type NB2A cells, which possessed all other proteins present in the cells expressing the full-size LPHN1 or mutant LPHN1 (and therefore allowed me to identify any effects induced without binding to the NTF of LPHN1).

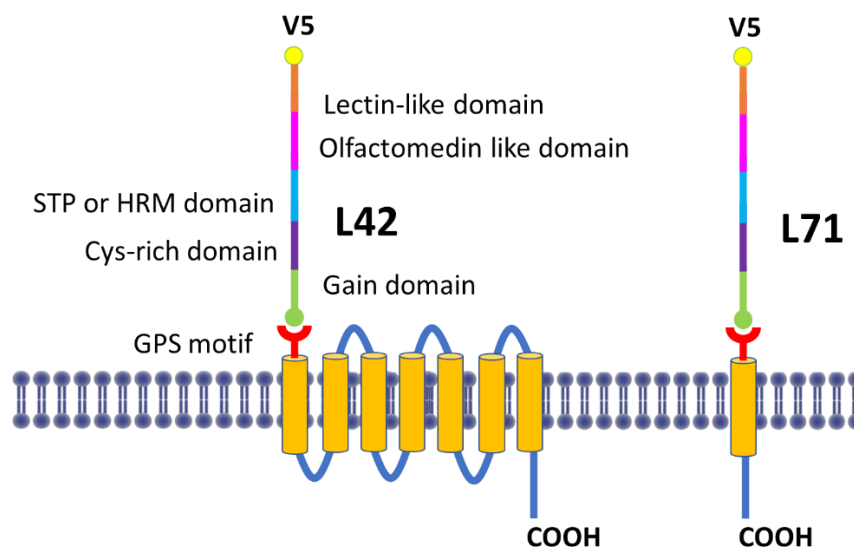


Figure 14: The structure of LPHN1 constructs: full-size LPH-42 and truncated LPH-71.

Two membrane anchored LPHN1 constructs were created in the lab: LPH-42 (L42) consist of the NTF, with an N-terminal V5 tag, and the complete CTF; LPH-71 (L71) contains the NTF and the first 18 amino acids of the CTF fused to the TMR from NRXN1 α . LPH-42 represents the full-size LPHN1 and is capable of all LPHN1 signalling, while LPH-71 contains a single TMR from another receptor and cannot signal as LPHN1. However, both constructs contain the complete NTF and therefore are able to interact with all ligands that bind the NTF of LPHN1.

Cytosolic Ca²⁺ concentration in NB2a cells was measured using the chemical dye Fluo-4 AM. A Fluoroskan Ascent fluorescent plate reader was used in order to obtain the readings as previously described in the Methods section. Cells were loaded with Fluo-4 AM before the recordings were performed. Cells were initially incubated in Ca²⁺

free buffer, followed by the administration of thapsigargin (TG), a SERCA pump inhibitor (Thastrup *et al.*, 1990). As a result of the irreversible SERCA blockade by TG, the stores rapidly lose accumulated Ca^{2+} , which leaks into the cytosol where it reacts with the Ca^{2+} sensor dye (**Figure 6, Figure 15**). However, subsequently, cytosolic Ca^{2+} concentration then decays slowly by mainly two mechanisms: the opening of PMCA, which removes cytosolic Ca^{2+} from the cell, and NCX exchanger, which exchanges three ions of sodium for one ion of Ca^{2+} . In addition to the plasma membrane presence of NCX exchanger it is also present on the surface of mitochondria which means that decrease of cytosolic Ca^{2+} concentrations is related to mitochondria as well (Berridge *et al.*, 2000). As these processes reduce the cytosolic Ca^{2+} concentration, they also lead to a corresponding decrease in Fluo-4 fluorescence. However, by measuring the peak level of Fluo-4- Ca^{2+} fluorescence, it is possible to determine the maximal size of the intracellular Ca^{2+} stores, a value that can be used as a reference point for measuring the intensity of intracellular Ca^{2+} signalling (**Figure 15**).

Cytosolic Ca^{2+} measurements, corresponding to calcium released from the stores, were performed in a Ca^{2+} free buffer. After the cytosolic Ca^{2+} concentration and dye fluorescence subsided to the basal level ($\sim 50 \text{ nM } \text{Ca}^{2+}$), the cells were exposed to 2 mM extracellular Ca^{2+} , which is the normal extracellular Ca^{2+} concentration outside the living cell. This usually leads to a rapid Ca^{2+} influx, driven by the re-establishment of a steep Ca^{2+} gradient and occurring through multiple mechanisms of Ca^{2+} entry. Such mechanisms include the reversal of the NCX and the opening of various Ca^{2+} -permeable channels. If the cells have not been treated with TG and retain their intact

Ca²⁺ stores, the initially fast influx of Ca²⁺ will quickly slow down in a logarithmic curve (**Figure 15**, black line). In resting cells, the increase in cytosolic Ca²⁺ concentration is related to constitutive Ca²⁺ influx, such as CICR mechanism that switches on when the increasing cytosolic Ca²⁺ activates IP₃Rs and RYRs on the ER membrane, resulting in Ca²⁺ release from stores (Berridge *et al.*, 2000). The plateau Ca²⁺ concentration is reached due to the gradual saturation of Ca²⁺ influx/extrusion mechanisms and leads to the establishment of a new equilibrium Ca²⁺ concentration (~100 nM). However, if the cells have undergone partial or complete loss of stored Ca²⁺ (for example due to TG treatment or receptor-mediated signalling), the SOCCs, specifically activated by the loss of Ca²⁺ from the stores, will be open prior to the addition of Ca²⁺ and will contribute to a much stronger Ca²⁺ influx. As the SOCCs are inactivated by cytosolic Ca²⁺, their contribution to Ca²⁺ influx is transient and appears as a sharp peak added on top of the cytosolic Ca²⁺ saturation curve (**Figure 15**, red line).

After the cells reached a new cytosolic steady state level, Triton X-100 was added to permeabilise the cells and achieve the maximum fluorescence intensity. This allows one to normalise fluorescence responses in different wells, compensating for the variability in cell numbers and dye loading (**Figure 15**). The size of intracellular Ca²⁺ stores in cells treated with TG or any other Ca²⁺ mobiliser was measured during the first phase of the experiment as the maximum difference in fluorescence amplitude, ΔF_n , compared to control cells. Similarly, SOCE was measured during the second (Ca²⁺ add-back) phase, as the maximum ΔF_n amplitude compared to the control cells. Cells were considered to reach a cytosolic Ca²⁺ equilibrium when SOCE exponentially decayed and reached a plateau phase. The average of ΔF_n was determined over at

least 60 s. Cytosolic Ca^{2+} equilibrium is an indirect reflection of constitutive Ca^{2+} influx (other than SOCE) which is balanced out by Ca^{2+} extrusion mechanisms. Different method can be used to measure the changes in cytosolic Ca^{2+} concentration, for example, by calculating the area under the ΔF_n curve over time. However, this approach is limited, as it can only be used when there is a peak in ΔF_n , for example, as in the case of TG-induced Ca^{2+} release peak or SOCE peak. Since most of the data shown here (except for TG does not show peaks), the ΔF_n amplitude was used.

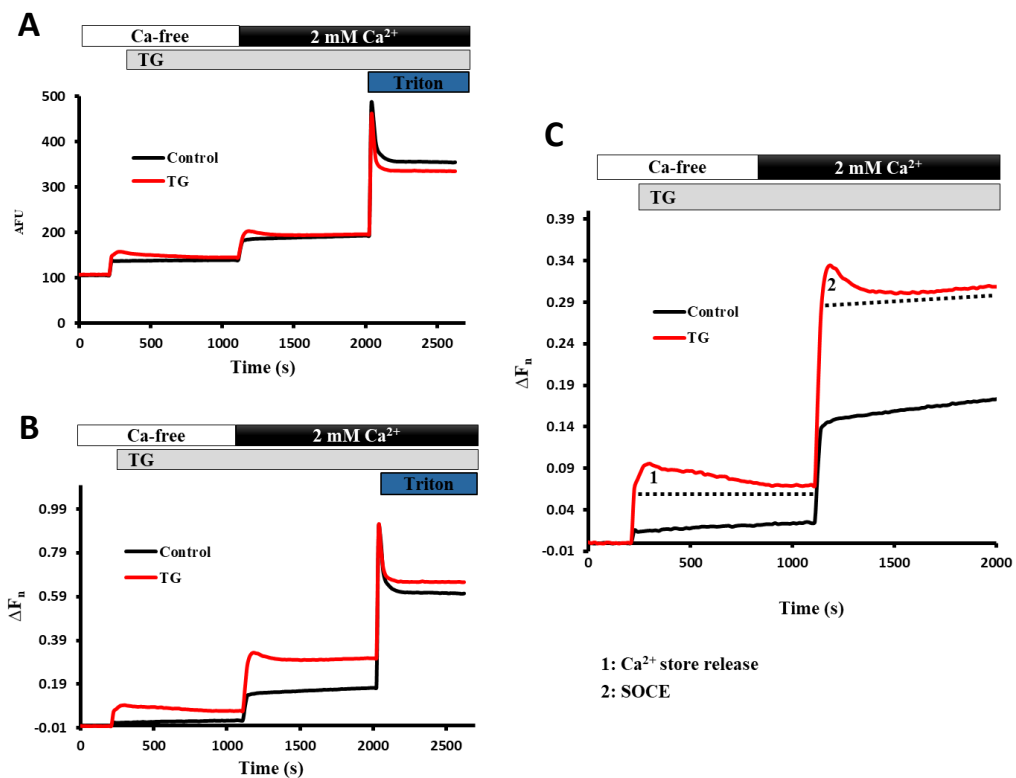


Figure 15: Measurement of cytosolic Ca^{2+} dynamics in live cells.

A) Example of averaged raw fluorescence traces with or without administration of $1 \mu\text{M}$ TG. NB2a cells were first incubated in Ca^{2+} free buffer. Measurement of baseline fluorescence was recorded for 210 s, then TG was added manually; this resulted in Ca^{2+} store release, which was recorded for 885 s. Next, buffer containing 2 mM Ca^{2+} was added automatically by Fluoroskan dispenser and Ca^{2+} influx was recorded for 885 s. Triton X-100 (0.1%) solution was added manually to permeabilise the cells and reach the maximum fluorescence intensity. B) Normalised fluorescence signal was

calculated using equation 1.1. C) Truncated normalised traces showing parts to be measured: Ca^{2+} store release, SOCE and cytosolic Ca^{2+} equilibrium.

In this section, the dynamic nature of cytosolic Ca^{2+} concentration will be described, based on the investigation of how different cellular conditions affect the changes in cytosolic Ca^{2+} concentration and what mechanisms may contribute to each part of cytosolic Ca^{2+} changes.

4.2. Ca^{2+} homeostasis in NB2A cells expressing full size and truncated LPHN1

The NB2A cells used in these experiments expressed either a full-size LPHN1, which contained 7 TMRs and thus represented a proper GPCR, or a truncated construct, which lacked the 7 TMRs and thus could not engage in G-protein-mediated signalling (**Figure 14**). The expression of a GPCR (LPHN1) that is known to be able to signal to intracellular Ca^{2+} could affect the viability of cells or at least the characteristics of their Ca^{2+} homeostasis. Indeed, GPCRs are known to show two different conformations, On and Off, and they spontaneously change between the two in the absence of ligands (Ango *et al.*, 2001). Agonist-independent GPCRs activation may lead to a conformational change and thus activation of downstream signalling. Such effect has been observed previously in glutamate GPCRs (Prézeau *et al.*, 1996), cannabinoid receptor (Nie and Lewis, 2001), and human CT receptor (Cohen *et al.*, 1997) mostly because of the C-terminal truncation and overexpression of these receptors. With overexpression of the full-size LPHN1 (LPH-42), Ca^{2+} signalling in NB2A cells may be constantly activated, leading to cell toxicity and death or to the

activation of some compensatory mechanisms. Therefore, I compared the features of Ca^{2+} stores and SOCE in cells expressing full-size LPHN1 (LPH-42) and cells expressing truncated LPHN1 (LPH-71).

This experiment was carried out using a standard approach, based on SERCA inhibition by TG and cytosolic Ca^{2+} detection using Fluo-4 (Figure 16). Both cell clones reacted to TG during the Ca^{2+} -free incubation phase by releasing Ca^{2+} from intracellular stores. On re-addition of 2 mM Ca^{2+} , both cell types demonstrated strong SOCE, with a characteristic transient peak of Ca^{2+} entry, followed by the

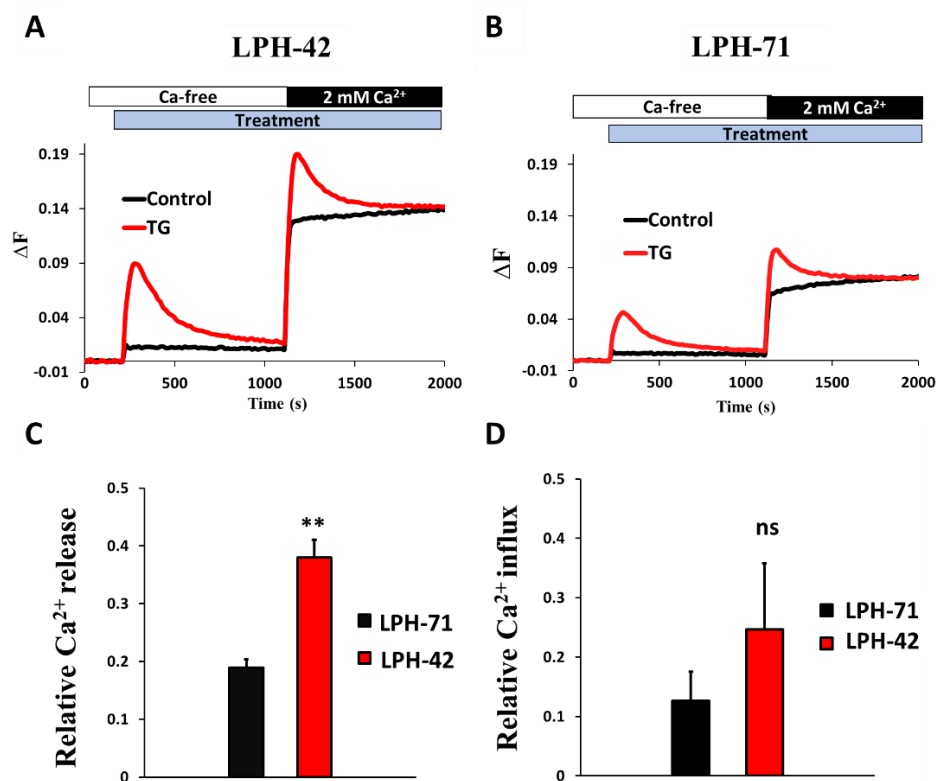


Figure 16: The effect of TG on cytosolic Ca^{2+} in cells expressing full-size or mutant LPHN1.

A-B: NB2a cells expressing full size LPHN1 and mutant LPHN1 (LPH-71) were treated with 1 μM TG in a Ca^{2+} free buffer, followed by the addition of extracellular 2 mM Ca^{2+} . C-D: Maximum amplitudes of ΔF . C: Ca^{2+} release from TG-sensitive stores. D: amount of SOCE. Traces are the averages of three independent experiments ($n = 3$) and error bars show SD. Asterisks indicate statistically significant

difference from cells expressing mutant LPHN1; t-test results: **, $p < 0.01$.

establishment of a new Ca^{2+} equilibrium (**Figure 16**). When the size of Ca^{2+} stores was compared in these cell lines, it was clear that it was significantly larger in the cells stably expressing full-size LPHN1 (LPH-42) compared to the mutant-expressing cells (due to LPHN1 mediated signalling thus an increase in IP3 production and therefore amplifying calcium release from internal stores by increased activation of IP3 receptors on the ER) (**Figure 16**). The latter did not differ from control, wild-type NB2A cells (not shown). Likewise, the amplitude of SOCE was consistently higher in the cells expressing LPHN1, although this effect was not statistically significant. This effect can be clearly seen when the specific Ca^{2+} fluorescence is calculated (the difference in fluorescence between the non-treated control and the experiment treated with TG) (**Figure 17**).

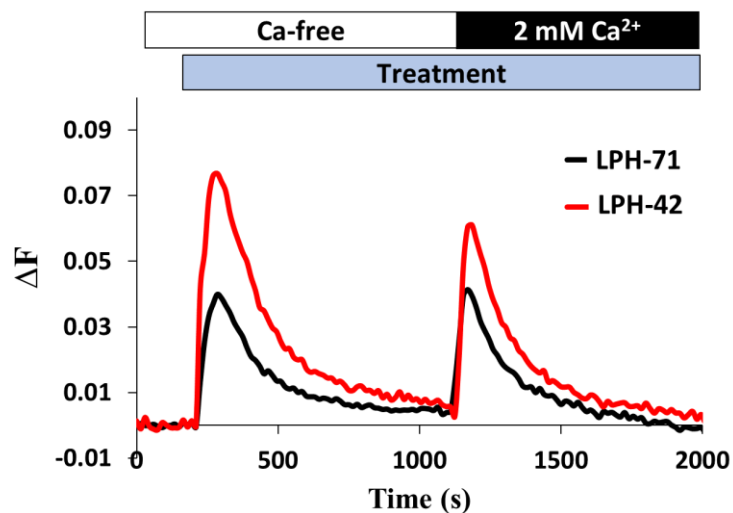


Figure 17: Increased Ca^{2+} stores and SOCE in cells expressing full-size LPHN1.

TG-induced Ca^{2+} mobilisation in cells expressing full size or mutant LPHN1. The data are from Figure 15, but the controls were subtracted.

4.3. Store operated Ca²⁺ channels

First, I needed to establish that the NB2A cells expressing LPHN1 possess SOCCs, which can be regulated by Ca²⁺ store depletion. This can be done by forced release of Ca²⁺ from the stores (for example by using TG to block SERCA), which causes subsequent opening of SOCCs. These channels are highly specific for Ca²⁺ and will not pass Na⁺ which is present in the medium during the whole experiment, but will only pass Ca²⁺ after it is added back at the second phase of the experiment. The SOCCs may have different features, but one of their characteristic traits is the sensitivity to La³⁺.

La³⁺ is one of the rare earth elements, which has a large atom size and a large positive charge and is known to inhibit SOCCs and other Ca²⁺ channels. Low micromolar concentrations of La³⁺ can block SOCE (Hoth and Penner, 1993). However higher concentrations of La³⁺ block other types of Ca²⁺ channels, such as VGCC, TRP channels, leak channels and the α -LTX pore (Clapham *et al.*, 2001) (Ashton *et al.*, 2001). Therefore, I used low La³⁺ concentrations to study the specific features of SOCCs in NB2A cells.

When cells were treated with 50 μ M La³⁺ in Ca²⁺-free conditions, fluorescence of the cytosolic dye increased sharply (**Figure 18**), but did not show a peak. This potentially indicated that La³⁺ could stimulate some mechanisms that very quickly depleted the ER stores. This hypothesis was tested by stimulating Ca²⁺ release by TG in the presence of La³⁺. This combination treatment still led to a transient increase in cytosolic Ca²⁺ concentration, typical of the effect of TG, which appeared above the

effect of La^{3+} , but was noticeably smaller than in the absence of La^{3+} (**Figure 18**). Thus, TG was still able to release stored Ca^{2+} by blocking SERCA, which means that the large increase in fluorescence in the presence of La^{3+} was not caused by store depletion. What could then be the reason for this sharp and significant increase in Fluo-4 fluorescence upon the addition of La^{3+} , alone or with TG? Although La^{3+} is known to block many Ca^{2+} channels, a small amount of it can be taken up by cells (Halaszovich *et al.*, 2000). Ca^{2+} indicator dyes have a higher affinity for La^{3+} than for Ca^{2+} , and 1 μM La^{3+} produces a higher dye fluorescence than 100 μM Ca^{2+} (Halaszovich *et al.*, 2000). Thus, it is most likely that the sharp rise of the cytosolic fluorescence in the presence of La^{3+} simply corresponds to fluorescence of the La^{3+} -Fluo-4 complex. However, La^{3+} also blocks many Ca^{2+} channels better from their cytosolic side, and it can inhibit the release of Ca^{2+} from the stores via IP_3R . This can explain the smaller apparent size of Ca^{2+} stores in the cells treated with both TG and La^{3+} .

Upon the addition of 2 mM external Ca^{2+} , cells treated with TG, as usual, demonstrated store-operated opening of SOCCs, which was observed as a large transient increase in Ca^{2+} fluorescence above that in control (**Figure 18**). La^{3+} alone showed an increased fluorescence at this stage, which was higher than the fluorescence increases due to constitutive Ca^{2+} influx in control conditions, but was

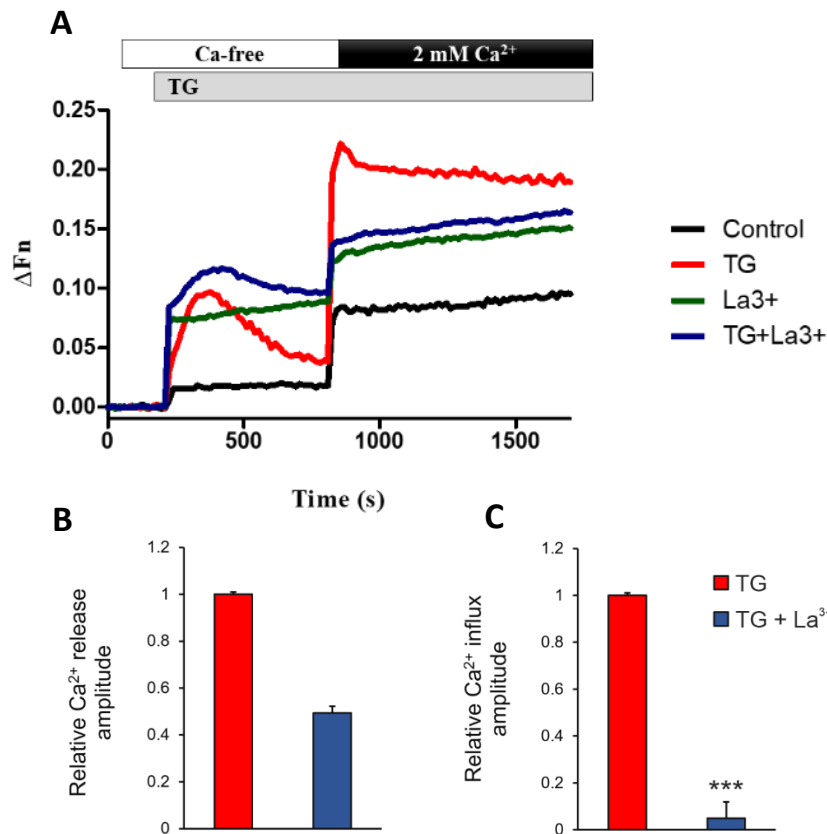


Figure 18: Features of the SOCCs in NB2A cells.

Cytosolic Ca²⁺ measurement in NB2a expressing full size LPHN1 when treated with 50 μM La³⁺, a Ca²⁺ channel blocker. NB2a cells were first treated with TG with or without La³⁺ in a Ca²⁺ free buffer, and then bathed in a Ca²⁺-containing medium. A) Average traces of cytosolic Ca²⁺ fluorescence under the conditions indicated (n = 3). B,C) Normalised peak values of Ca²⁺ release from the stores (B) and Ca²⁺ influx via SOCE (C), in cells treated with TG ± La³⁺ (respective values in cells treated with TG only were normalised to 1); n = 5. Results of a t-test comparing the SOCE amplitudes induced by TG ± La³⁺ are shown by asterisks (***, p < 0.001).

equal to the La³⁺-induced additional fluorescence during the Ca²⁺-free stage of the experiment and remained unchanged. Therefore, it was caused by the fluorescence of cytosolic La³⁺ and Ca²⁺. However, when La³⁺ was added together with TG, the usual effect of TG at this stage disappeared (**Figure 18**): there was no further transient increase in fluorescence above that in the presence of La³⁺ alone. This clearly shows that the SOCCs in NB2A cells can be fully blocked by La³⁺.

4.4. α -LTX signalling via LPHN1

Having established the presence of Ca^{2+} stores and SOCE in the NB2A cells expressing LPHN1, I then studied LPHN1-mediated signalling in these cells. As explained above, I had access to NB2A cells expressing the full-size protein (LPH-42, consisting of the NTF without TMRs and the CTF that has 7 TMRs) and a truncated protein (LPH-71, which has one TMR from NRXN1). G-protein-mediated signalling could only be mediated by the former, but not the latter construct.

As the most reliable ligand to stimulate LPHN1, I selected α -LTX, described in the Introduction. This toxin binds to several receptors (LPHN1, NRXN1 and RPTP σ) and forms transmembrane pores. Obviously, when Ca^{2+} influx occurs through such toxin pores, it is hard to distinguish it from receptor-mediated increase in Ca^{2+} signalling. However, comparison between the effects of α -LTX on the cells expressing the full-size LPHN1 and on the cells expressing the truncated LPH-71 construct would allow me to detect the signalling mediated by the CTF of LPHN1.

However, first, I carried out experiments to establish the ability of α -LTX to bind to the cells of these two types. For this purpose, I incubated large amounts (25 million) of the LPH-42 cells and LPH-71 cells with 5 nM α -LTX for 30 min, then washed and lysed the cells. Both the lysed cell pellets and supernatants (which had been concentrated by chloroform/methanol-precipitation, as described under Methods) were analysed by Western blotting with anti- α -LTX antibodies (**Figure 19**). As the results clearly demonstrate, both LPHN1-expressing cells specifically bound significantly more α -LTX than the WT cells, which appeared to non-specifically entrap

some small amounts of the toxin. Interestingly, the cells expressing the truncated mutant LPHN1 (LPH-71) bound more α -LTX than the cells expressing the full-size receptor (LPH-42) (**Figure 19**).

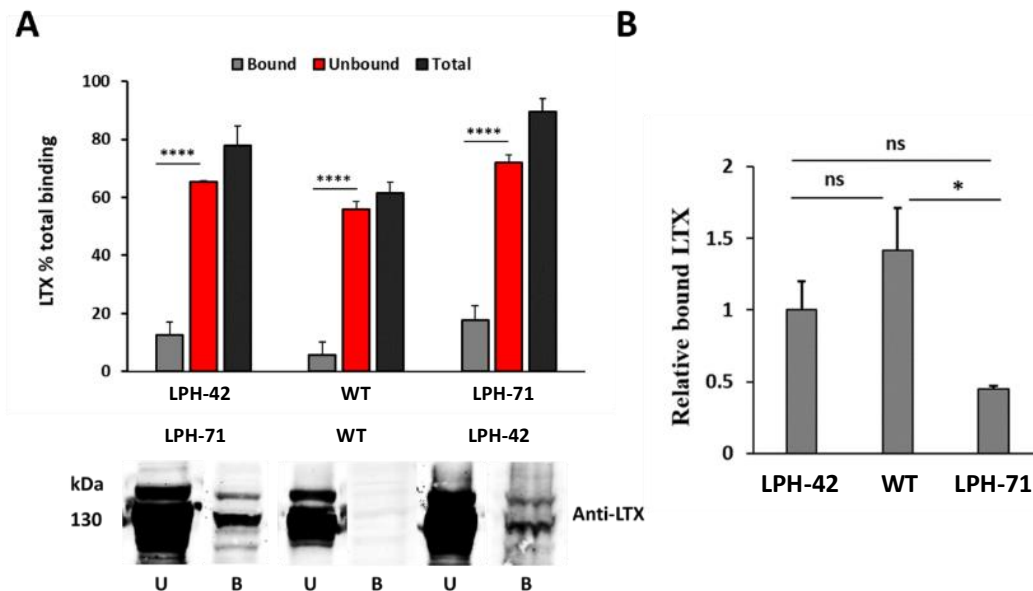


Figure 19: α -LTX binding to different LPHN1 constructs in NB2a cells.

A NB2a Cells expressing full size LPHN1, mutant LPHN1 and WT cells were treated with 5 nM LTX (see materials and Methods). Unbound LTX in the supernatant (U) and LPHN1-bound LTX in whole cell lysates (B) were separated in 8% SDS-PAGE, blotted, and probed with anti-LTX. The blots are representative of three independent experiments (n=3). B) Specifically, bound LTX in LPHN1 expressing and WT NB2A cells.

To measure LPHN1-mediated signalling, I used the same methodology of cytosolic Ca^{2+} detection based on cells loading with a fluorescent Ca^{2+} dye, as described above. As previously, the size of the Ca^{2+} stores and the SOCE dynamics were controlled by using TG during the Ca^{2+} -free phase and the Ca^{2+} -add back phase, respectively.

As shown in **Figure 20**, and consistent with the experiments shown above (**Figure 17**), the NB2A cells expressing full-size LPHN1 showed a very strong response to TG during the Ca^{2+} -free phase of the experiment. By contrast, α -LTX caused a gradual, but

substantial increase in cytosolic Ca^{2+} , which did not subside within the timeframe of the experiment. Upon the re-addition of Ca^{2+} to the extracellular medium, the TG-treated cells demonstrated a strong SOCE and a gradual return to a new Ca^{2+} equilibrium. The cells treated with α -LTX demonstrated a very similar response (**Figure 20**, blue line). The cells expressing mutant LPH-71 also responded to TG poisoning by Ca^{2+} release from the stores and by activating SOCE. However, when treated with α -LTX, the mutant-expressing cells did not show any increase in cytosolic Ca^{2+} during the Ca^{2+} -free phase; although they enabled an influx of Ca^{2+} during the Ca^{2+} re-addition phase, this did not demonstrate a transient peak of Ca^{2+} influx (SOCE) (**Figure 20**). Thus, the mutant LPH-71 cannot support the same intracellular signalling, leading to Ca^{2+} release and subsequent opening of SOCCs, that is mediated by the full-size LPHN1.

4.5. FLRT3 does not induce fast signalling via LPHN1

In the experiment with α -LTX (**Figure 20**), I also used FLRT3, a known LPHN1 ligand (see Chapter 3), which will be used in many experiments described in my project. 150 nM FLRT3 did not increase Ca^{2+} during the first, Ca^{2+} -free phase of the experiment, and this consistently did not lead to any influx of Ca^{2+} above background during the

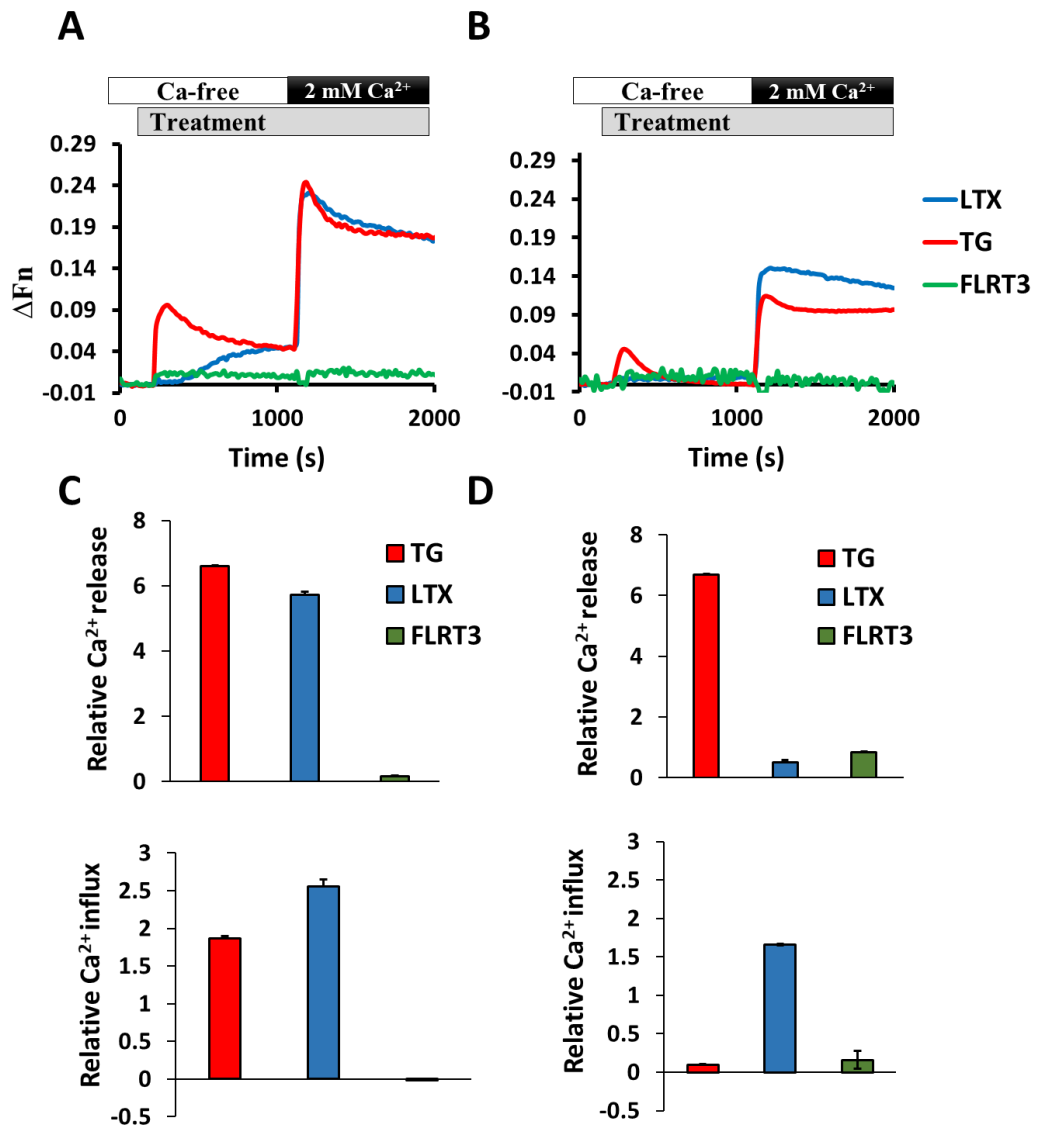


Figure 20: Ca^{2+} signalling induced by α -LTX in NB2a cells expressing full size or mutant LPHN1.

NB2a cells expressing full size LPHN1 (A, C) and NB2a cells expressing the non-signalling mutant LPH-71 (B, D) were treated with 2 μM TG, 5 nM α -LTX or 150 nM FLRT3. A, B) Average traces ($n = 4$) of cytosolic Ca^{2+} fluorescence in respective cell types treated as indicated. C, D) Peak increases in cytosolic Ca^{2+} concentration due to Ca^{2+} release (top graphs) and Ca^{2+} influx (bottom graphs). In the cells expressing mutant LPH-71, α -LTX causes pore formation, which does not lead to Ca^{2+} release from stores but supports continuous Ca^{2+} influx after Ca^{2+} add-back. In the cell expressing full-size LPHN1, the toxin also forms pores, but in addition it causes intracellular signalling, which leads to Ca^{2+} release from stores and a large transient peak of Ca^{2+} influx due to the opening of SOCCs.

second (2 mM Ca^{2+}) phase of the test (**Figure 20**, green line). This lack of Ca^{2+} signalling during the course of that experiment did not depend on the expression of the full-

size or truncated LPHN1.

4.6. FLRT3 binding to LPHN1-expressing NB2A cells

Given the unexpected lack of FLRT3 signalling via LPHN1 in NB2A cells (**Figure 20**), it was possible that FLRT3, for some reason, did not bind to the cells and therefore could not induce any signalling. Therefore, I decided to check FLRT3 binding to cells expressing full-size LPHN1, by incubating these cells with FLRT3 and then detecting any bound protein by Western blotting of the cell lysate. However, when LPHN1-expressing cells were incubated with 150 nM FLRT3 over 1 h (the approximate length of my Ca²⁺ signalling experiments), no FLRT3 could be detected bound to the cells (data not shown).

One reason for the failure to detect FLRT3 binding to these cells was the possibility that only a small amount of protein remained bound after the wash stage and this was below the detection limit. To identify the detection threshold of the anti-FLRT3 antibodies, I tested their sensitivity. For this purpose, different amounts of FLRT3 (1-10 ng) were analysed by Western blotting, alone or in the presence of a carrier protein, BSA, to avoid potential FLRT3 losses due to its adsorption to plastic. The results (**Figure 21**) demonstrate that the antibody detected 5 ng of FLRT3, but failed to detect 1 ng. This information was used to design a new experiment, where the number of cells incubated with FLRT3 was adjusted, to ensure that the amount of FLRT3 bound to the cell pellet would be detectable with our antibodies, even if only 1% of FLRT3 present in the reaction remained bound.

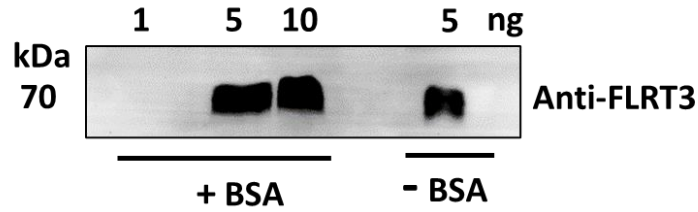


Figure 21: Sensitivity of FLRT3 detection.

To test the antibody sensitivity, a test experiment was conducted: 1, 5 or 10 ng of FLRT3 was mixed with 1% BSA and analysed using 8% SDS-PAGE, in parallel with a BSA-free FLRT3 sample (5 ng), blotted and probed with an anti-FLRT3 antibody. FLRT3 amounts below 5 ng are not detectable by our Western blotting procedure, even in the presence of the carrier protein.

In addition, the length of binding reaction was increased from 1 to 16 h, similar to that used in previous publications (Boucard *et al.*, 2014). FLRT3 concentration in the reaction was also increased to 300 nM. After the cells expressing full-size LPHN1 (or untransfected cells, as a negative control) were incubated with FLRT3, centrifuged and washed very briefly (only a few seconds), it was possible to detect a small amount of FLRT3 specifically bound to the LPHN1-expressing cells (**Figure 22**). The amount of specifically bound protein constituted about 0.6% of the unbound FLRT3.

4.7. Possible LPHN1 ligands in the blood plasma

Given the presence of LPHN1 on the surface of AML cells (Gonçalves Silva *et al.*, 2017), it was possible that an endogenous ligand of LPHN1, which is expressed ectopically in malignant cells, could be present in the blood plasma. The Ca²⁺ signal recording system, with a good internal control, described in this chapter might be useful for detecting specific LPHN1 ligands in the plasma or any fractions isolated from it.

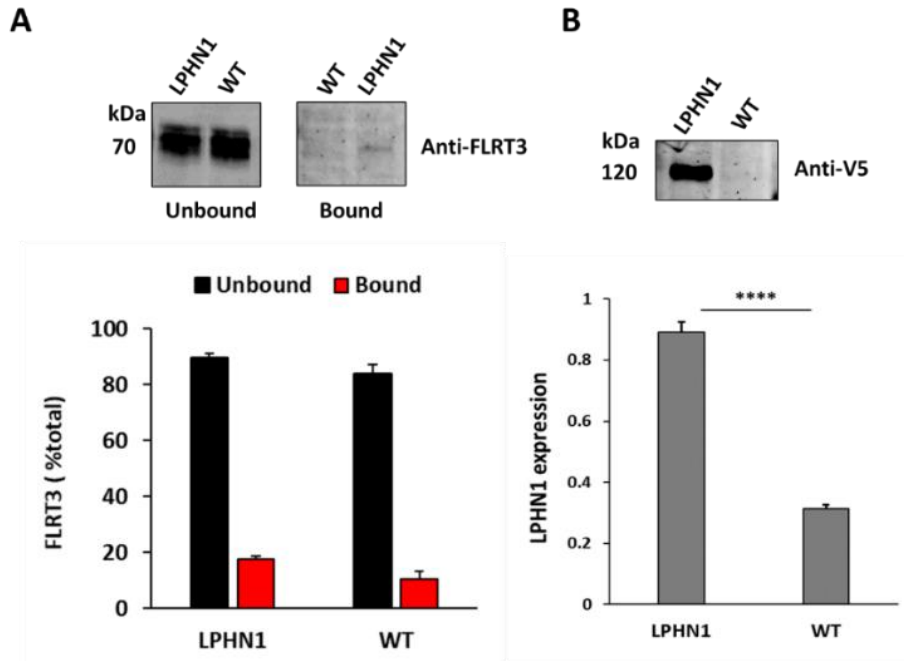


Figure 22: FLRT3 interaction with NB2a cells expressing full-size or mutant LPHN1.

A) NB2a cells were preincubated with 300 nM FLRT3 overnight at 4 °C. The supernatants and whole cell lysates (concentrated 10-fold by chloroform/methanol precipitation) were separated in an 8% SDS-PAGE, blotted and probed with anti-FLRT3 antibodies. B) LPHN1 expression in NB2a cells and WT cells was quantified using Western blot analysis. The bottom panels show the 10x percent of FLRT3 bound to LPHN1-expressing and WT NB2A cells (left) and the 1x percent of bound FLRT3 adjusted to LPHN1 expression (right).

Therefore, I decided to test if any proteins or other substances present in blood plasma could stimulate fast signalling via LPHN1. The human serum was diluted 1:1 or 1:4 with Ca²⁺-free buffer and applied to WT or LPHN1-expressing NB2A cells (**Figure 23**). The results demonstrate that, within the timeframe of the experiment, there was no significant differences between the WT and LPHN1-expressing cells in terms of Ca²⁺ release or subsequent influx, except for some delayed increase in Ca²⁺ equilibrium level achieved after the addition of 2 mM calcium.

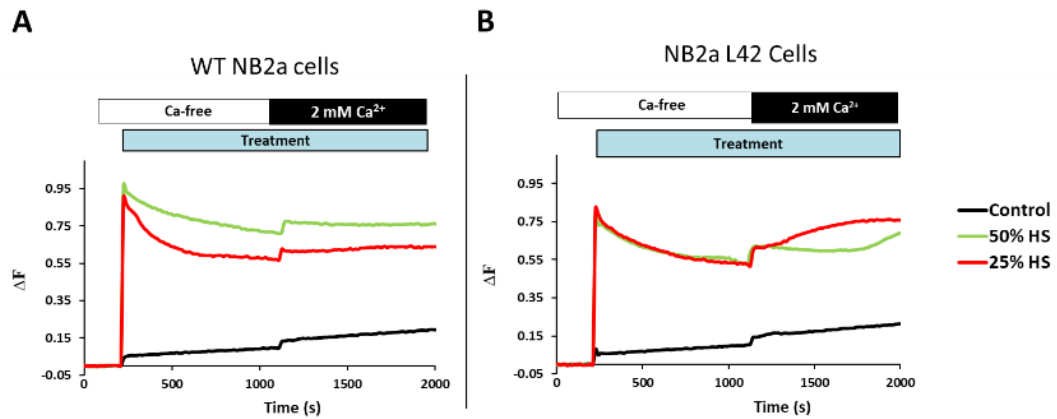


Figure 23: Intracellular Ca^{2+} dynamics in NB2a cells stimulated with human serum.

NB2a cells with or without LPHN1 were treated with human serum diluted with Ca^{2+} free recording buffer at a 1:1 or 1:4 ratio (50% and 25%, respectively). Cells were then exposed to 2 mM extracellular Ca^{2+} . Traces are the averages of 2 independent experiments.

4.8. Discussion

The experiments described in this section clearly established that the methodology adopted in this project enabled me to measure the size of intracellular stores and the features of SOCE. I have also found that the expression of LPHN1 did not dramatically affect these parameters, making this system a good model for studying the role of LPHN1 in intracellular signalling.

Interestingly, the cells expressing full-size LPHN1 possessed either bigger or more sensitive Ca^{2+} stores and responded to their depletion by a large SOCE than the cells expressing its non-signalling homologue (**Figure 16, Figure 20**). This was probably due to the fact that only full-size LPHN1, as a true GPCR, is likely to be spontaneously activated for short periods of time, even in the absence of a ligand. Such an activation would lead to store depletion, SOCC activation and their desensitisation. These effects would require some compensatory changes from the cell, in order to

counteract frequent losses of Ca^{2+} from the stores and to support house-keeping Ca^{2+} -dependent processes. These changes might lead to relative hypertrophy of the Ca^{2+} stores and upregulation of the SOCCs (**Figure 17**).

We also hypothesised that a ligand of LPHN1 might be present in mammalian blood. Normally, it would not be able to interact with this receptor, which is not expressed in blood cells or endothelial cells of blood vessels, but is very abundant in the brain and also present in autonomic neurons in the kidneys and lungs. However, if LPHN1 is ectopically expressed in malignant blood cells (as described in Chapter 5), then it may be exposed to such a ligand, and this may be important for activation and proliferation of cancer cells. Although we have not seen any short-term changes in Ca^{2+} dynamics in our experiments with treating LPHN1-expressing cells with human serum (**Figure 23**), this lack of effect may simply be due to the short time-frame of our Ca^{2+} recording or involvement of this ligand in a different signalling mechanism such as activation of cAMP pathway or may simply be due to the fact that the ligand is cell membrane bound and does not get secreted to the blood plasma. Moreover, human serum in our experiments did cause some LPHN1-specific changes in late SOCE (**Figure 23**). In this respect, it is important to remember that NB2A cells are normally cultured in the presence of 10% bovine serum, while malignant blood cells in human blood would be exposed to 100% serum. Therefore, it is possible that full-size LPHN1 expressed in NB2A can be subliminally activated by long-term incubation with a small concentration of its ligand present in the cell culture medium, leading to store and SOCE hypertrophy detected in our experiments (**Figure 17**).

It is also interesting, that there was a difference in α -LTX binding to the two types of

cells used here: cells expressing full-size LPHN1 bound less α -LTX than those expressing the truncated LPH-71 construct (**Figure 19**). It was not possible to remove this difference by several rounds of cell sorting (not shown), which may further suggest that overexpression of full-size LPHN1 could have a modest detrimental effect on cell viability.

Despite this, the system developed in my project allowed me to test the effect of known fast-acting LPHN1 ligand, α -LTX (**Figure 19**, **Figure 20**). Although the cells expressing the truncated LPHN1 mutant, LPH-71, bound more α -LTX than the cells expressing the full size receptor (**Figure 19**), they did not show any signalling during the Ca^{2+} -free recording phase (**Figure 20B**, blue line). By contrast, the LPHN1-expressing cells, while binding less toxin, demonstrated a gradual build-up of Ca^{2+} in the cytosol (**Figure 20A**, blue line). These differences in intracellular signalling led to substantial differences in SOCE: the mutant-expressing cells showed some increased Ca^{2+} influx, which was caused by the pore formed by α -LTX in the plasma membrane, but they did not demonstrate SOCE (**Figure 20B**, blue line). As opposed to this, the LPHN1-expressing cells responded to α -LTX-induced signalling by maximal SOCE (**Figure 20A**, blue line), commensurate with that caused by TG (**Figure 20A**, red line).

My experiments using this system also allowed me to identify one of the important features of the SOCCs involved in SOCE in these cells: they can be completely blocked by La^{3+} (**Figure 18**). This limits the number of channel types that can serve as SOCCs in NB2A cells, because for example, such transient receptor potential classical (TRPC) channels as TRPC1, 3, 6 and 7 are blocked by La^{3+} , while TRPC2 is not. Interestingly, TRPC4 is instead activated by La^{3+} , while TRPC5 is activated by micromolar La^{3+}

concentrations and blocked by millimolar La^{3+} (Armstrong *et al.*, 2019).

This system can now be used by the laboratory to study intricate features of LPHN1 signalling and the SOCCs involved in Ca^{2+} influx. This can be done using various inhibitors, such as SOCC blockers 2-aminoethoxydiphenyl borate (2-APB), SKF96365, U73122 and many others, or blockers of G-protein signalling, such as inhibitors of adenylyl cyclase or phosphodiesterase, or a selective $\text{G}\alpha_q$ inhibitor UBO-QIC. However, it is also amenable to transfection with various proteins that could attenuate or enhance different types of signalling downstream of G-protein activation.

In particular, this system has allowed me to study the effects of another known LPHN1 ligand, FLRT3. This ligand did not cause any Ca^{2+} signalling during the course of the experiment (10-15 min). While this result is fully consistent with some data from the Ushkaryov laboratory, it seems to contradict the data obtained in my experiments with other types of malignant cells, such as AML, THP-1 and MCF-7 cells, and described in subsequent Chapters. One possible explanation can be that the effect of FLRT3 only develops over a longer period of time than the Ca^{2+} release experiments described here. Indeed, in subsequent experiments (Chapter 5) FLRT3 was allowed to activate cells for 4-24 h in a cell culture environment, while this was not possible in our fluorescence experiments, which were conducted in the absence of CO_2 and therefore were limited to about 1-1.5 h overall.

Nevertheless, any rapid Ca^{2+} changes induced by such LPHN1 ligands as α -LTX and Ten2 (Silva *et al.*, 2012) could be easily tested using this system. Thus, having been optimised in these model experiments, the fluorescent dye-based methodology of

determining the size of Ca^{2+} stores and SOCE was used to study LPHN1-mediated signalling in other types of malignant cells.

5. The role of LPHN1 in AML cells

5.1. Introduction

LPHN1 was always thought to be present mainly in the brain and in very small amounts in the kidney and in the lungs, but recently the Sumbayev and Ushkaryov groups discovered the expression of LPHN1 in acute myeloid leukaemia (AML) cells. They also showed that LPHN1 is absent in healthy leukocytes. This important discovery shed new light on the functions of LPHN1 in non-neuronal tissues/cells. More importantly, this revealed the potential use of LPHN1 as a leukaemia biomarker or eventually as a therapeutic target. However, little is still known about the LPHN1 function in leukaemia in terms of cell signalling and its role in SOCE. Finally, its functional ligand in AML cells remains to be discovered. Therefore, the aim of this chapter is to study the ligand/s of LPHN1 and to reveal the signalling pathways downstream of LPHN1 in AML cells.

5.2. Identification of LPHN1 in THP-1 cells

THP-1 cells are immortalised monocyte-like cells; they have been derived from the peripheral blood of an AML patient and are often used as a laboratory model of AML cells (Sumbayev *et al.*, 2016). Immunocytochemical detection of LPHN1 in THP-1 cells was carried out, using NB2a cells as a negative control. THP-1 cells show clearly high expression of cell surface LPHN1, as opposed to NB2a cells. For comparison with primary AML cells, Western blot analysis of LPHN1 expression was performed in primary human leukocytes, THP-1 cell line and primary human AML cells. As previously reported by Sumbayev and Ushkaryov (Sumbayev *et al.*, 2016), LPHN1 was absent in healthy leukocytes and present in both primary AML cells and THP-1 cells,

but considerably higher levels were observed in AML primary cells compared to THP-1 cells (**Figure 24**)

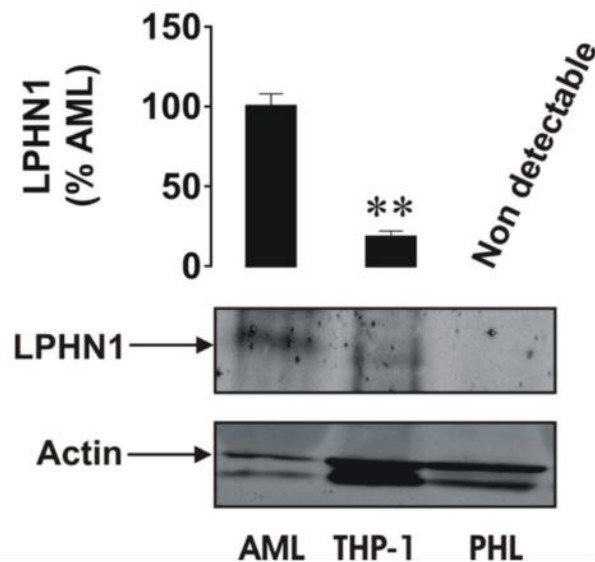


Figure 24: LPHN1 protein expression in human primary AML cells, THP-1 cells, and primary healthy leukocytes.

Lysates of each cell type were analysed by Western blotting as outlined under Materials and Methods. Images are from one of three experiments, which gave similar results. Data are the mean values \pm SEM of three independent experiments: **, $p < 0.01$ vs. AML cells.

5.3. Presence of soluble LPHN1 fragments in AML blood

plasma

It has been previously demonstrated that LPHN1 was expressed in the membrane of blood cells (Sumbayev *et al.*, 2016), and our data above confirmed this. Therefore, we thought that LPHN1 may be released from these cells and shed into the blood stream. To study this possibility, blood plasma samples from AML patients were obtained and subjected to immunoprecipitation followed by Western blot analysis,

utilizing different LPHN1 antibodies. A series of bands was observed between 45 and 68 kDa, using an anti-LPHN1 antibody (**Figure 25A**). Lower molecular weight bands were also observed when stained with different anti-LPHN1 antibodies. The NTF of

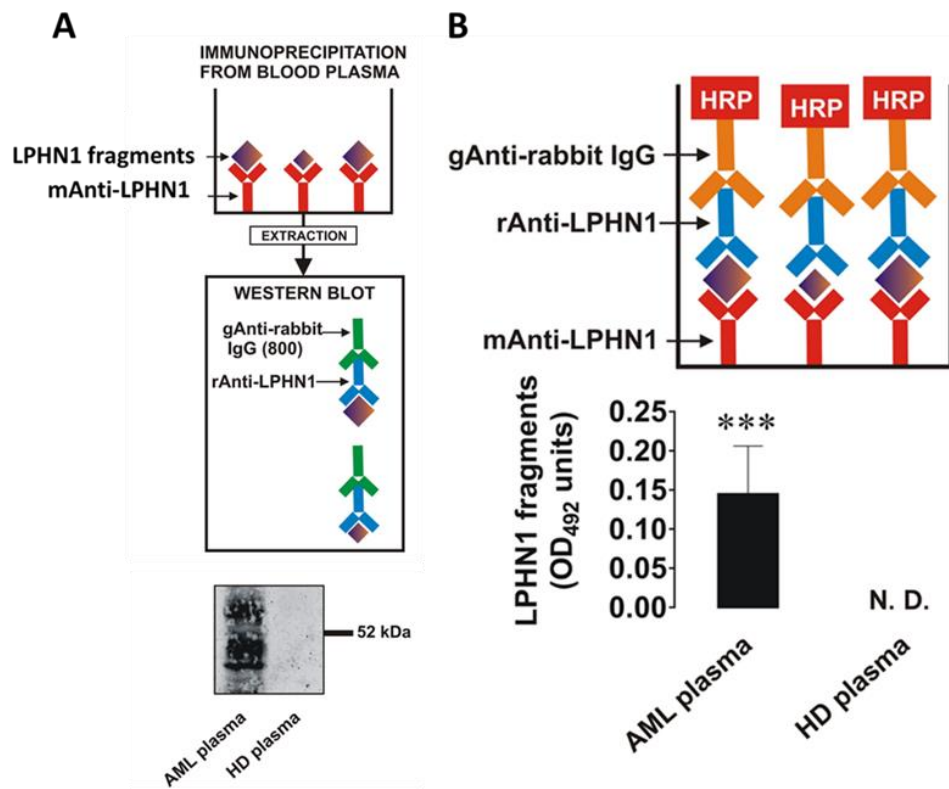


Figure 25: Soluble LPHN1 fragments in the blood plasma of AML patients.

A) Blood plasma of ten healthy donors and ten AML patients was subjected to immunoprecipitation employing Santa Cruz mouse monoclonal antibody, as a capture antibody. The wells were then extracted, and the extracts obtained were analysed by Western blotting using rabbit anti-LPHN1 antibody (PAL-1 or Abcam anti-LPHN1 antibody) for detection (A). Specific detection of soluble LPHN1 fragments (in the same blood samples) was performed using ELISA as outlined in Material and Methods (B). Images are from one experiment representative of six, which gave similar results. Data are the mean values \pm SEM of ten independent experiments; *t*-test results are indicated by asterisk: ***, $p < 0.01$ vs control. Modified from (Sakhnevych et al., 2018).

LPHN1 expressed on the cell surface usually migrates as a 120 kDa band. Therefore, the presence of lower molecular weight fragments of LPHN1 in the blood stream of AML patients may indicate that LPHN1 is cleaved and or shed by malignant blood

cells. Indeed, none of these bands was observed in blood plasma samples from healthy donors (**Figure 25A**). AML patients' blood and healthy donors' blood were also subjected to ELISA analysis, which confirmed the presence of LPHN1 fragments in the blood of AML patient but not in healthy patients.

5.4. Upregulation of LPHN1 expression in AML cells and haematopoietic stem cells

Since AML cells and haematopoietic stem cells (HSCs) are generally present in bone marrow or blood vessels, the search for potential LPHN1 expression inducers mainly focused on bone marrow and blood vessels. We also considered the known fact that stress hormones, including cortisol (hydrocortisone), are significantly upregulated in AML patients (Singh *et al.*, 1989) and that cortisone is a strong immunosuppressor. To investigate its effects on LPHN1 transcription and translation, 1 μ M cortisol was used to treat in primary human AML cells, THP-1 cells, primary human HSCs, and primary healthy human leukocytes for 24 h. After that, qRT-PCR was used to analyse the amounts of LPHN1 mRNA and showed that detectable amounts of LPHN1 mRNA levels were found in AML, THP-1 and HSC cells and were significantly upregulated after treatment with cortisol. However, in primary healthy leukocytes LPHN1 was absent both before and after the cortisol treatment (**Figure 26**).

Our previous data indicated that LPHN1 can control the release of Gal-9 (Goncalves Silva *et al.*, 2017). Therefore, we also tested the effect of cortisol on Gal-9 release. Gal-9 levels in the medium conditioned by these three cell types were subjected to ELISA analysis with or without cortisol treatment (**Figure 26B, C and D**). Results

showed that cortisol treatment did not affect the Gal-9 release by all cell types (**Figure 26B, C and D**). This may indicate that LPHN1 alone does not stimulate Gal-9 release, but needs to be activated by a ligand in order to induce Gal-9 release by AML cells.

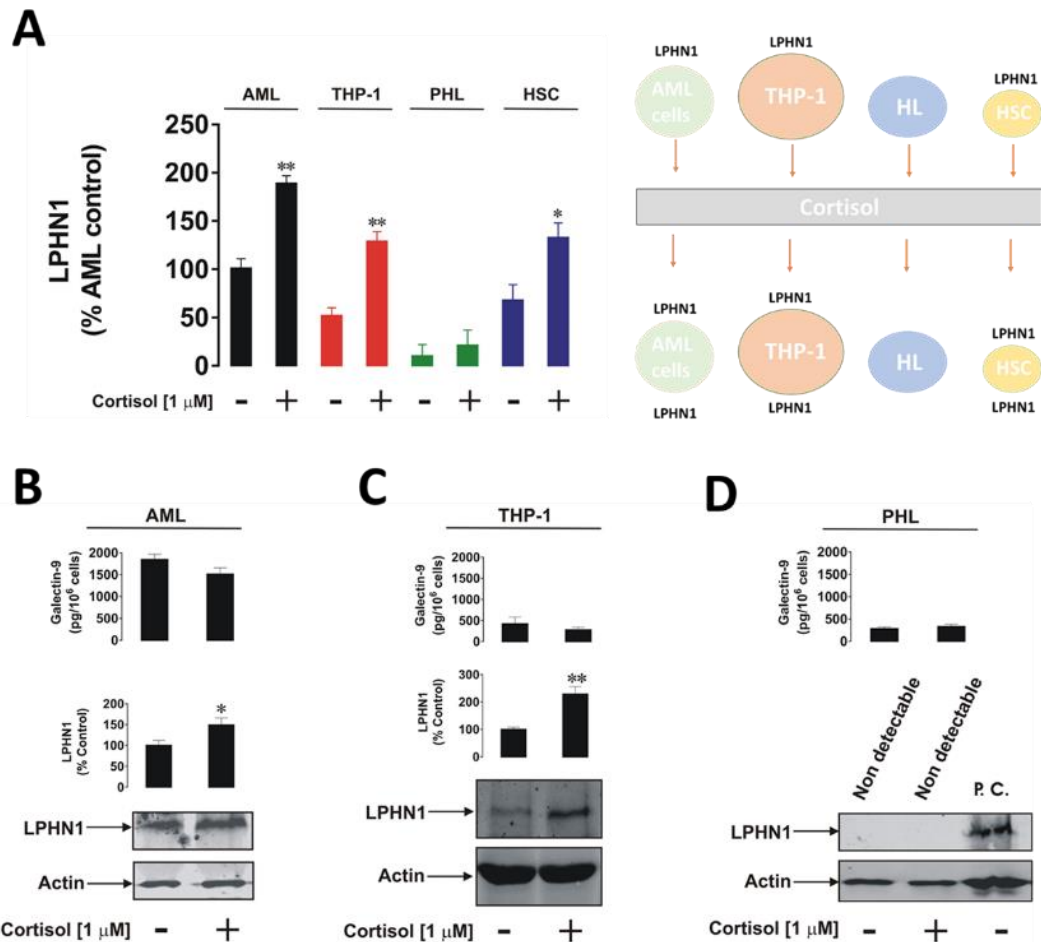


Figure 26: Cortisol induces LPHN1 expression in human hematopoietic stem cells (HSC), AML cells and THP-1 cells, but not in healthy primary leukocytes.

Primary human AML cells, HSC, THP-1 cells and primary healthy leukocytes (PHL) were treated for 24 h with 1 μ M cortisol followed by qRT-PCR analysis for LPHN1 gene transcription A) and Western blot analysis in primary AML cells B), THP-1 cells C), and primary healthy leukocytes D). In PHL experiment, NB2a cells overexpressing LPHN1 were used as a positive control. Images are from one experiment, but are representative of 4–6 replicates, all of which showed similar results. Data represent the mean values \pm SEM of 6–10 independent experiments. The results of t-tests are indicated by asterisks: *, $p < 0.05$; **, $p < 0.01$ vs. control. Modified from (Sakhnevych et al., 2018).

We also tested the concentrations of cortisol and Gal-9 in blood plasma samples taken from AML patients and healthy donors. Results showed that cortisol and Gal-9 were both significantly higher in blood plasma of AML patients compared to healthy donors (**Figure 27**).

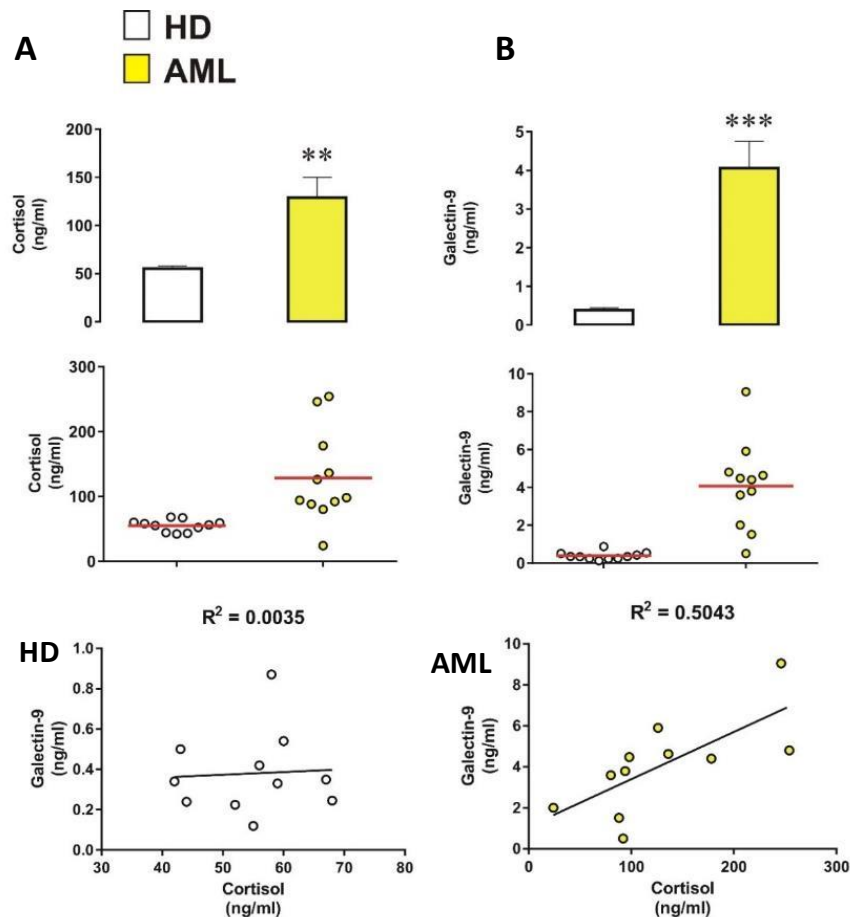


Figure 27: Cortisol and Gal-9 levels in the blood plasma of AML patients and healthy donors.

Blood plasma samples were collected from ten healthy donors and 10 AML patients at the same time of the day to avoid the influence of circadian dynamics and ensure comparability of cortisol levels. The levels of cortisol (A) and Gal-9 (B) were measured by ELISA, and the correlation between these two proteins was analysed. Data are the mean values \pm SEM of ten independent experiments. The results of t-tests are indicated by asterisks: **, $p < 0.01$; ***, $p < 0.01$ vs control. Modified from (Sakhnevych *et al.*, 2018)

Furthermore, these results showed that there is no correlation between cortisol and Gal-9 levels in healthy patients, while, by contrast, a clear correlation was observed

in blood plasma of AML patients, suggesting that LPHN1 presence in AML cells may have induced Gal-9 secretion.

5.5. Upregulation of Gal-9 in AML cells by FLRT3 and LPHN1 interaction

To investigate whether FLRT3-LPHN1 interaction was the reason behind the increase in galectin-9 secretion in THP-1 and AML cells, specific anti-LPHN1 neutralizing antibody (RL1) was used. A test experiment was performed first, to assess the specificity of this antibody on THP-1 cells and untransfected NB2a cells as a negative control. RL1 interaction with receptors on the cell surface of THP-1 and NB2a cells was studied by immunocytochemistry (**Figure 28**). The results demonstrate that the RL1 antibody specifically recognizes LPHN1 on THP-1 cells, but does not interact with the surface of NB2A cells.

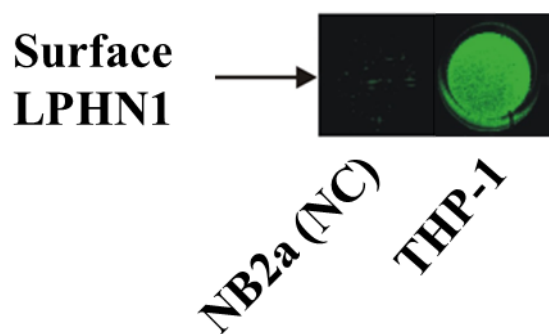


Figure 28: Detection of LPHN1 on the surface of THP-1 cells.

Non-permeabilised LPHN1-negative, wild-type NB2A cells (negative control, NC) and THP-1 cells were stained using a polyclonal rabbit anti-LPHN1 antibody (RL1) and a anti-rabbit fluorescently labelled secondary antibody (green), followed by fluorescence imaging. The image shown is representative of three experiments which gave similar results.

Subsequently, THP-1 cells were incubated for 16 h with or without RL1 antibody. After incubation, ELISA analysis was employed in order to measure the release of Gal-9. Data showed that RL1 preincubation did not affect Gal-9 release (data not shown), indicating that RL1 antibody does not serve as an LPHN1 agonist. After understanding the neutralizing effect of RL1 antibody, a study of LPHN1 involvement in Gal-9 secretion by THP-1 cells and AML cells was carried out. THP-1 cells were preincubated for 1 h with or without RL1 antibody followed by incubation of cells overnight with or without 10 nM FLRT3. After that, release of Gal-9 levels in cell culture media was analysed by ELISA. Results showed that RL1 antibody decreased the induction of Gal-9 by FLRT3 in THP-1 cells (**Figure 29A**). Most likely, the long-term interaction of the RL1 antibody with cell-surface LPHN1 led to its internalisation as described previously (Volynski *et al.* 2004). Thus, the removal of LPHN1 from the cell surface of THP-1 cells blocked the action of FLRT3 on Gal-9 release from these cells, suggesting that LPHN1 was involved in FLRT3-induced Gal-9 release. Moreover, this suggestion was further confirmed by the fact that FLRT3 incubation with primary healthy leukocytes did not increase Gal-9 release (negative control) (**Figure 29C**).

However, these experiments were conducted using an exogenous FLRT3, and it was necessary to show that FLRT3 is present in the blood of AML patients. For measurement of FLRT3 presence, blood plasma samples were taken from AML patients and healthy donors and subjected to Western blot analysis. Two bands at ~55 kDa and ~27-28 kDa were detected by anti-FLRT3 antibody in both samples (**Figure 29B**) and represented shed and proteolytically cleaved fragments of FLRT3. Interestingly, soluble FLRT3 fragments were present in approximately the same

amounts in both groups.

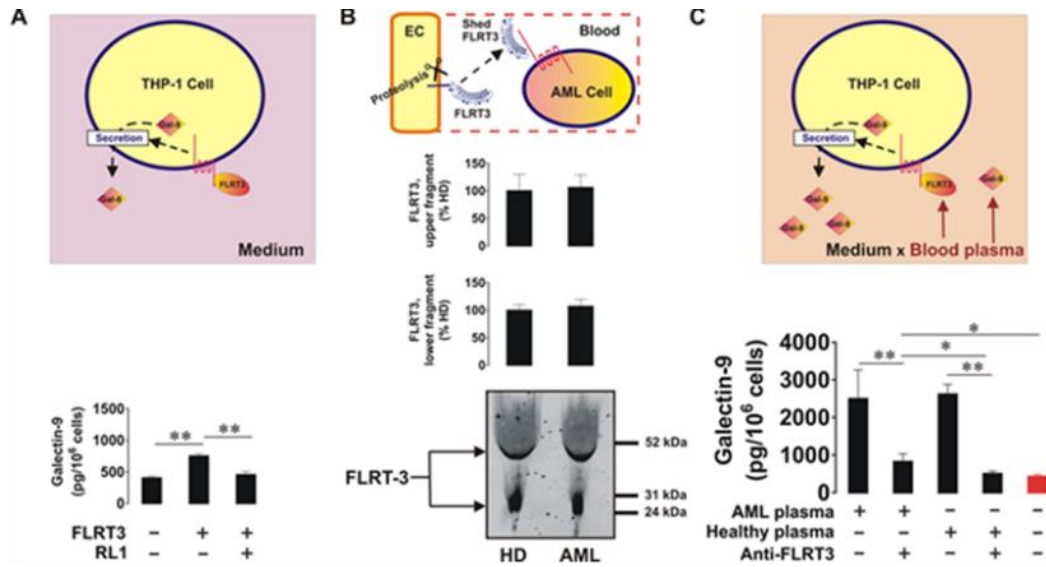


Figure 29: FLRT3 circulating in blood plasma induces Gal-9 secretion in AML cells in a LPHN1-dependent manner.

THP-1 cells and PHL were exposed to 10 nM human recombinant FLRT3 for 16 h followed by detection of secreted Gal-9 by ELISA. In THP-1 cells, the treatment was performed with or without 1 h pre-exposure to RL1 anti-LPHN1 polyclonal antibody (A). The levels of shed FLRT3 and its fragments were analysed in the blood plasma of healthy donors and AML patients using Western blot (B). THP-1 cells were exposed for 16 h to 10% blood plasma either from healthy donors or AML patients with or without pre-treatment with anti-FLRT3 neutralising antibody. The levels of secreted Gal-9 were analysed using ELISA (C). The data are shown as the mean values \pm SEM from four independent experiments; t-test results indicated by asterisks: *, $p < 0.05$; **, $p < 0.01$ vs. control.

To study whether soluble FLRT3 fragments were able to stimulate Gal-9 secretion in AML cells by binding to LPHN1, THP-1 cells were maintained in RPMI 1640 media as mentioned in Materials and Methods, except the usual 10% foetal bovine serum in experimental samples was replaced with blood plasma obtained from AML patients or healthy donors. Thus, THP-1 cells were incubated overnight with or without 10% blood plasma, which had been preincubated with or without the anti-FLRT3 antibody,

and Gal-9 secretion levels in culture media were measured by ELISA. The results (**Figure 29C**) showed that Gal-9 secretion was significantly higher when cells were maintained in 10% blood plasma compared to 10% FBS (negative control, red bar). In addition, the presence of anti-FLRT3 antibody decreased Gal-9 secretion (**Figure 29C**). These data indicate that FLRT3 present in the medium was specifically responsible for Gal-9 release from THP-1 cells.

5.6. Fast Ca²⁺ signalling in THP-1 cells

After we studied the effects of FLRT3 on THP-1 cells using the standard immunological approaches and incubation times, as described above, it was interesting to correlate the effects observed with transient calcium signalling that reflects fast GPCR-mediated effects. This was done using our established cytosolic Ca²⁺ detection system based on Fluo-4 fluorescence. While there was an *a priori* large difference in the time course of these effects (4-16 h vs. 15-30 min), it was possible that the long-term changes could be initiated by the short-term Ca²⁺ signalling.

When the THP-1 cells were treated with TG to block the SERCA and induce Ca²⁺ from intracellular stores, the cells responded with a robust, but unremarkable, transient peak of Ca²⁺ release (**Figure 30A**). However, the subsequent SOCE (induced by the re-addition of extracellular Ca²⁺) and the new Ca²⁺ equilibrium level appeared to be much higher than in NB2A cells (**Figure 30A**). As demonstrated in **Figure 30B**, the SOCE in THP-1 cells was 2-4 times higher than in NB2A cells.

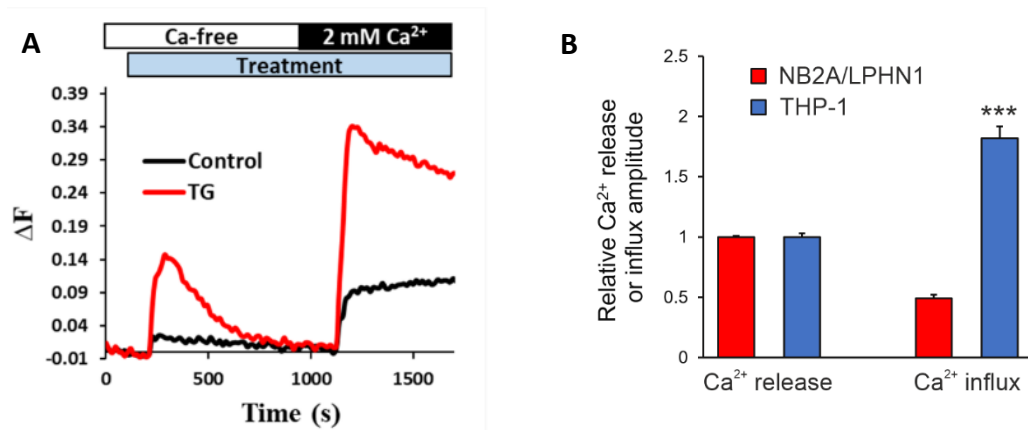


Figure 30: Intracellular Ca²⁺ stores and SOCE in THP-1 cells.

A) THP-1 cells expressing LPHN1 were treated with 1 μM TG in Ca²⁺ free buffer for 20 min followed by addition of 2 mM extracellular Ca²⁺. B) Relative TG-induced Ca²⁺ influx in LPHN1-expressing NB2A cells and THP-1 cells, compared to respective Ca²⁺ release (normalised to 1). Representative traces shown are the averages of three replicates. The error bars show SEM (n=3). Student's t test was performed, and asterisks (***, p < 0.001) show statistical significance when comparing SOCE in LPHN1-expressing NB2A cells and THP-1 cells.

To test whether LPHN1, which has been shown to be present in THP-1 cells, had a normal sensitivity to α-LTX and could possibly be sensitive to its other agonists, I treated THP-1 cells with α-LTX and compared its effect to that of TG (**Figure 31**). Similar to its action in NB2A cells expressing full size LPHN1, α-LTX caused in THP-1 cells a strong gradual release of Ca²⁺ (during the Ca²⁺-free phase of the experiment), whose amplitude was similar to the amplitude of TG-induced peak of Ca²⁺ release (**Figure 31A, B**). However, the subsequent SOCE induced by the addition of extracellular Ca²⁺ was even stronger than SOCE caused by TG (**Figure 31A, C**). Thus, consistent with the overall high sensitivity of THP-1 cells to store depletion, they also reacted to LPHN1-mediated intracellular Ca²⁺ signalling by an exaggerated Ca²⁺ influx via SOCCs.

The equilibrium Ca^{2+} concentration in THP-1 cells (at the end of experiment) was also higher than in LPHN1-expressing NB2A cells, when they were stimulated by α -LTX, but not when the SOCE was induced by TG (**Figure 31D**). This is likely to be the result of increased membrane pore formation by α -LTX in THP-1 cells.

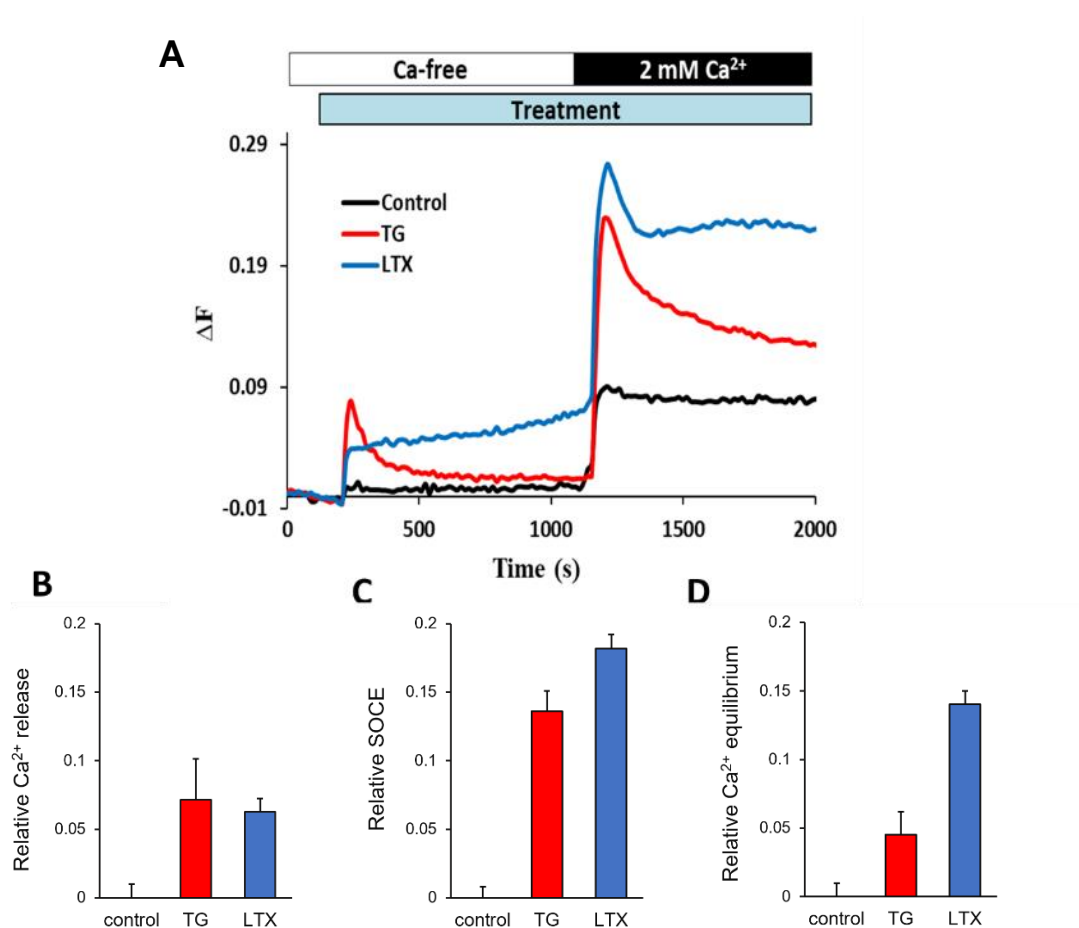


Figure 31: Stimulation of LPHN1 by α -LTX in THP-1 cells.

A) THP-1 cells were treated with $1 \mu\text{M}$ TG and stimulated with 5 nM LTX in Ca^{2+} free buffer for 15 min. Cells were then exposed to 2 mM Ca^{2+} containing buffer. Representative trace shows the averages of three replicates. B – D) Cytosolic Ca^{2+} concentration that reflects: Ca^{2+} release (B), Ca^{2+} influx (C) and Ca^{2+} equilibrium (D), relative to control (normalised to 0). The error bars show SEM ($n=3$).

The most logical next step in this analysis was to test whether THP-1 cells could respond to FLRT3 in our short-term Ca^{2+} fluorescence experiment. However, similar

to LPHN1-expressing NB2A cells, FLRT3 did not cause Ca²⁺ release from stores or the SOCE in THP-1 cells, within the time-frame of the Ca²⁺ fluorescence test (**Figure 32**).

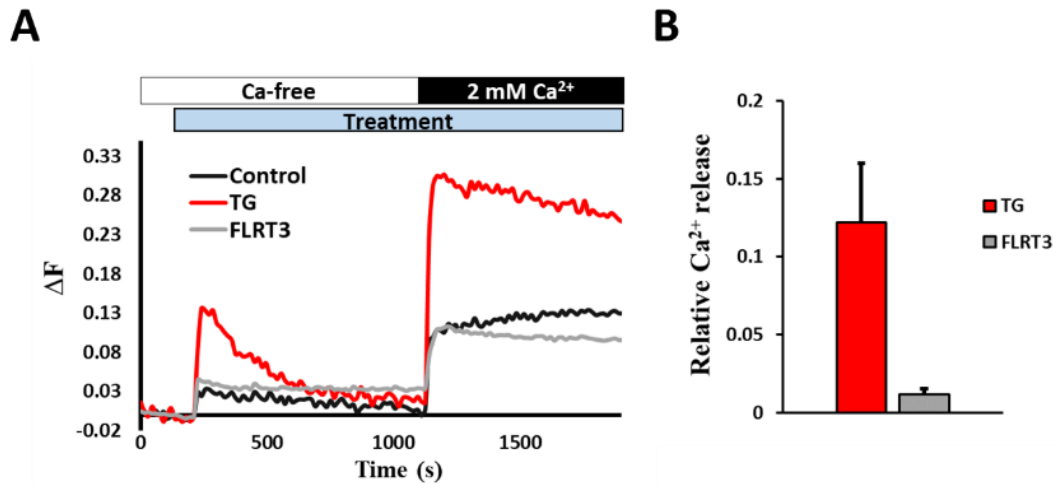


Figure 32: FLRT3 does not induce fast release of stored Ca²⁺ in THP-1 cells.

A) THP-1 cells were treated with 100 nM FLRT3 and 1 μ M TG in Ca²⁺ free buffer for 15 min. Cells were then exposed to 2 mM Ca²⁺ containing buffer. Representative traces show the averages of three replicates. B) Ca²⁺ release after induced by TG or FLRT3, relative to control (normalised to 0). Error bars show SEM (n=3).

5.7. Discussion

Cortisol is a glucocorticoid hormone known widely as the stress hormone produced by the adrenal gland in response to long-term stress (Torpy and Chrousos, 1996). AML is known for its rapid progression, which leads with time to lower glucose levels (Gonçalves Silva *et al.*, 2016). This will stimulate the hypothalamic-pituitary-adrenal axis to continuously release high amounts of cortisol into the bloodstream. These facts were in line with our results. Cortisol was found in higher amounts in blood samples of AML patients compared to healthy donors. The data showed also that cell surface

LPHN1 expression in AML cells was upregulated by the presence of cortisol and that FLRT3, LPHN1 endogenous ligand, could interact with it. LPHN1 and FLRT3 interaction in the blood led to upregulation of Gal-9 release (see Figure 32). It has been shown that both Tim-3 and Gal-9 needs activation of PKC α and mTOR pathway in addition to proteolytic enzymes to get released (Gonçalves Silva *et al.*, 2017). Moreover, activation of PKC α pathways leads to agglomeration of SNAP receptor (SNARE) proteins, which are essential for vesicles fusion and therefore exocytosis (Morgan *et al.*, 2005). Our theory, based on our publications (Gonçalves Silva *et al.*, 2017; Sakhnevych *et al.*, 2018) suggests that Tim3 and Gal-9 serve to protect AML cells from cytotoxic immune cells by inducing interferon-gamma (IFN- γ) release from NK cells (Gleason *et al.*, 2012), which will interact with AML cells and induce the activation of indoleamine 2,3-dioxygenase (IDO1); an enzyme that converts L-tryptophan into formyl-L-kynurenine and eventually L-kynurenine (Corm *et al.*, 2009; Folgiero *et al.*, 2015). L-kynurenine was shown to affects the capability of NK cells to attack AML cells.

However, HSCs also express LPHN1 mRNA and its transcription is also increased by cortisol presence. LPHN1 expression in HSCs was also observed at the protein level. However, LPHN1 observed in HSCs was slightly higher in terms of its molecular weight (~140 kDa) compared to MW of LPHN1 in AML cells (~120 kDa). In addition, unlike AML cells, HSCs do not show detectable levels of Gal-9 and Tim3 expression, which means that LPHN1 in HSCs may use different biochemical mechanisms and would not induce the secretion of the Tim3-Gal-9 complex.

On the other hand, primary healthy leukocytes showed an ability to produce detectable amounts of Gal-9, but independently to LPHN1 presence, as LPHN1 was not observed in healthy leukocytes either at the mRNA or protein level. Furthermore, LPHN1 transcription and translation in healthy leukocytes was independent of cortisol, possibly due to its gene repression. Consistently, soluble LPHN1 fragments were easily detected by Western blot analysis and ELISA, in blood plasma of AML patients, but not healthy donors.

It is important that LPHN1 expressed in THP-1 cells was sensitive to its specific ligands, such as α -LTX, to which it reacted by the usual gradual release of Ca^{2+} and subsequent strong SOCE, both of which happened within 15-30 min (**Figure 31**). However, FLRT3 was unable to cause similarly fast activation of LPHN1 in THP-1 cells (**Figure 32**), and this is fully consistent with the lack of fast FLRT3 effect on LPHN1-expressing NB2A cells in this experimental paradigm (**Figure 22**). Thus, unlike α -LTX, which induces strong and fast LPHN1-dependent signalling and SOCCs activation, both in cells naturally expressing LPHN1 (THP-1) and in artificially transfected cells (NB2A expressing LPHN1), FLRT3 is apparently incapable of similarly fast signalling. Instead, FLRT3 causes an effect that develops over a long time period (4-16 h), but still involves LPHN1. Therefore, it is possible that FLRT3 induces its effects only after (1) a slow conformational adjustment to LPHN1 molecule and (2) via a mechanism that may not involve the usual, GPCR-mediated, fast Ca^{2+} signalling. The specific mechanism by which FLRT3 induces LPHN1-mediated Gal-9 secretion will have to be investigated in detail in a separate project.

Finally, reflecting on our discovery of the physiological role of LPHN1 in AML cells, it is important to consider its practical use. While LPHN1 expressed in AML cells is an absolute biomarker of AML and can be used for AML diagnosis, the use of the whole blood for LPHN1 detection may not be convenient or sensitive. Therefore, further studies must be carried out in order to investigate the difference in the composition of blood plasma, which will might lead to faster AML diagnosis.

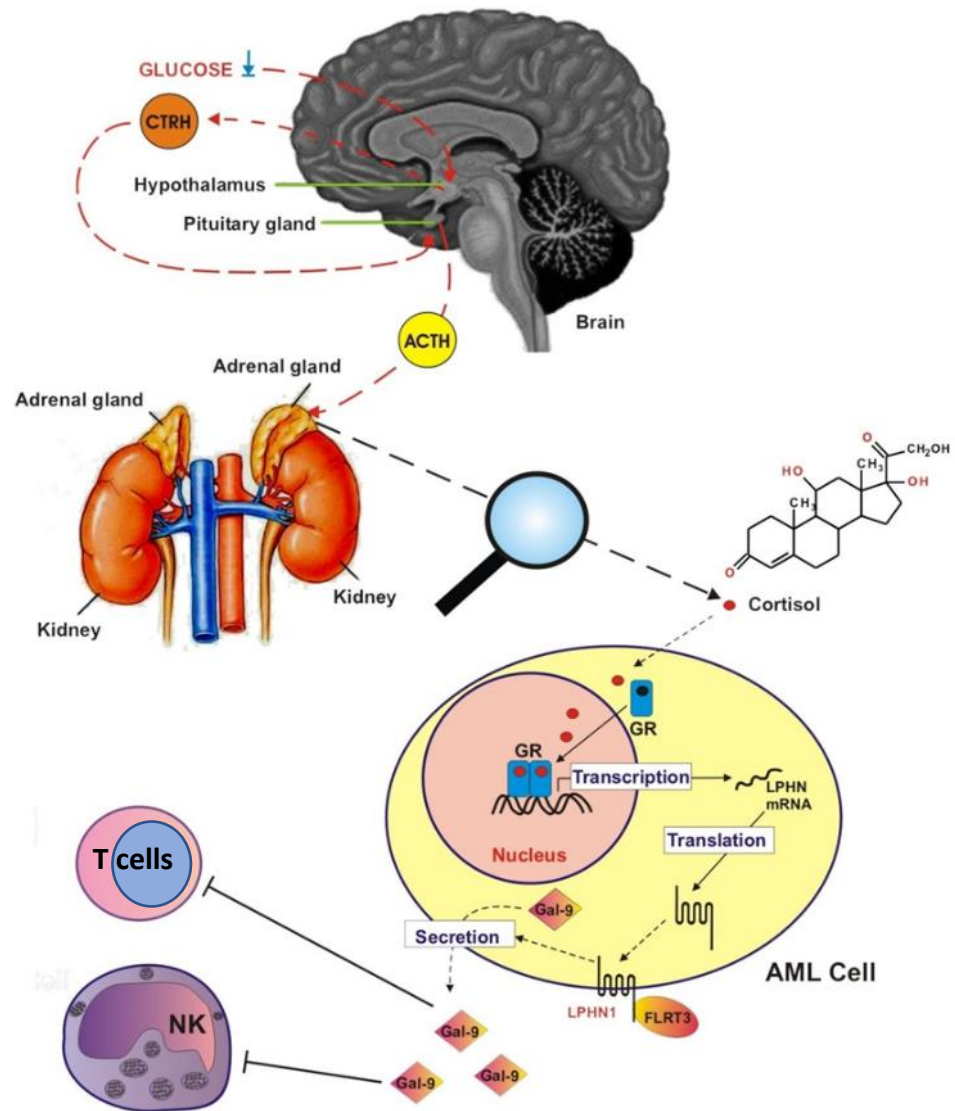


Figure 33: A proposed mechanism of cortisol-induced increase in LPHN1 expression in AML cells followed by increased Gal-9 secretion.

AML is linked with lower blood plasma glucose levels, that usually upregulates the secretion of corticotropin-releasing hormone (CTRH) by the hypothalamus. CTRH induces secretion of adrenocorticotropic hormone (ACTH) by the pituitary gland. Released ACTH increases cortisol levels by the adrenal cortex, therefore leading to cortisol-induced increase of LPHN1 levels in AML cells. Gal-9, secreted in a FLRT3-LPHN1-dependent manner reduces anti-cancer activity of cytotoxic T cells and natural killer (NK) cells.

6. Signalling pathways in human breast cancer cells

It has been shown by several scientist that aGPCRs may be involved in breast cancer. In particular, LPHN2 was upregulated in breast cancer cells compared to healthy cells (White *et al.*, 1998). Moreover, other components of this complex machinery, such as Gal-9 and Tim3, have been found to be expressed in breast cancer cells. Cancer cells release Gal-9 in complex with Tim3 to prevent being detected and destroyed by the immune system (Yasinska *et al.*, 2019). Therefore, we decided to investigate the role of LPHN in Ca²⁺ signalling in breast cancer cells and its impact on expression and release of the Tim3-Gal-9 complex, and suppression of immune attack.

6.1. Autocrine loop proteins in human tissues

Expression of LPHN2, FLRT3, Tim3 and Gal-9 was confirmed by Western blot analysis. Proteins present in breast cancer tissue were resolved in 12% SDS-PAGE and detected by specific antibodies.

The NTF of LPHN2 (~120 kDa) was identified in both healthy and malignant human tissues, but was ~3 times more abundant in the breast tumour tissue (**Figure 34A**). The extracellular domain of FLRT3 was detected at 76 kDa in healthy and breast cancer tissues (**Figure 34A**). However, FLRT3 appeared to be fragmented, probably due to proteolysis, and another FLRT3-positive band around 55 kDa was also detected. The breast tumour tissue also showed a third fragment, at around 40 kDa, which was absent in the healthy tissues from the same patients. The malignant tissues expressed visibly higher amounts of each of the three fragments than healthy tissues, and the combined difference in FLRT3 expression was ~1.5 times more abundant in the cancerous tissue. However, this difference was not statistically

significant, due to high variability of FLRT3 expression in malignant cells.

Interestingly, Gal-9 was also detected in a band around 55 kDa in both healthy and malignant tissues (**Figure 34B**). Given that the molecular weights of Gal-9 and Tim3 are around 32 and 38 kDa, respectively, and the two proteins are known to form an SDS-resistant complex, we thought that the 55 kDa band could correspond to Tim3-

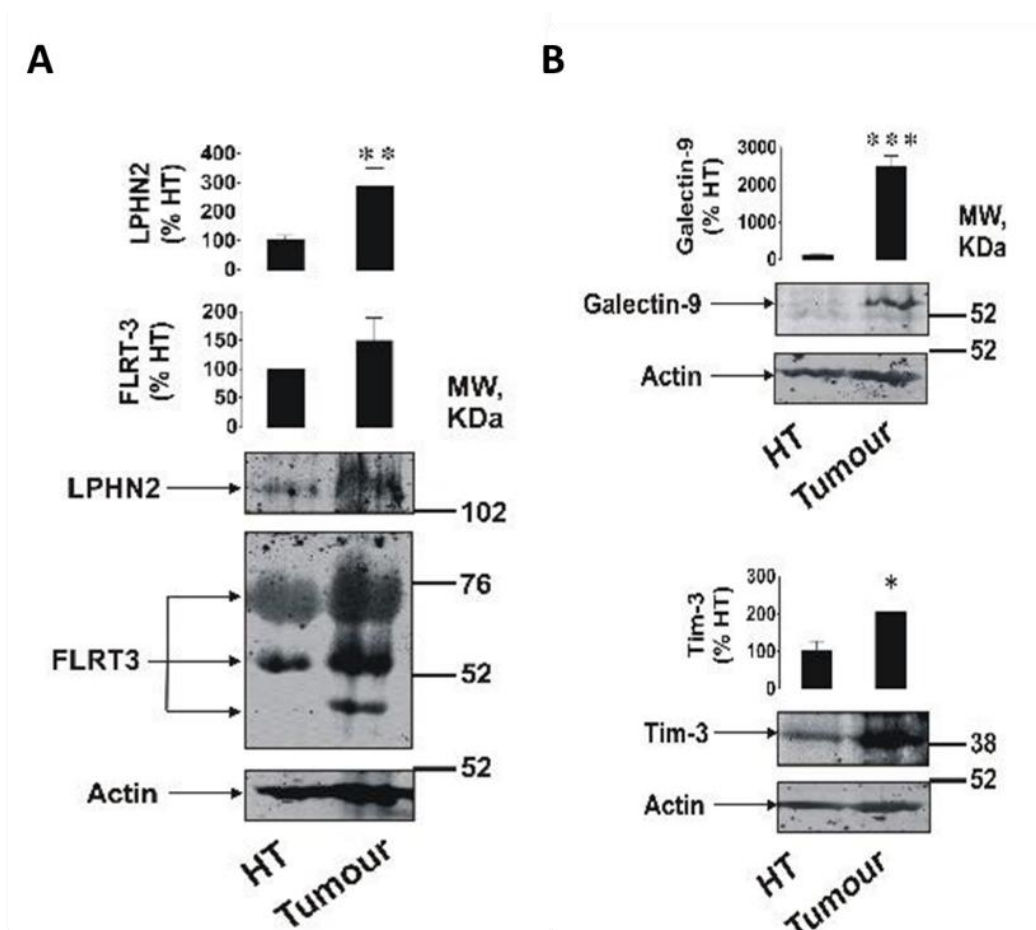


Figure 34: Expression of LPHN2, FLRT3, Gal-9 and Tim3 in primary human breast cancer tissues.

Expression levels of LPHN2 and FLRT3 (A); and Gal-9 and Tim3 (B) in primary breast tumour samples were compared to healthy tissues (n=5) using Western blot analysis as described under Materials and Methods. Blots are representative of 5 experiments. Blot quantifications are shown as the mean values \pm SEM, where statistical significance is shown in comparison to control; *, $p < 0.05$; **, $p < 0.01$ and ***, $p < 0.001$ vs control.

Gal9 complex. However, an anti-Tim3 antibody did not detect the 55 kDa band stained with Gal-9 antibodies. Thus, the 55 kDa band stained by the Gal-9 antibodies may correspond to a highly glycosylated isoform of Gal-9. When the same sample was subsequently analysed by Western blotting using a 10% SDS-PAGE and anti-Gal-9 antibody, a band around 32 kD was indeed detected (**Figure 35**). This may signify that due to protein glycosylation or other post translational modifications a slower migrating band of Gal-9 appeared in all tissues tested. The analysis also showed that both Gal-9 and Tim3 were expressed in small amounts in healthy tissues isolated from cancer patients, but were upregulated in malignant breast tumours from the same patients (**Figure 34B**). However, these proteins were upregulated in malignant cells to different extents: while Gal-9 was 25 times more abundant in breast cancer than healthy tissues, this ratio for Tim3 was only 1.5 times.

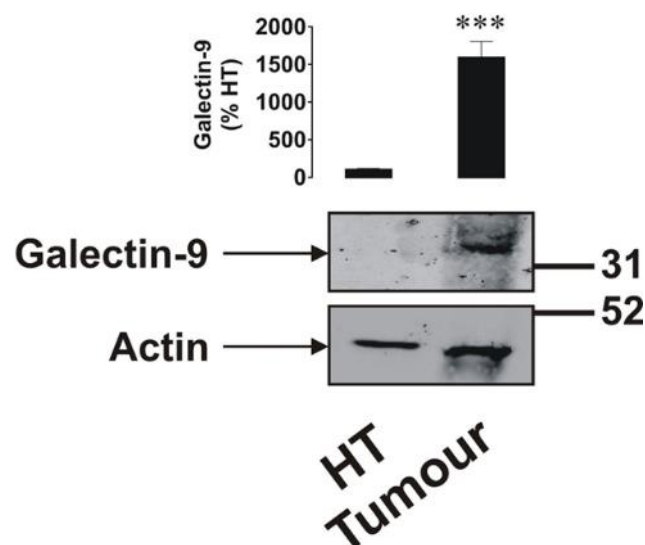


Figure 35: Gal-9 expression in primary human breast cancer and healthy tissues.

Western blot analysis of five ($n=5$) primary breast tumours and five healthy tissue lysates were done using 10% SDS-PAGE. The blot shown is a representative of 5 blots which gave similar results. Quantification of the blot is shown as the mean \pm SEM where ***, $p<0.001$ vs HT.

PLC, PKC- α and mTOR activities were also measured in five healthy and breast cancer patients. The activities of PKC- α and PLC were significantly higher in breast cancer patients compared to healthy patients (**Figure 36A**). By contrast, the levels of phosphorylated pS2448-mTOR (the active form of mTOR) were similar in both tissue samples (**Figure 36A**). We also tested the changes in eIF4E-BP, an mTOR substrate. The ratio between the phosphorylated phospho-S65-eIF4E-BP and the total eIF4E-BP amount was also similar in both tissues, even though the amount of phospho-S65 and total eIF4E-BP was higher in tumour tissues.

As indicated above, Tim3 and Gal-9 are more abundant in the breast cancer tissue. Importantly, these proteins can form a strong complex, which aides in Gal-9 secretion. Therefore, the presence of a Tim3-Gal-9 complex in both healthy and malignant tissues was verified. The investigation was carried out in two steps: first, ELISA test showed that there is a clear difference between the healthy and tumorous cells in terms of the amount of Tim3-Gal9 complex present (**Figure 37A**). Second, these results were confirmed by confocal microscopy, which showed that Gal-9 and Tim3 were clearly present in tumours tissues and co-localised in individual cells, most likely forming a complex (**Figure 37B**).

Following these experiments, it was possible that overproduced Tim3-Gal-9 complex in cancer patients could be detected not only in the primary tumorous tissues, but also in patients' blood. Therefore, we decided to measure the blood plasma levels of Gal-9, Tim3 and IL-2 in healthy donors (HD), primary breast cancer (PBC) patients and metastatic breast cancer (MBC) patients. The results showed (**Figure 38**) that the levels of Gal-9 and Tim3 were significantly lower in PBC and MBC patients' blood

plasma compared to HD plasma samples. By contrast, IL2 level was non-significantly higher in PBC and MBC patients compared to HD.

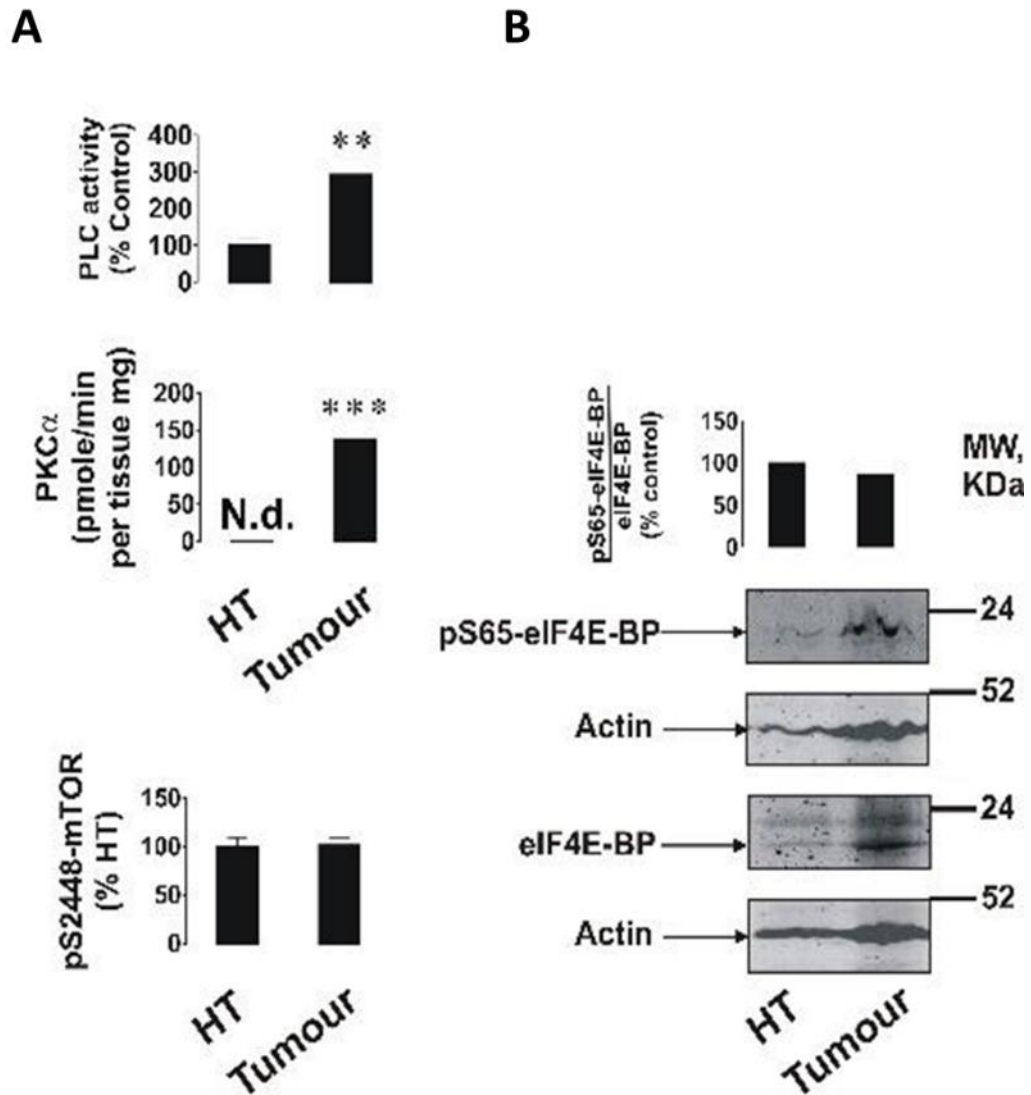


Figure 36: PLC, PKC α and mTOR activity in human breast cancer primary tissues.

A) The activities of PLC, PKC and mTOR were measured in 5 healthy and 5 breast cancer tissue samples, as mentioned in Methods section. (B) phospho-S65 and total eIF4E-BP (mTOR substrate) were subject to Western blot analysis. The blots shown are a representative of 5 blots, which gave similar results. Quantifications of blots and activities are shown as the means \pm SEM, where *, $p < 0.05$; **, $p < 0.01$ and ***, $p < 0.001$ vs control.

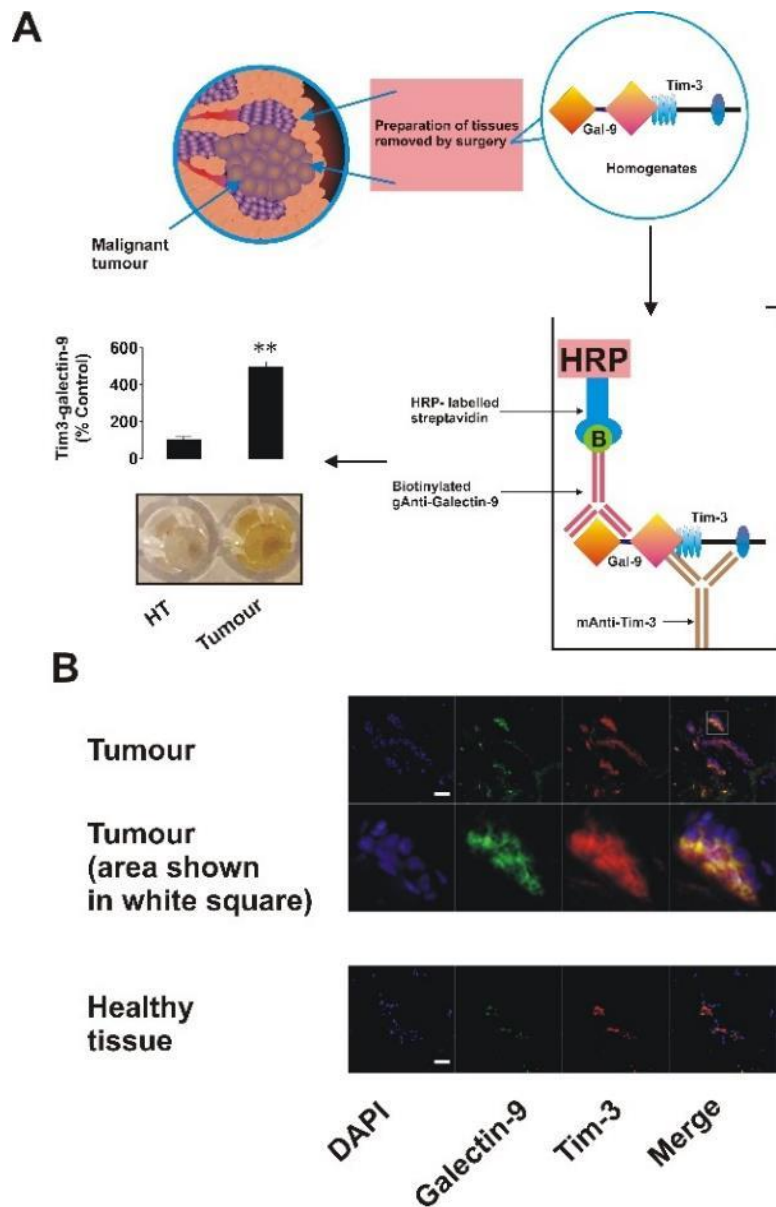


Figure 37: The presence of Tim3-Gal9 complex in primary human breast cancer.

A) Expression of Tim3-Gal9 complex in primary breast tumours and in healthy tissues was assessed by ELISA as described in Materials and Methods. (B) Presence and co-localisation of Tim3 and Gal9 in primary human breast tumours and healthy tissues of five patients ($n = 5$) using confocal microscopy (see Materials and Methods for details). Images represent one out of 5 experiments, which all gave similar results. Modified from (Yasinska et al., 2019).

Thus, it was possible that the breast cancer cells and especially aggressive metastatic forms of breast cancer do not release the overexpressed Tim-3-Gal-9 complex into

the bloodstream, but, instead, expose it on their surface to avoid detection by the patient's immune system – similar to the behaviour of the AML cells. To study whether the immunosuppressive mechanism used by AML cells to escape immune attack can also be applied by breast tumour tissues, a model cell was needed in order to carry out this investigation. We used an oestrogen receptor-positive breast cancer cell line, MCF-7 cells, the only breast cancer cell line that expresses a significant amount of LPHN2, oestrogen positive, similar to that found in primary breast tumours (Figure 39). In addition, MCF-7 cells express detectable amounts of Gal-9, Tim3 and their complex which serve as the best model cell that will represent primary breast cancer rather than metastatic cells (Figure 39).

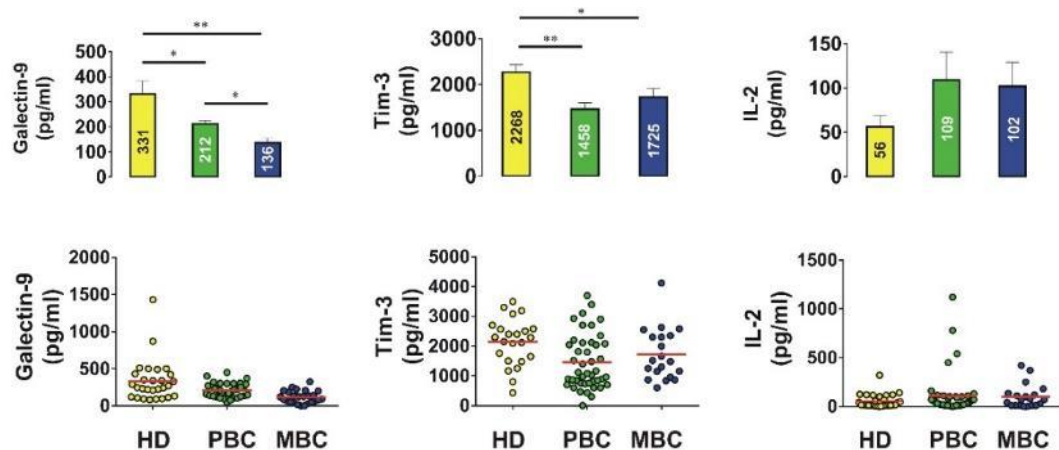


Figure 38: Gal-9, Tim-3 and IL-2 blood plasma levels in human healthy donors, primary breast cancer patients and metastatic breast cancer patients.

The levels of Gal-9, Tim3 and IL-2 were measured in blood plasma by ELISA. Data are shown as the means \pm SEM of 20 healthy donors (HD), 42 primary breast cancer (PBC) patients and 20 metastatic breast cancer (MBC) patients. The results of a t-test are shown by asterisks (*, $p < 0.05$; **, $p < 0.01$). from (Yasinska et al., 2019).

LPHN2 is a member of aGPCRs, which means that a G protein can bind to the CTF of

LPHN to mediate signal transduction. Therefore, MCF-7 cells and tumour lysates were subjected to Western blot analysis for Gαq detection. The results showed that both MCF-7 cells and breast cancer tissues have Gαq (not shown). Once all the components of the LPHN2, FLRT3, Tim3 and Gal-9 pathway were determined in MCF-

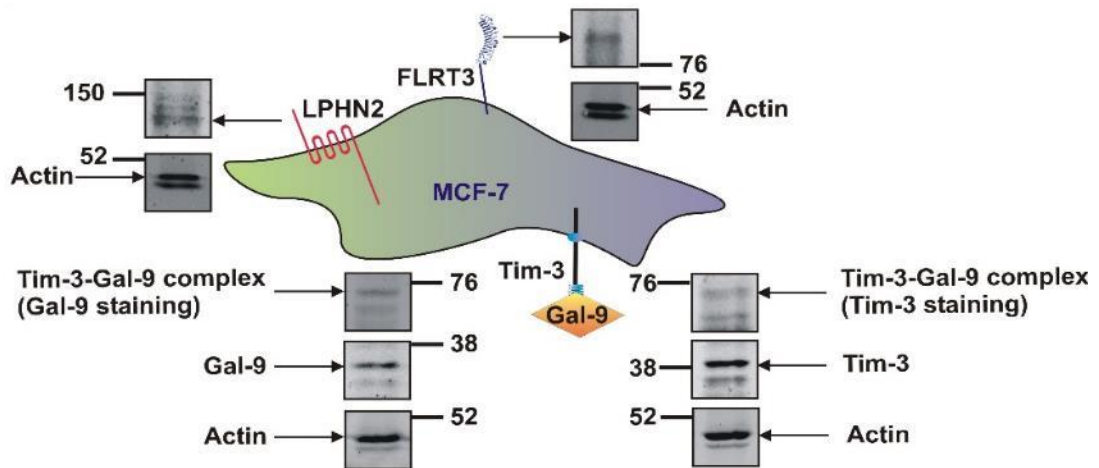


Figure 39: Expression of LPHN2, Gal-9, Tim3 and Tim3-Gal-9 complex in a breast cancer cell line.

Western blot analysis of MCF-7 cells (breast cancer cell line) shows expression of LPHN2, Gal-9, Tim3 and their complex. The blots are from one experiment representative of at least three, which gave similar results.

7 cells, the signalling pathway involved with LPHN2 activation was investigated by treating the cells with the extracellular domain of human recombinant FLRT3. Ca²⁺ recordings for MCF-7 cells were performed in the presence of 10 and 100 nM of FLRT3. TG was used to control of the size of Ca²⁺ stores (**Figure 40A**). Addition of 1 mM TG in a Ca²⁺ free solution showed an effect similar to that observed in NB2a cells and THP-1 cells. This indicates that MCF-7 cells can signal via Ca²⁺. While the addition of 10 nM FLRT3 in a Ca²⁺ free solution showed a small Ca²⁺ release from intracellular stores, 100 nM FLRT3 caused a similar response. This indicates that Ca²⁺ release from

intracellular stores is not ligand concentration dependent in these cells. Next, MCF-7 cells were incubated with 10 nM extracellular FLRT3 fragment for 4 h (as a control, the cells were incubated without FLRT3) (**Figure 40A**). After incubation, PLC and PKC-

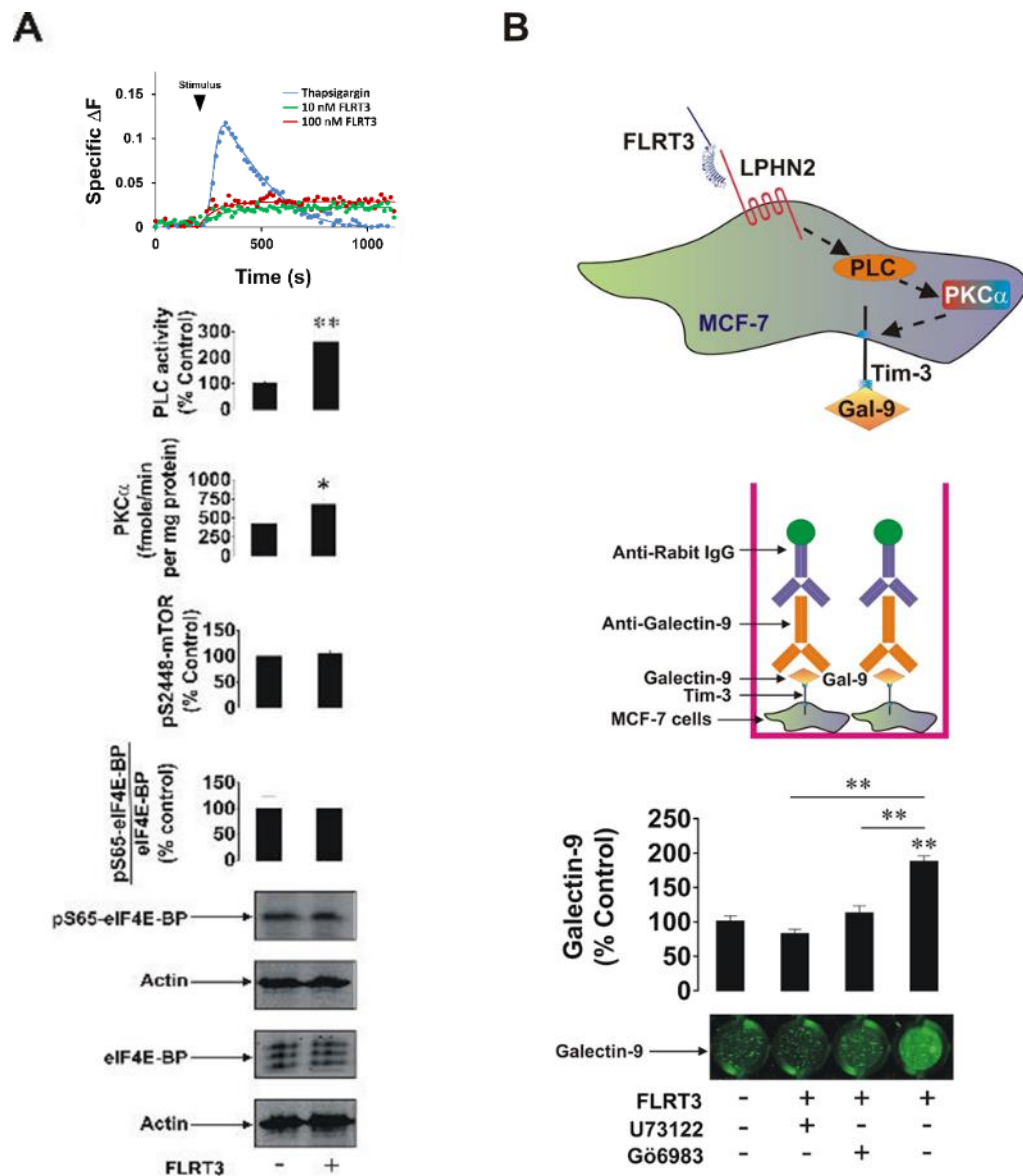


Figure 40: FLRT3 causes translocation of Gal-9 to the cell surface in breast cancer MCF-7 cells.

A) MCF-7 cells were treated with 10 nM or 100 nM of extracellular domain of FLRT3, or 1 μ M mM TG in Ca^{2+} -free medium and medium containing 2 mM Ca^{2+} . The activity of PLC and PKC α , the levels of phospho-S2448 mTOR and amounts of phospho-S65 and total eIF4E-BP were measured after incubating MCF-7 cells with 10 nM FLRT3 for 4 h, as described under Materials and Methods. B) MCF-7 cells were treated with 10 nM extracellular FLRT3 for 4 h with or without pre-treatment with 30 μ M of PLC inhibitor (U73122) or 70 nM PKC α inhibitor (Gö6983) followed by

*immunocytochemistry for detection of cells surface presence of Gal-9. The blots are from one out of four experiments, which all showed similar results. Other results are shown as the mean values \pm SEM of at least three independent experiments. * $p < 0.05$; **, $p < 0.01$ vs control.*

α activities were determined, as described under Materials and Methods, followed by Western blot analysis of cell lysates to detect phospho-S2448 mTOR and phospho-S65/total eIF4E-BP. Results showed that FLRT3 significantly (2-2.5 fold) increased PLC and PKC- α activities, while phospho-S2440 mTOR and phosphorylation of eIF4E-BP did not change.

Since soluble Gal-9 was absent from the MCF-7 cells medium (data not shown) and was not induced by FLRT3, the cell surface presence of Gal-9 was determined, as shown in **Figure 40B**. Administration of FLRT3 increased cell-surface Gal-9 and this effect was reduced by PLC and PKC inhibitors, U73122 and Gö6983, respectively. This may indicate that upregulation of Gal-9 on the cell surface is somehow related to a PLC/PKC α -dependent pathway.

6.2. Ca²⁺ dynamics in MCF-7 cells

To determine whether any of the FLRT3 effects on MCF-7 cells were due to regular, fast GPCR signalling, I studied the size of intracellular Ca²⁺ stores and the features of SOCE in MCF-7 cells. For this purpose, I used our well-developed method with SERCA inhibition by TG (**Figure 41**).

As demonstrated by the results of this experiment, MCF-7 are indeed sensitive to TG and possess substantial Ca²⁺ stores (**Figure 41**). The SOCE induced by store depletion

in these cells is robust and similar to that in THP-1 cells (**Figure 30**), but substantially higher than SOCE in NB2A cells (**Figure 16**).

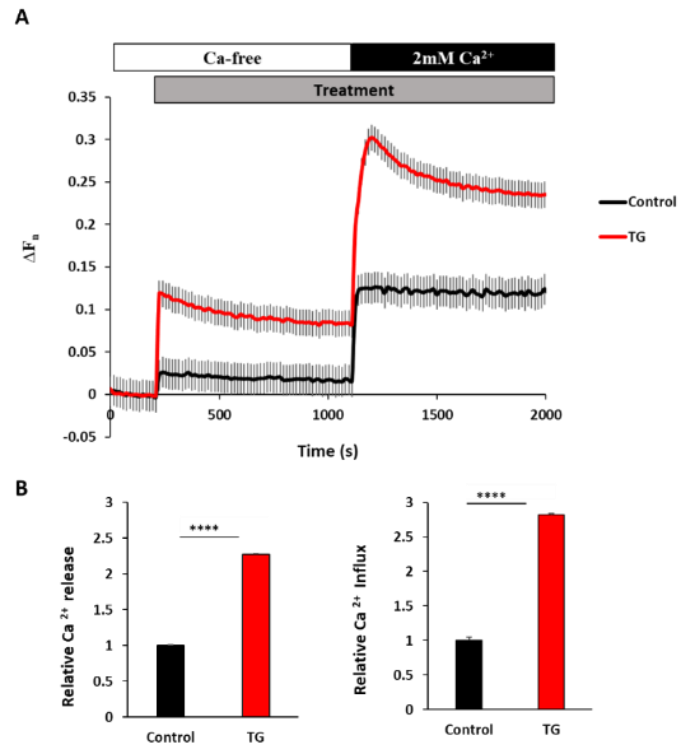


Figure 41: Intracellular Ca²⁺ dynamics in breast cancer cells.

A) MCF-7 cells were loaded with Fluo-4 AM and incubated in Ca²⁺ free buffer. 1 μM TG was added to induce Ca²⁺ store release. SOCE was induced by adding 2 mM Ca²⁺. B) Maximum amplitude of ΔF_n were measured for Ca²⁺ release from TG-sensitive stores, and Ca²⁺ influx due to SOCE. Traces shown are the averages of four independent experiments with three replicates each. Asterisks indicate statistically significant difference from control: ****, *p* < 0.0001. Error bars show SEM (*n*=4).

6.3. FLRT3 binding to LPHN2

Obviously, the effects of the extracellular domain of FLRT3 could be mediated by other proteins than LPHN2. However, we confirmed, using SRCD spectroscopy, that the NTF of LPHN2 binds FLRT3. This analysis was performed on LPHN2 and FLRT3 alone, or together, in equimolar concentrations (**Figure 42**). SRCD result showed that FLRT3 and LPHN2 interaction lead to conformational changes in LPHN2 similar to the

ones observed with FLRT3-LPHN1 interaction (see **Figure 12**). This lines up with the fact that the olfactomedin domains of all three LPHN homologues share high similarity. A 3D model of the interaction between the LPHN3 olfactomedin-like domain and extracellular (LRR) domain of FLRT3 is shown in **Figure 42**.

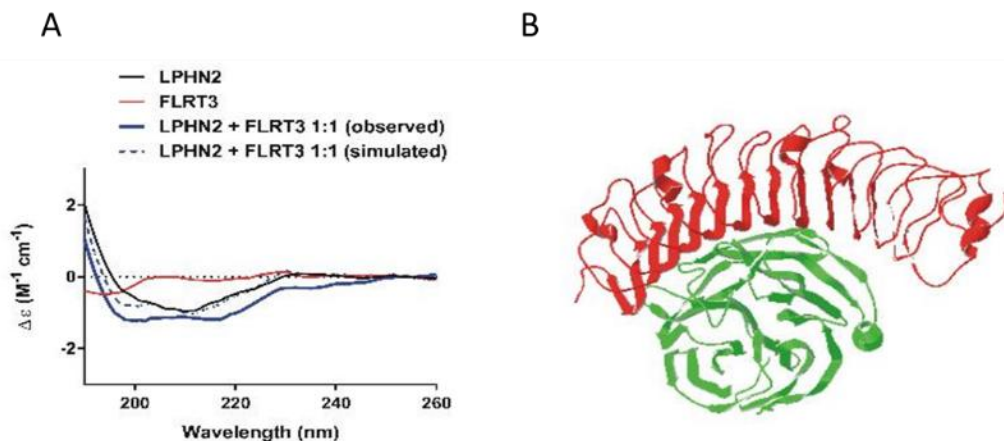


Figure 42: An interaction between the extracellular domain of FLRT3 and the olfactomedin-like domain of LPHN2.

A) SRCD spectroscopy of LPHN2 olfactomedin-like domain, extracellular domain of FLRT3 and their complex was conducted as described under Methods. B) A model of interaction between olfactomedin-like domain of LPHN3 and FLRT3 generated by Swiss PDB viewer (5cmn.pdb).

6.4. α -LTX does not activate Ca^{2+} signalling in MCF-7 cells

MCF-7 cells do not express LPHN1, but instead have LPHN2. This homologue has been shown to bind α -LTX with low affinity (Ichtchenko *et al.*, 1999), and it was interesting whether LPHN2 could respond to α -LTX in the same manner as LPHN1. I carried out fluorescence-based detection of intracellular Ca^{2+} dynamics in MCF-7 cells stimulated by 5 nM α -LTX. As shown in **Figure 43**, α -LTX had no effect on Ca^{2+} release or subsequent Ca^{2+} influx these cells. Thus, MCF-7 cells may have a different mechanism of activation compared to LPHN1-expressing THP-1 cells.

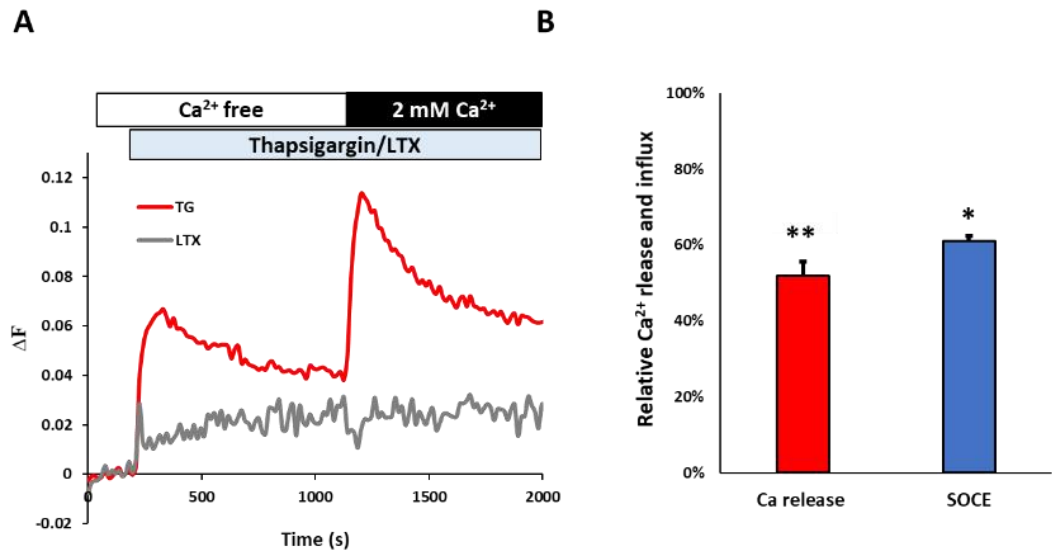


Figure 43: α -LTX does not stimulate fast Ca^{2+} mobilisation in MCF-7 cells.

A) MCF-7 cells were treated with 1 μ M TG or 5 nM α -LTX in a Ca^{2+} -free solution. Then 2 mM Ca^{2+} was added to the cells as indicated. MCF-7 cell did not show any Ca^{2+} release or influx when treated with α -LTX, while TG induced Ca^{2+} release and opening of SOCCs. B) TG-induced Ca^{2+} release and influx amplitudes normalised to control. Traces in A are the averages of five experiments. Error bars show SD. Student's t-test was performed in B; asterisks show statistical significance compared to control (normalised to 0), **, $p < 0.01$.

6.5. Discussion

Our results show that LPHN2, FLRT3, Tim3 and Gal-9 are present in breast cancer cells. LPHN2 can be activated, leading to surface expression of Gal-9 and Tim3 and used by these cells as a protector from cytotoxic immune attack. FLRT3 is expressed on the cell surface of MCF-7 cells and binds LPHN2. This binding leads to an upregulation of PLC and PKC α activities, which causes an increase in Gal-9 cell-surface expression. Contrary to AML, when MCF-7 cells were exposed to the extracellular domain of FLRT3 for 4 h, mTOR activity was not upregulated. This may indicate that MCF-7 cells, in contrast to AML cells, do not release Gal-9. Moreover, the biological

nature of blood cancer cells are constantly in contact with cytotoxic immune cells, which may explain why high amounts of expressed and released Gal-9 were observed compared to solid tumour (such as breast cancer). Therefore, upregulation of mTOR activity in AML cells was probably due to the continuous stimulation by FLRT3, the endogenous ligand of LPHN1 and 2. By contrast, in breast cancer cells, FLRT3 induced low to moderate Ca^{2+} release and, therefore, moderate PLC and PKC- α activation, which was still sufficient for tumorous cells to escape immune attack. These results were in line with what was shown in breast tumours compared with healthy breast tissues: indeed, LPHN2, Tim3 and Gal-9 were all expressed significantly higher in tumour cells compared to healthy breast tissues. Western blot analysis and confocal microscopy both showed the presence of a Tim3-Gal-9 complex in breast tissues. Most importantly, the amount of this complex was significantly higher in breast cancer tissues compared to healthy tissues. Although PLC and PKC α activities were upregulated in cancer tissues, the phosphorylation of mTOR levels were comparable in cancerous cells and healthy tissues. Furthermore, Gal-9 levels were lower in the blood plasma of patients with breast cancer than in healthy patients, and lower release of Gal-9 was also observed in MCF-7 cells. This may indicate that MCF-7 cells keep Gal-9 on the cell surface rather than release it into the surrounding medium. This can support cancer cells from host immune attack. Blood plasma levels of Tim3 in breast cancer patients were significantly lower compared to those in healthy donors. Consistently, IL-2 levels were not higher in cancer patients compared to healthy donors. In fact, lower levels of Tim3 permit higher secretion of IL-2, that has been shown to be downregulated by soluble Tim-3.

Overall, Gal-9 seems to protect tumour cells from immune attack but does not promote metastasis.

It is interesting to note that α -LTX did not stimulate fast Ca^{2+} signalling in MCF-7 cells. This suggests that when LPHN affinity for its ligand is low (K_d higher than 20 nM), little or no receptor activation takes place. Given that even the best ligand of LPHNs was unable to induce fast signalling to Ca^{2+} stores, it is unlikely that FLRT3 would induce G-protein-dependent Ca^{2+} signalling in MCF-7 cells, although FLRT3 interacts with LPHN2 (**Figure 42**). This is consistent with our observations made on THP-1 cells (**Figure 32**): these cells express LPHN1 and respond to α -LTX, but still do not show fast Ca^{2+} signalling when stimulated by FLRT3. Therefore, I conclude that the two ligands of LPHN1 (α -LTX and FLRT3) have different mechanisms of action. While α -LTX action depends on LPHN1-mediated $\text{G}\alpha_q$ activation and release of Ca^{2+} (with subsequent increased influx of Ca^{2+}), the mechanism of action of FLRT3 is much slower and does not involve G-protein-mediated signalling to Ca^{2+} stores.

7. General Discussion and Conclusions

In this project, I have studied receptor expression and release of immune-protective proteins in two types of cancer cells, AML and breast cancer cells.

Together with other members of the laboratory, I have shown that an aGPCR LPHN1 is expressed in AML cells and can be used as their biomarker. Furthermore, in AML cells the interaction of FLRT3 with LPHN1 results in translocation of tim-3-gal-9 on to the cell surface via Gαq coupling which will activate PLC. Activation of PLC results in release of IP3 and formation of DAG. IP3 will then bind to IP3R and eventually release of Ca²⁺ from intracellular stores. Accumulation of cytosolic Ca²⁺ concentration and production of DAG results in activation of PKCα which will lead to trafficking of tim-3-gal-9 vesicles on to the cell surface followed by proteolytic shedding. This helps AML cells to protect themselves from immune system attack (see Figure 43). These findings may serve as a promising approach for developing the new generation of immunotherapy. Over the past decade, immune checkpoint inhibitors such as monoclonal antibodies that target the programmed cell death protein 1 (PD-1) and its ligand PD-L1 have shown a dramatic change in therapeutic strategies. However, it is now well accepted that targeting immune checkpoint pathways does not always restore T cell function indicating a counterattack mechanism such as tim-3-gal-9 that keeps T cells continuously exhausted. Therefore, newly developed therapeutic targets are much needed to maximise the efficacy of immunotherapy. Tim-3 is often co-expressed with PD-1 on tumour infiltrating T cells, and its highly expressed on T cells in AML patients, therefore it is most likely to be a strong potential target as a monotherapy or in combination with PD-1 monoclonal antibody (Sakuishi *et al.*, 2010; Ngiow *et al.*, 2011). However, due to the wide expression of tim-3 on innate and

adaptive immune cells, blockade of tim-3 might result in a pleiotropic effects therefore further studies are needed to understand better the function of tim-3 in tumour microenvironments.

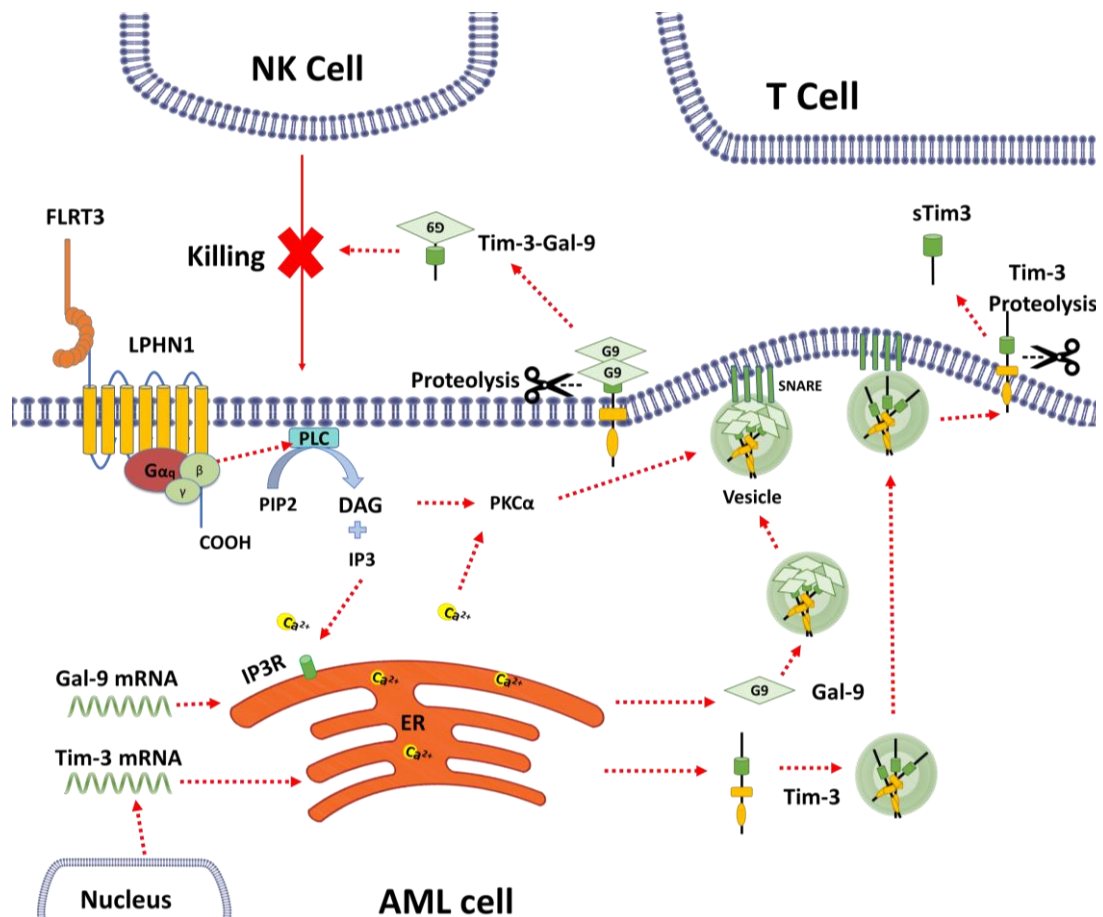


Figure 44: Schematic representation of LPHN1 induced translocation of Tim-3 and Galectin-9 onto cell surface in Acute myeloid leukaemia cells.

When FLRT3 interact with LPHN1 for a long period of time (4-16 h) an activation of PKCα occurs, most likely through the classical Gαq/PLC/Ca²⁺ pathway. Ligand-bound LPHN1 stimulates PLC production through Gαq. This leads to degradation of phosphatidylinositol-bisphosphate (PIP2) into inositol-trisphosphate (IP3) and diacylglycerol (DAG). PKCα gets activated by DAG and cytosolic Ca²⁺. PKCα will then provoke the agglomeration of SNARE proteins that promote vesicle attachment to the plasma membrane. Proteolytic enzymes will then shed soluble Tim-3 and tim-3-gal-9 complex. Tim-3-gal-9 complex will then impair the cancer cell killing activity of NK cells and other cytotoxic lymphocytes.

I have also shown that breast cancer cells, from solid tumours, express a LPHN1 homologue, LPHN2. These cells also react to FLRT3, but do not secrete the Gal-9-Tim3 complex as in the case with AML cells and instead display it on the cell surface (see Figure 34). Interestingly, tim3 and gal-9 were both expressed significantly higher in primary breast tumours compared to healthy tissues. This finding may serve in using tim-3 and gal-9 as a potential therapeutic target. Moreover, using anti-tim-3 monoclonal antibody as a monotherapy or in combination with other immunotherapy/chemotherapy or targeting tim-3-gal-9 complex (highly expressed on the cell surface) are all potential targets possibilities for breast cancer drugs.

I also developed a fluorescence-based versatile system for detecting cytosolic Ca^{2+} changes and studying fast signalling from cell-surface receptors to intracellular Ca^{2+} stores and subsequent SOCE. I used this system to investigate the LPHN-mediated signalling in the AML and breast cancer cells. I have found that all cells expressing LPHN1 can be activated by an LPHN1 ligand, α -LTX, which induces Ca^{2+} signalling. However, the other LPHN1 ligand, FLRT3, is unable to cause similar short-term Ca^{2+} signalling. The interaction between LPHN1/2 and FLRT3 may require much longer interaction and structural adjustment, which leads to a much slower response and possibly involves a mechanism that does not involve G protein-mediated signalling.

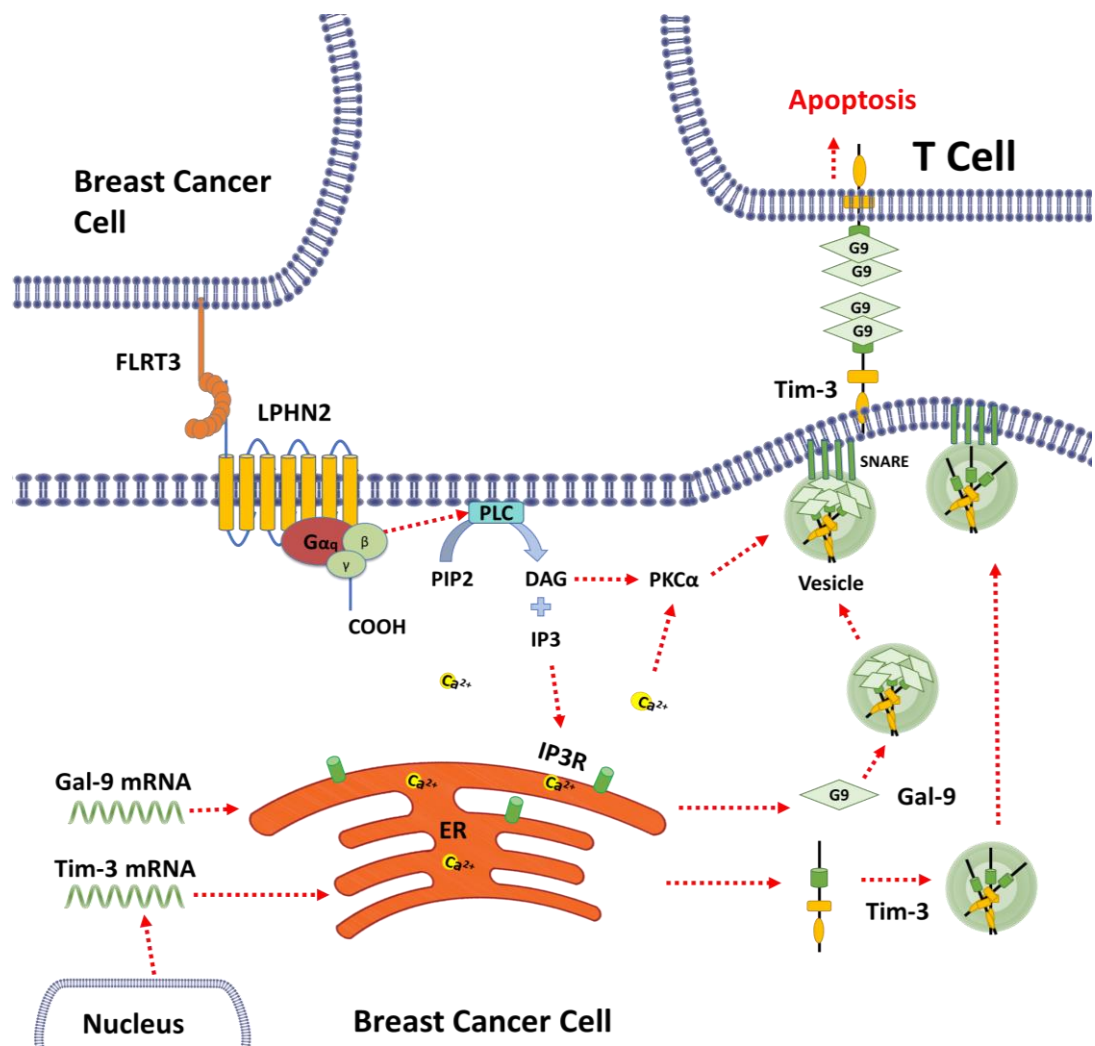


Figure 45: Schematic representation of LPHN2 induced translocation of Tim-3-Gal-9 complex to the plasma membrane in breast cancer cells.

When FLRT3 interact with LPHN2 for a long period (4-16 h) an activation of PKC α occurs, most likely through the classical G α q/PLC/Ca $^{2+}$ pathway. Ligand-bound LPHN2 stimulates PLC production through G α q binding. This leads to degradation of phosphatidyl-inositol-bisphosphate (PIP2) into inositol-trisphosphate (IP3) and diacylglycerol (DAG). PKC α gets activated by DAG and cytosolic Ca $^{2+}$. PKC α will then provokes the agglomeration of SNARE proteins that promote vesicle attachment to the plasma membrane. Tim-3-Gal-9 complex will then impair the cancer cell killing activity of cytotoxic T cells (and other cytotoxic lymphocytes).

While my studies have uncovered more complex signalling interactions than was previously thought, this work has led to the identification of LPHN1 as an absolute biomarker of AML cells and a potential target not only for AML diagnosis, but also for leukaemia treatment in the future.

Future studies will need to concentrate on specific mechanisms that underpin FLRT3 signalling to Gal-9-Tim3 surface delivery in many types of malignant cells, on the distinct roles of different LPHN homologues in cancer, and on the exploitation of the exquisitely specific LPHN1 expression in AML cells.

8. References

- Abu-Omar, N., Das, J., Szeto, V. and Feng, Z. P. (2018) 'Neuronal Ryanodine Receptors in Development and Aging', *Molecular Neurobiology*, 55(2), pp. 1183–1192. doi: 10.1007/s12035-016-0375-4.
- Aicher, B., Lerch, M. M., Müller, T., Schilling, J. and Ullrich, A. (1997) 'Cellular redistribution of protein tyrosine phosphatases LAR and PTP σ by inducible proteolytic processing', *Journal of Cell Biology*, 138(3), pp. 681–696. doi: 10.1083/jcb.138.3.681.
- Albrecht, M. A., Colegrove, S. L. and Friel, D. D. (2002) 'Differential regulation of ER Ca²⁺ uptake and release rates accounts for multiple modes of Ca²⁺-induced Ca²⁺ release', *Journal of General Physiology*, 119(3), pp. 211–233. doi: 10.1085/jgp.20028484.
- Ango, F., Prézeau, L., Muller, T., Tu, J. C., Xiao, B., Worley, P. F., Pin, J. P., Bockaert, J. and Fagni, L. (2001) 'Agonist-independent activation of metabotropic glutamate receptors by the intracellular protein Homer', *Nature*, 411(6840), pp. 962–965. doi: 10.1038/35082096.
- Araç, D., Boucard, A. A., Bolliger, M. F., Nguyen, J., Soltis, S. M., Südhof, T. C. and Brunker, A. T. (2012) 'A novel evolutionarily conserved domain of cell-adhesion GPCRs mediates autoproteolysis', *EMBO Journal*, 31(6), pp. 1364–1378. doi: 10.1038/emboj.2012.26.
- Araç, D., Strater, N. and Seiradake, E. (2016) 'Understanding the Structural Basis of Adhesion GPCR Functions', *Springer International Publishing*, 234, p. 408. doi: 10.1007/978-3-319-41523-9.
- Ashton, A. C., Volynski, K. E., Lelianova, V. G., Orlova, E. V., Van Renterghem, C., Canepari, M., Seagar, M. and Ushkaryov, Y. A. (2001) ' α -Latrotoxin, Acting via Two Ca²⁺-dependent Pathways, Triggers Exocytosis of Two Pools of Synaptic Vesicles', *Journal of Biological Chemistry*, 276(48), pp. 44695–44703. doi: 10.1074/jbc.M108088200.
- Aust, G., Zhu, D., Van Meir, E. G. and Xu, L. (2016) 'Adhesion GPCRs in Tumorigenesis', *Handbook of Experimental Pharmacology*, 234, pp. 369–396. doi: 10.1007/978-3-319-41523-9.
- Behrmann, L., Wellbrock, J. and Fiedler, W. (2018) 'Acute myeloid leukemia and the bone marrow niche - Take a closer look', *Frontiers in Oncology*, 8(OCT), pp. 1–13. doi: 10.3389/fonc.2018.00444.
- Berridge, M. J., Bootman, M. D. and Roderick, H. L. (2003) 'Calcium signalling: Dynamics, homeostasis and remodelling', *Nature Reviews Molecular Cell Biology*, 4(7), pp. 517–529. doi: 10.1038/nrm1155.
- Berridge, M. J., Lipp, P. and Bootman, M. D. (2000) 'The versatility and universality of calcium signalling', *Nature Reviews Molecular Cell Biology*, 1(1), pp. 11–21. doi: 10.1038/35036035.
- Bers, D. M. (2002) 'Cardiac excitation-contraction coupling', *Nature*, 415, pp. 198–205.
- Birks, B. R., Huxley, H. E. and Katz, B. (1960) 'THE FINE STRUCTURE OF THE NEUROMUSCULAR JUNCTION OF THE FROG', *Journal of Physiology*, 150, pp. 134–144.
- Bittner, M. A., Mo, W., Buryanovsky, L., Neubert, T. A., Holz, R. W., Ichtchenko, K. and Petrenko, A. G. (2002) 'Protein-tyrosine phosphatase- σ is a novel member of the functional family of α -latrotoxin receptors', *Journal of Biological Chemistry*, 277(39), pp. 35887–35895. doi: 10.1074/jbc.M205478200.
- Bootman, M. D. (2012) 'Calcium Signaling', *Cold Spring Harbor Perspectives in Biology*, 4, pp. 1–4.
- Boucard, A. A., Maxeiner, S. and Südhof, T. C. (2014) 'Latrophilins function as heterophilic cell-adhesion molecules by binding to teneurins: Regulation by alternative splicing', *Journal of Biological Chemistry*, 289(1), pp. 387–402. doi: 10.1074/jbc.M113.504779.
- Brini, M. and Carafoli, E. (2011) 'The Plasma Membrane Ca²⁺ ATPase and the NCX cooperate in the regulation of cell calcium', *Cold Spring Harbor Perspectives in Biology*, pp. 1–15.

Bygravel, F. L. and Benedetti, A. (1996) 'What is the of calcium ions in the endoplasmic reticulum?', *Commentary Cell Calcium*, 19(6), p. 19.

Capogna, M., Volynski, K. E., Emptage, N. J. and Ushkaryov, Y. A. (2003) 'The α -latrotoxin mutant LTXN4C enhances spontaneous and evoked transmitter release in CA3 pyramidal neurons', *Journal of Neuroscience*, 23(10), pp. 4044–4053.

Catterall, W. A. (2011) 'Voltage-gated calcium channels', *Cold Spring Harbor Perspectives in Biology*, 3, pp. 1–4. doi: 10.1016/B978-008055232-3.60392-7.

Al Chawaf, A., St. Amant, K., Belsham, D. and Lovejoy, D. A. (2007) 'Regulation of neurite growth in immortalized mouse hypothalamic neurons and rat hippocampal primary cultures by teneurin C-terminal-associated peptide-1', *Neuroscience*, 144(4), pp. 1241–1254. doi: 10.1016/j.neuroscience.2006.09.062.

Civelli, O., Reinscheid, R. K., Zhang, Y., Wang, Z., Fredriksson, R. and Schiöth, H. B. (2013) 'G Protein-Coupled Receptor Deorphanizations', *Annual Review of Pharmacology and Toxicology*, 53(1), pp. 127–146. doi: 10.1146/annurev-pharmtox-010611-134548.

Civini, S., Jin, P., Ren, J., Sabatino, M., Castiello, L., Jin, J., Wang, H., Zhao, Y., Marincola, F. and Stroncek, D. (2013) 'Leukemia cells induce changes in human bone marrow stromal cells', *Journal of Translational Medicine*, 11(1), pp. 1–14. doi: 10.1186/1479-5876-11-298.

Clapham, D. E. (2007) 'Calcium Signaling', *Cell*, 131(6), pp. 1047–1058. doi: 10.1016/j.cell.2007.11.028.

Clapham, D. E., Runnels, L. W. and Strübing, C. (2001) 'The TRP ion channel family', *Nature reviews Neuroscience*, 2(July), pp. 387–396. doi: 10.1038/35077544.

Cohen, D. P., Thaw, C. N., Varma, A., Gershengorn, M. C. and Nussenzveig, D. R. (1997) 'Human calcitonin receptors exhibit agonist-independent (constitutive) signaling activity', *Endocrinology*, 138(4), pp. 1400–1405. doi: 10.1210/endo.138.4.5046.

Corm, S., Berthon, C., Imbenotte, M., Biggio, V., Lhermitte, M., Dupont, C., Briche, I. and Quesnel, B. (2009) 'Indoleamine 2,3-dioxygenase activity of acute myeloid leukemia cells can be measured from patients' sera by HPLC and is inducible by IFN- γ ', *Leukemia Research*, 33(3), pp. 490–494. doi: 10.1016/j.leukres.2008.06.014.

D'Arcy, V., Pore, N., Docquier, F., Abdullaev, Z. K., Chernukhin, I., Kita, G. X., Rai, S., Smart, M., Farrar, D., Pack, S., Lobanenkov, V. and Klenova, E. (2008) 'BORIS, a paralogue of the transcription factor, CTCF, is aberrantly expressed in breast tumours', *British Journal of Cancer*, 98(3), pp. 571–579. doi: 10.1038/sj.bjc.6604181.

Davletov, B. A., Meunier, F. A., Ashton, A. C., Matsushita, H., Hirst, W. D., Lelianova, V. G., Wilkin, G. P., Dolly, J. O. and Ushkaryov, Y. A. (1998) 'Vesicle exocytosis stimulated by α -latrotoxin is mediated by latrophilin and requires both external and stored Ca^{2+} ', *EMBO Journal*, 17(14), pp. 3909–3920. doi: 10.1093/emboj/17.14.3909.

Davletov, B. A., Shamotienko, O. G., Lelianova, V. G., Grishin, E. V. and Ushkaryov, Y. A. (1996) 'Isolation and biochemical characterization of a Ca^{2+} -independent α -latrotoxin-binding protein', *Journal of Biological Chemistry*, 271(38), pp. 23239–23245. doi: 10.1074/jbc.271.38.23239.

Davydov, I. I., Fidalgo, S., Khaustova, S. A., Lelyanova, V. G., Grebenyuk, E. S., Ushkaryov, Y. A. and Tonevitsky, A. G. (2009) 'Prediction of Epitopes in Closely Related Proteins Using a New Algorithm', *Bulletin of Experimental Biology and Medicine*, 148(6), pp. 869–873. doi: 10.1007/s10517-010-0838-y.

Deák, F., Liu, X., Khvotchev, M., Li, G., Kavalali, E. T., Sugita, S. and Südhof, T. C. (2009) ' α -Latrotoxin stimulates a novel pathway of Ca^{2+} -dependent synaptic exocytosis independent of the classical

synaptic fusion machinery', *Journal of Neuroscience*, 29(27), pp. 8639–8648. doi: 10.1523/JNEUROSCI.0898-09.2009.

Deri, Z. and Adam-Vizi, V. (1993) 'Detection of Intracellular Free Na⁺ Concentration of Synaptosomes by a Fluorescent Indicator, Na⁺-Binding Benzofuran Isophthalate: The Effect of Veratridine, Ouabain, and α -Latrotoxin', *Journal of Neurochemistry*, 61(3), pp. 818–825. doi: 10.1111/j.1471-4159.1993.tb03592.x.

Dickson, E. J., Falkenburger, B. H. and Hille, B. (2013) 'Quantitative properties and receptor reserve of the IP3 and calcium branch of Gq-coupled receptor signaling', *Journal of General Physiology*, 141(5), pp. 521–535. doi: 10.1085/jgp.201210886.

Dupont, G., Combettes, L., Bird, G. S. and Putney, J. W. (2011) 'Calcium Oscillations', *Cold Spring Harbor Perspectives in Biology*, 3, pp. 1–18.

Fasler-Kan, E., Baiken, Y., Vorobjev, I. A. and Barteneva, N. S. (2016) 'Imaging Flow Cytometry Methods and protocols', *Methods in Molecular Biology*, 1389(November), pp. 2–12. doi: 10.1007/978-1-4939-3302-0.

Fasler-Kan, E., Barteneva, N., Ketterer, S., Wunderlich, K., Huwyler, J., Gygax, D., Flammer, J. and Meyer, P. (2010) 'Activation of the JAK-STAT intracellular pathway in human retinal pigment epithelial cell line ARPE-19', *International Journal of Interferon, Cytokine and Mediator Research*, 2(1), pp. 127–136. doi: 10.2147/IJICMR.S13642.

Fill, M. and Copello, J. (2002) 'Ryanodine receptor calcium release channels', *Physiological Reviews*, 82, pp. 893–922. doi: 10.1007/978-94-007-2888-2_7.

Finkelstein, A., Rubin, L. and Tzeng, M. (1976) 'Black Widow Spider Venom: Effect of Purified Toxin on Lipid Bilayer Membranes.', *Science*, 193(4257)(SEPTEMBER), pp. 1009–1011.

Folgiero, V., Cifaldi, L., Pira, G. L., Goffredo, B. M., Vinti, L. and Locatelli, F. (2015) 'TIM-3/Gal-9 interaction induces IFN γ -dependent IDO1 expression in acute myeloid leukemia blast cells', *Journal of Hematology and Oncology*. ???, 8(1), pp. 4–8. doi: 10.1186/s13045-015-0134-4.

Fornera, S. and Walde, P. (2010) 'Spectrophotometric quantification of horseradish peroxidase with o-phenylenediamine', *Analytical Biochemistry*. Elsevier Inc., 407(2), pp. 293–295. doi: 10.1016/j.ab.2010.07.034.

Foskett, J. K., White, C., Cheung, K. H. and Mak, D. O. D. (2007) 'Inositol trisphosphate receptor Ca²⁺ release channels', *Physiological Reviews*, 87(2), pp. 593–658. doi: 10.1152/physrev.00035.2006.

Fredriksson, R., Lagerström, M. C., Lundin, L. G. and Schiöth, H. B. (2003) 'The G-protein-coupled receptors in the human genome form five main families. Phylogenetic analysis, paralogon groups, and fingerprints', *Molecular Pharmacology*, 63(6), pp. 1256–1272. doi: 10.1124/mol.63.6.1256.

Galione, A. (2011) 'NAADP Receptors', *Cold Spring Harbor Perspectives in Biology*, 3, pp. 1–17.

Gleason, M. K., Lenvik, T. R., McCullar, V., Felices, M., O'Brien, M. S., Cooley, S. A., Verneris, M. R., Cichocki, F., Holman, C. J., Panoskaltis-Mortari, A., Niki, T., Hirashima, M., Blazar, B. R. and Miller, J. S. (2012) 'Tim-3 is an inducible human natural killer cell receptor that enhances interferon gamma production in response to galectin-9. *Blood.*', *Blood*, 119(13), pp. 3064–3072.

Gonçalves Silva, I., Rüegg, L., Gibbs, B. F., Bardelli, M., Fruewirth, A., Varani, L., Berger, S. M., Fasler-Kan, E. and Sumbayev, V. V. (2016) 'The immune receptor Tim-3 acts as a trafficker in a Tim-3/galectin-9 autocrine loop in human myeloid leukemia cells', *Oncolmmunology*, 5(7). doi: 10.1080/2162402X.2016.1195535.

Gonçalves Silva, I., Yasinska, I. M., Sakhnevych, S. S., Fiedler, W., Wellbrock, J., Bardelli, M., Varani, L., Hussain, R., Siligardi, G., Ceccone, G., Berger, S. M., Ushkaryov, Y. A., Gibbs, B. F., Fasler-Kan, E. and Sumbayev, V. V (2017) 'The Tim-3-galectin-9 Secretory Pathway is Involved in the Immune Escape of Human Acute Myeloid Leukemia Cells.', *EBioMedicine*. Elsevier, 22, pp. 44–57. doi: 10.1016/j.ebiom.2017.07.018.

Gorio, A., Hurlbut, W. P. and Ceccarelli, B. (1978) 'Acetylcholine compartments in mouse diaphragm: Comparison of the effects of black widow spider venom, electrical stimulation, and high concentrations of potassium', *Journal of Cell Biology*, 78(3), pp. 716–733. doi: 10.1083/jcb.78.3.716.

Haines, B. P., Wheldon, L. M., Summerbell, D., Heath, J. K. and Rigby, P. W. J. (2006) 'Regulated expression of FLRT genes implies a functional role in the regulation of FGF signalling during mouse development', *Developmental Biology*, 297(1), pp. 14–25. doi: 10.1016/j.ydbio.2006.04.004.

Halaszovich, C. R., Zitt, C., Jungling, E. and Luckoff, A. (2000) 'Inhibition of TRP3 channels by lanthanides. Block from the cytosolic side of the plasma membrane', *Journal of Biological Chemistry*, 275(48), pp. 37423–37428. doi: 10.1074/jbc.M007010200.

Hamann, J., Aust, G., Araç, D., Engel, F. B., Formstone, C., Fredriksson, R., Hall, R. A., Harty, B. L., Kirchhoff, C., Knapp, B., Krishnan, A., Liebscher, I., Lin, H. H., Martinelli, D. C., Monk, K. R., Peeters, M. C., Piao, X., Prömel, S., Schöneberg, T., Schwartz, T. W., Singer, K., Stacey, M., Ushkaryov, Y. A., Vallon, M., Wolfrum, U., Wright, M. W., Xu, L., Langenhan, T. and Schiöth, H. B. (2015) 'International union of basic and clinical pharmacology. XCIV. adhesion G protein-coupled receptors', *Pharmacological Reviews*, 67(2), pp. 338–367. doi: 10.1124/pr.114.009647.

Harmar, A. J. (2001) 'Family-B G-protein-coupled receptors', *Genome Biology*, 2(12), pp. 1–10. doi: 10.1186/gb-2001-2-12-reviews3013.

Vander Heiden, M., Cantley, L. and Thompson, C. (2009) 'Understanding the Warburg Effect: The Metabolic Requirements of Cell Proliferation', *Science*, 324(5930), pp. 1029–1033. doi: 10.1126/science.1160809.Understanding.

Hoth, M. and Penner, R. (1993) 'calcium release-activated calcium current in rat mast cells', *Journal of Physiology*, 465, pp. 359–386.

Hsu, Y., Yuan, S., Chen, H., Yu, S., Liu, C., Hsu, P., Wu, G., Lin, C., Chang, G. and Li, K. (2009) 'A Four-Gene Signature from NCI-60 Cell Line for Survival Prediction in Non – Small Cell Lung Cancer', *Clin Cancer Res*, 15(23), pp. 7309–7316. doi: 10.1158/1078-0432.CCR-09-1572.

Huang, Y.-S., Chiang, N.-Y., Hu, C.-H., Hsiao, C.-C., Cheng, K.-F., Tsai, W.-P., Yona, S., Stacey, M., Gordon, S., Chang, G.-W. and Lin, H.-H. (2012) 'Activation of Myeloid Cell-Specific Adhesion Class G Protein-Coupled Receptor EMR2 via Ligation-Induced Translocation and Interaction of Receptor Subunits in Lipid Raft Microdomains', *Molecular and Cellular Biology*, 32(8), pp. 1408–1420. doi: 10.1128/mcb.06557-11.

Husić, M., Barsyte-Lovejoy, D. and Lovejoy, D. A. (2019) 'Teneurin C-terminal associated peptide (TCAP)-1 and latrophilin interaction in HEK293 cells: Evidence for modulation of intercellular adhesion', *Frontiers in Endocrinology*, 10(FEB), pp. 1–17. doi: 10.3389/fendo.2019.00022.

Hussain, R., Benning, K., Javorfi, T., Longo, E., Rudd, T. R., Pulford, B. and Siligardi, G. (2015) 'CDApps: Integrated software for experimental planning and data processing at beamline B23, Diamond Light Source', *Journal of Synchrotron Radiation*. International Union of Crystallography, 22(2), pp. 465–468. doi: 10.1107/S1600577514028161.

Ichtchenko, K., Bittner, M. A., Krasnoperov, V., Little, A. R., Chepurny, O., Holz, R. W. and Petrenko, A. G. (1999) 'A novel ubiquitously expressed α -latrotoxin receptor is a member of the CIRL family of G-protein-coupled receptors', *Journal of Biological Chemistry*, 274(9), pp. 5491–5498. doi:

10.1074/jbc.274.9.5491.

Ichtchenko, K., Khvotchev, M., Kiyatkin, N., Simpson, L., Sugita, S. and Südhof, T. C. (1998) 'α-latrotoxin action probed with recombinant toxin: Receptors recruit α-latrotoxin but do not transduce an exocytotic signal', *EMBO Journal*, 17(21), pp. 6188–6199. doi: 10.1093/emboj/17.21.6188.

Islam, M. S. (2011) 'Calcium Signaling in the Islets', *Advances in Experimental Medicine and Biology*, (3), pp. 20–26. doi: 10.1007/978-90-481-3271-3.

Jackson, V. A., Del Toro, D., Carrasquero, M., Roversi, P., Harlos, K., Klein, R. and Seiradake, E. (2015) 'Structural basis of latrophilin-FLRT interaction', *Structure*, 23, pp. 774–781. doi: 10.1016/j.str.2015.01.013.

Kan, Z., Jaiswal, B. S., Stinson, J., Janakiraman, V., Bhatt, D., Stern, H. M., Yue, P., Haverty, P. M., Bourgon, R., Zheng, J., Moorhead, M., Chaudhuri, S., Tomsho, L. P., Peters, B. A., Pujara, K., Cordes, S., Davis, D. P., Carlton, V. E. H., Yuan, W., Li, L., Wang, W., Eigenbrot, C., Kaminker, J. S., Eberhard, D. A., Waring, P., Schuster, S. C., Modrusan, Z., Zhang, Z., Stokoe, D., Sauvage, F. J. De, Faham, M. and Seshagiri, S. (2010) 'Diverse somatic mutation patterns and pathway alterations in human cancers', *Nature Letters*, 466(August), pp. 869–873. doi: 10.1038/nature09208.

Kirichok, Y., Krapivinsky, G. and Clapham, D. E. (2004) 'The mitochondrial calcium uniporter is a highly selective ion channel.', *Nature*, 427(972)(January 2004), pp. 1874–1878.

Krasnoperov, V., Bittner, M. A., Holz, R. W., Chepurny, O. and Petrenko, A. G. (1999) 'Structural Requirements for α-Latrotoxin Binding and α-Latrotoxin-stimulated Secretion', *Journal of Biological Chemistry*, 274(February 5), pp. 3590–3596. doi: 10.1074/jbc.274.6.3590.

Krasnoperov, V., Deyev, I. E., Serova, O. V., Xu, C., Lu, Y., Gabibov, A. G., Neubert, T. A. and Alexander, G. (2009) 'Dissociation of the subunits of the calcium-independent receptor of α-latrotoxin as a result of two-step proteolysis', *Biochemistry*, 48(14), pp. 3230–3238. doi: 10.1021/bi802163p.Dissociation.

Krasnoperov, V. G., Bittner, M. A., Beavis, R., Kuang, Y., Salnikow, K. V., Chepurny, O. G., Little, A. R., Plotnikov, A. N., Wu, D., Holz, R. W. and Petrenko, A. G. (1997) 'α-Latrotoxin stimulates exocytosis by the interaction with a neuronal G-protein-coupled receptor', *Neuron*, 18(6), pp. 925–937. doi: 10.1016/S0896-6273(00)80332-3.

Krasnoperov, V., Lu, Y., Buryanovsky, L., Neubert, T. A., Ichtchenko, K. and Petrenko, A. G. (2002) 'Post-translational proteolytic processing of the calcium-independent receptor of α-latrotoxin (CIRL), a natural chimera of the cell adhesion protein and the G protein-coupled receptor: Role of the G protein-coupled receptor proteolysis site (GPS) motif', *Journal of Biological Chemistry*, 277(48), pp. 46518–46526. doi: 10.1074/jbc.M206415200.

Kwan, C. Y., Takemura, H., Obie, J. F., Thastrup, O. and Putney, J. W. (1990) 'Effects of MeCh, thapsigargin, and La³⁺ on plasmalemmal and intracellular Ca²⁺ transport in lacrimal acinar cells', *American Journal of Physiology - Cell Physiology*, 258(6 27-6). doi: 10.1152/ajpcell.1990.258.6.c1006.

Lacy, S. E., Bönnemann, C. G., Buzney, E. A. and Kunkel, L. M. (1999) 'Identification of FLRT1, FLRT2, and FLRT3: A novel family of transmembrane leucine-rich repeat proteins', *Genomics*, 62(3), pp. 417–426. doi: 10.1006/geno.1999.6033.

Lanner, J., Georgiou, D., Joshi, A. and Hamilton, S. (2010) 'Ryanodine Receptors: Structure, Expression, Molecular Details, and Function in Calcium Release', *Cold Spring Harbor perspectives in biology*, 2, pp. 1–21. doi: 10.1093/nq/s1-III.67.105-f.

Lelianova, V. G., Davletov, B. A., Sterling, A., Rahman, M. A., Grishin, E. V., Totty, N. F. and Ushkaryov, Y. A. (1997) 'α-Latrotoxin receptor, latrophilin, is a novel member of the secretin family of G protein-coupled receptors', *Journal of Biological Chemistry*, 272(34), pp. 21504–21508. doi:

10.1074/jbc.272.34.21504.

Lelyanova, V. G., Thomson, D., Ribchester, R. R., Tonevitsky, E. A. and Ushkaryov, Y. A. (2009) 'Activation of α -latrotoxin receptors in neuromuscular synapses leads to a prolonged splash acetylcholine release', *Bulletin of Experimental Biology and Medicine*, 147(6), pp. 701–703. doi: 10.1007/s10517-009-0600-5.

Li, C., Lev, S., Desmarini, D., Kaufman-Francis, K., Saiardi, A., Silva, A. P. G., Mackay, J. P., Thompson, P. E., Sorrell, T. C. and Djordjevic, J. T. (2017) 'IP3-4 kinase Arg1 regulates cell wall homeostasis and surface architecture to promote clearance of *Cryptococcus neoformans* infection in a mouse model', *Virulence*. Taylor & Francis, 8(8), pp. 1833–1848. doi: 10.1080/21505594.2017.1385692.

Li, J., Shalev-Benami, M., Sando, R., Jiang, X., Kibrom, A., Wang, J., Leon, K., Katanski, C., Nazarko, O., Lu, Y. C., Südhof, T. C., Skiniotis, G. and Arac, D. (2018) 'Structural basis for teneurin function in circuit-wiring: A toxin motif at the synapse', *Cell*, 173(3), pp. 139–148. doi: 10.1016/j.physbeh.2017.03.040.

Lin, H. H., Chang, G. W., Davies, J. Q., Stacey, M., Harris, J. and Gordon, S. (2004) 'Autocatalytic cleavage of the EMR2 receptor occurs at a conserved G protein-coupled receptor proteolytic site motif', *Journal of Biological Chemistry*, 279(30), pp. 31823–31832. doi: 10.1074/jbc.M402974200.

Longenecker, H. E., Hurlbert, W. P., Mauro, A. and Clark, A. W. (1970) 'Effects of black widow spider venom on the frog neuromuscular junction. Effects on end-plate potential, miniature end-plate potential and nerve terminal spike.', *Nature Publishing Group*, 228, pp. 726–734. Available at: <http://www.mendeley.com/research/discreteness-conductance-change-n-bimolecular-lipid-membrane-presence-certain-antibiotics/>.

Lopez, J. J., Jardin, I., Albarrán, L., Sanchez-Collado, J., Cantonero, C., Salido, G. M., Smani, T. and Rosado, J. A. (2020) 'Molecular Basis and Regulation of Store-Operated Calcium Entry', *Advances in experimental medicine and biology*, 1131, pp. 445–469. doi: 10.1007/978-3-030-12457-1_17.

Lu, Y. C., Nazarko, O. V., Sando, R., Salzman, G. S., Südhof, T. C. and Araç, D. (2015) 'Structural Basis of Latrophilin-FLRT-UNC5 Interaction in Cell Adhesion', *Structure*. doi: 10.1016/j.str.2015.06.024.

Lyttonsg, J., Westlins, M. and Hanleyll, M. R. (1991) 'Thapsigargin Inhibits the Sarcoplasmic or Endoplasmic Reticulum Ca-ATPase Family of Calcium Pumps', *The journal of biological chemistry*, 266(26), pp. 17067–17071.

Maravall, M., Mainen, Z. F., Sabatini, B. L. and Svoboda, K. (2000) 'Estimating intracellular calcium concentrations and buffering without wavelength ratioing', *Biophysical Journal*. Elsevier, 78(5), pp. 2655–2667. doi: 10.1016/S0006-3495(00)76809-3.

Matsushita, H., Lelyanova, V. G. and Ushkaryov, Y. A. (1999) 'The latrophilin family: Multiply spliced G protein-coupled receptors with differential tissue distribution', *FEBS Letters*, 443(3), pp. 348–352. doi: 10.1016/S0014-5793(99)00005-8.

Meissner, G. (2004) 'Molecular regulation of cardiac ryanodine receptor ion channel', *Cell Calcium*, 35(6), pp. 621–628. doi: 10.1016/j.ceca.2004.01.015.

Micol, V., Sánchez-Piñera, P., Villalaín, J., De Godos, A. and Gómez-Fernández, J. C. (1999) 'Correlation between protein kinase C α activity and membrane phase behavior', *Biophysical Journal*, 76(2), pp. 916–927. doi: 10.1016/S0006-3495(99)77255-3.

Mikoshiba, K. (2015) 'Role of IP3 receptor signaling in cell functions and diseases', *Advances in Biological Regulation*. Elsevier Ltd, 57, pp. 217–227. doi: 10.1016/j.jbior.2014.10.001.

Minke, B. and Cook, B. (2002) 'TRP channel proteins and signal transduction', *Physiological Reviews*, 82(2), pp. 429–472. doi: 10.1152/physrev.00001.2002.

Mironov, S. L., Sokolov, Y. V., Chanturiya, A. N. and Lishko, V. K. (1986) 'Channels produced by spider venoms in bilayer lipid membrane: mechanisms of ion transport and toxic action', *BBA - Biomembranes*, 862(1), pp. 185–198. doi: 10.1016/0005-2736(86)90482-7.

Morgan, A., Burgoyne, R., Barclay, J., Craig, T., Prescott, G., Ciuffo, L., Evans, G. and Graham, M. (2005) 'Regulation of exocytosis by protein kinase C.', *Biochemical Society Transactions*, 33(6), pp. 1342–4.

Munaron, L., Antoniotti, S. and Lovisolò, D. (2004) 'Intracellular calcium signals and control of cell proliferation: how many mechanisms?', *Journal of Cellular and Molecular Medicine*, 8(2), pp. 161–168.

Nagul, E. A., McKelvie, I. D., Worsfold, P. and Kolev, S. D. (2015) 'The molybdenum blue reaction for the determination of orthophosphate revisited: Opening the black box', *Analytica Chimica Acta*. Elsevier Ltd, 890, pp. 60–82. doi: 10.1016/j.aca.2015.07.030.

Ngiow, S. F., Von Scheidt, B., Akiba, H., Yagita, H., Teng, M. W. L. and Smyth, M. J. (2011) 'Anti-TIM3 antibody promotes T cell IFN- γ -mediated antitumor immunity and suppresses established tumors', *Cancer Research*, 71(10), pp. 3540–3551. doi: 10.1158/0008-5472.CAN-11-0096.

Nie, J. and Lewis, D. L. (2001) 'Structural domains of the CB1 cannabinoid receptor that contribute to constitutive activity and G-protein sequestration.', *Journal of Neuroscience*, 15;21(22), pp. 8758–64.

O'Sullivan, M. L., de Wit, J., Savas, J. N., Comoletti, D., Otto-Hitt, S., Yates, J. R. and Ghosh, A. (2012) 'FLRT Proteins Are Endogenous Latrophilin Ligands and Regulate Excitatory Synapse Development', *Neuron*, 73(5), pp. 903–910. doi: 10.1016/j.neuron.2012.01.018.

Orlova, E. V., Atiqur Rahman, M., Gowen, B., Volynski, K. E., Ashton, A. C., Manser, C., Van Heel, M. and Ushkaryov, Y. A. (2000) 'Structure of α -latrotoxin oligomers reveals that divalent cation-dependent tetramers form membrane pores', *Nature Structural Biology*, 7(1), pp. 48–53. doi: 10.1038/71247.

Pathak, T. and Trebak, M. (2018) 'Mitochondrial Ca²⁺ signalling', *Pharmacology and Therapeutics*, 192(1), pp. 112–123. doi: 10.1016/j.physbeh.2017.03.040.

Periasamy, M., Bhupathy, P. and Babu, G. J. (2008) 'Regulation of sarcoplasmic reticulum Ca²⁺ ATPase pump expression and its relevance to cardiac muscle physiology and pathology', *Cardiovascular Research*, 77(2), pp. 265–273. doi: 10.1093/cvr/cvm056.

Periasamy, M. and Kalyanasundaram, A. (2007) 'SERCA pump isoforms: Their role in calcium transport and disease', *Muscle and Nerve*, 35(4), pp. 430–442. doi: 10.1002/mus.20745.

Periasamy, M., Maurya, S. K., Sahoo, S. K., Singh, S., Reis, F. C. G. and Bal, N. C. (2017) 'Role of SERCA pump in muscle thermogenesis and metabolism', *Comprehensive Physiology*, 7(3), pp. 879–890. doi: 10.1002/cphy.c160030.

Petrenko, A. G., Kovalenko, V. A., Shamotienko, O. G., Surkova, I. N., Tarasyuk, T. A., Ushkaryov, Y. A. and Grishin, E. V. (1990) 'Isolation and properties of the α -latrotoxin receptor The receptor protein of α -latrotoxin (caLTx, a neurotoxin', *The EMBO Journal*, 9(6), pp. 2023–2027.

Prézeau, L., Gomeza, J., Ahern, S., Mary, S., Galvez, T., Bockaert, J. and Pin, J. P. (1996) 'Changes in the carboxyl-terminal domain of metabotropic glutamate receptor 1 by alternative splicing generate receptors with differing agonist-independent activity.', *Molecular Pharmacology*, 49(3), pp. 422–429.

Prokhorov, A., Gibbs, B. F., Bardelli, M., Rüegg, L., Fasler-Kan, E., Varani, L. and Sumbayev, V. V. (2015) 'The immune receptor Tim-3 mediates activation of PI3 kinase/mTOR and HIF-1 pathways in human myeloid leukaemia cells', *International Journal of Biochemistry and Cell Biology*. Elsevier Ltd, 59, pp. 11–20. doi: 10.1016/j.biocel.2014.11.017.

Putney, J. W. (1986) 'A model for receptor-regulated calcium entry', *Cell Calcium*, 7(1), pp. 1–12. doi: 10.1016/0143-4160(86)90026-6.

Putney, J. W. (2005) 'Capacitative calcium entry: Sensing the calcium stores', *Journal of Cell Biology*, 169(3), pp. 381–382. doi: 10.1083/jcb.200503161.

Rahman, M. A., Ashton, A. C., Meunier, F. A., Davletov, B. A., Dolly, J. O. and Ushkaryov, Y. A. (1999) 'Norepinephrine exocytosis stimulated by α -latrotoxin requires both external and stored Ca^{2+} and is mediated by latrophilin, G proteins and phospholipase C', *Philosophical Transactions of the Royal Society B: Biological Sciences*, 354(1381), pp. 379–386. doi: 10.1098/rstb.1999.0390.

Rahman, M. A., Manser, C., Benlaouer, O., Suckling, J., Blackburn, J. K., Silva, J. P. and Ushkaryov, Y. A. (2019) 'C-terminal phosphorylation of latrophilin-1/adgrl1 affects the interaction between its fragments', *Annals of the New York Academy of Sciences*, 1456(1), pp. 122–143. doi: 10.1111/nyas.14242.

Rohou, A., Nield, J. and Ushkaryov, Y. A. (2007) 'Insecticidal toxins from black widow spider venom', *Toxicon*. Elsevier Ltd, 49(4), pp. 531–549. doi: 10.1016/j.toxicon.2006.11.021.

Roos, J., DiGregorio, P. J., Yeromin, A. V., Ohlsen, K., Lioudyno, M., Zhang, S., Safrina, O., Kozak, J. A., Wagner, S. L., Cahalan, M. D., Velichelebi, G. and Stauderman, K. A. (2005) 'STIM1, an essential and conserved component of store-operated Ca^{2+} channel function', *Journal of Cell Biology*, 169(3), pp. 435–445. doi: 10.1083/jcb.200502019.

Röthe, J., Thor, D., Winkler, J., Knierim, A. B., Binder, C., Huth, S., Kraft, R., Rothmund, S., Schöneberg, T. and Prömel, S. (2019) 'Involvement of the Adhesion GPCRs Latrophilins in the Regulation of Insulin Release', *Cell Reports*, 26(6), pp. 1573–1584.e5. doi: 10.1016/j.celrep.2019.01.040.

Saimi, Y. and Kung, C. (2002) 'Calmodulin as an ion channel subunit.', *Annual Review of Physiology*, 64(1), pp. 289–311.

Sakhnevych, S. (2019) 'Tim-3-galectin-9 immunosuppressive pathway in human acute myeloid leukaemia and solid tumour cells and biochemical functions of its crucial components Thesis by', (September).

Sakhnevych, S. S., Yasinska, I. M., Bratt, A. M., Benlaouer, O., Gonçalves Silva, I., Hussain, R., Siligardi, G., Fiedler, W., Wellbrock, J., Gibbs, B. F., Ushkaryov, Y. A. and Sumbayev, V. V. (2018) 'Cortisol facilitates the immune escape of human acute myeloid leukemia cells by inducing latrophilin 1 expression', *Cellular and Molecular Immunology*. doi: 10.1038/s41423-018-0053-8.

Sakuishi, K., Apetoh, L., Sullivan, J. M., Blazar, B. R., Kuchroo, V. K. and Anderson, A. C. (2010) 'Targeting Tim-3 and PD-1 pathways to reverse T cell exhaustion and restore anti-tumor immunity', *Journal of Experimental Medicine*, 207(10), pp. 2187–2194. doi: 10.1084/jem.20100643.

Schiöth, H. B. and Fredriksson, R. (2005) 'The GRAFS classification system of G-protein coupled receptors in comparative perspective', *General and Comparative Endocrinology*, 142(1-2 SPEC. ISS.), pp. 94–101. doi: 10.1016/j.ygcen.2004.12.018.

Serova, O. V., Popova, N. V., Deyev, I. E. and Petrenko, A. G. (2008) 'Identification of proteins in complexes with α -latrotoxin receptors', *Russian Journal of Bioorganic Chemistry*, 34(6), pp. 668–673. doi: 10.1134/S1068162008060046.

Sheer, H. and Meldolesi, J. (1985) 'Purification of the putative α -latrotoxin', *EMBO Journal*, 4(2), pp. 323–327.

Short, N. J., Rytting, M. E. and Cortes, J. E. (2018) 'Acute myeloid leukaemia', *The Lancet*. Elsevier Ltd, 392(10147), pp. 593–606. doi: 10.1016/S0140-6736(18)31041-9.

Silva, J. P., Lelianova, V. G., Ermolyuk, Y. S., Vysokov, N., Hitchen, P. G., Berninghausen, O., Rahman, M. A., Zangrandi, A., Fidalgo, S., Tonevitsky, A. G., Dell, A., Volynski, K. E. and Ushkaryov, Y. A. (2011) 'Letrophilin 1 and its endogenous ligand Lasso/teneurin-2 form a high-affinity transsynaptic receptor pair with signaling capabilities', *Proceedings of the National Academy of Sciences of the United States of America*, 108(29), pp. 12113–12118. doi: 10.1073/pnas.1019434108.

Silva, J. P., Lelianova, V., Hopkins, C., Volynski, K. E. and Ushkaryov, Y. (2009) 'Functional cross-interaction of the fragments produced by the cleavage of distinct adhesion G-protein-coupled receptors', *Journal of Biological Chemistry*, 284(10), pp. 6495–6506. doi: 10.1074/jbc.M806979200.

Silva, J. P. and Ushkaryov, Y. A. (2010) 'The letrophilins, "split-personality" receptors', *Advances in Experimental Medicine and Biology*, 706(706), pp. 59–75. doi: 10.1007/978-1-4419-7913-1_5.

Silva, J., Suckling, J. and Ushkaryov, Y. (2009) 'Penelope' s web: using α -letrotoxin to untangle the mysteries of exocytosis', *J Neurochem*, 111(2), pp. 275–290. doi: 10.1111/j.1471-4159.2009.06329.x.Penelope.

Silva, J. and Ushkaryov, Y. A. (2011) 'The letrophilins , " split-personality " receptors', *Advances in Experimental Medicine and Biology*, 706, pp. 59–75.

Simms, B. A. and Zamponi, G. W. (2012) 'Trafficking and stability of voltage-gated calcium channels', *Cellular and Molecular Life Sciences*, 69(6), pp. 843–856. doi: 10.1007/s00018-011-0843-y.

Stacey, M., Lin, H. H., Hilyard, K. L., Gordon, S. and McKnight, A. J. (2001) 'Human Epidermal Growth Factor (EGF) Module-containing Mucin-like Hormone Receptor 3 is a New Member of the EGF-TM7 Family that Recognizes a Ligand on Human Macrophages and Activated Neutrophils', *Journal of Biological Chemistry*, 276(22), pp. 18863–18870. doi: 10.1074/jbc.M101147200.

Stanika, R. I., Villanueva, I., Kazanina, G., Brian Andrews, S. and Pivovarov, N. B. (2012) 'Comparative impact of voltage-gated calcium channels and NMDA receptors on mitochondria-mediated neuronal injury', *Journal of Neuroscience*, 32(19), pp. 6642–6650. doi: 10.1523/JNEUROSCI.6008-11.2012.

Südhof, T. C. and Starke, K. (2008) *Preface, Handbook of Experimental Pharmacology*. doi: 10.1007/978-3-540-74805-2.

Sugita, S., Ichtchenko, K., Khvotchev, M. and Südhof, T. C. (1998) ' α -Letrotoxin receptor C1RL/letrophilin 1 (CL1) defines an unusual family of ubiquitous G-protein-linked receptors: G-protein coupling not required for triggering exocytosis', *Journal of Biological Chemistry*, 273(49), pp. 32715–32724. doi: 10.1074/jbc.273.49.32715.

Sumbayev, V. V., Silva, I. G., Blackburn, J., Bernhard, F., Yasinska, I. M., Garrett, M. D., Tonevitsky, A. G. and Yuri, A. (2016a) 'Expression of functional neuronal receptor letrophilin 1 in human acute myeloid leukaemia cells', *Oncotarget*, 7(29), pp. 45575–45583.

Tang, X., Jin, R., Qu, G., Wang, X., Li, Z., Yuan, Z., Zhao, C., Siwko, S., Shi, T., Wang, P., Xiao, J., Liu, M. and Luo, J. (2013) 'GPR116, an adhesion G-protein-coupled receptor, promotes breast cancer metastasis via the G α -p63 Rho GEF-Rho GTPase pathway', *Cancer Research*, 73(20), pp. 6206–6218. doi: 10.1158/0008-5472.CAN-13-1049.

Thastrup, O., Cullen, P. J., Drobak, B. K., Hanley, M. R. and Dawson, A. P. (1990) 'Thapsigargin, a tumor promoter, discharges intracellular Ca²⁺ stores by specific inhibition of the endoplasmic reticulum Ca²⁺-ATPase', *Proceedings of the National Academy of Sciences of the United States of America*, 87(7), pp. 2466–2470. doi: 10.1073/pnas.87.7.2466.

Torpy, D. and Chrousos, G. (1996) 'The three-way interactions between the hypothalamic-pituitary-adrenal and gonadal axes and the immune system', *Rheumatic Disease Clinics of North America*, 10(2), pp. 181–198. doi: 10.1016/s0889-857x(05)70181-2.

Toyoshima, C. and Inesi, G. (2004) 'Structural Basis of Ion Pumping by Ca²⁺-ATPase of the Sarcoplasmic Reticulum', *Annual Review of Biochemistry*, 73(1), pp. 269–292. doi: 10.1146/annurev.biochem.73.011303.073700.

Toyoshima, C., Nomura, H. and Tsuda, T. (2004) 'Lumenal gating mechanism revealed in calcium pump crystal structures with phosphate analogues', *Nature*, 432(7015), pp. 361–368. doi: 10.1038/nature02981.

Tsang, C. W., Elrick, D. B. and Charlton, M. P. (2000) 'α-Latrotoxin releases calcium in frog motor nerve terminals', *Journal of Neuroscience*, 20(23), pp. 8685–8692. doi: 10.1523/JNEUROSCI.20-23-08685.2000.

Tzeng, M. chin and Siekevitz, P. (1978) 'The effect of the purified major protein factor (α-latrotoxin) of black widow spider venom on the release of acetylcholine and norepinephrine from mouse cerebral cortex slices', *Brain Research*, 139(1), pp. 190–196. doi: 10.1016/0006-8993(78)90073-2.

Ushkaryov, Y. A., Lelianova, V. and Vysokov, N. V. (2019) 'Catching Latrophilin With Lasso: A Universal Mechanism for Axonal Attraction and Synapse Formation', *Frontiers in Neuroscience*, 13(March), pp. 1–9. doi: 10.3389/fnins.2019.00257.

Ushkaryov, Y. A., Petrenko, A. G., Geppert, M. and Südhof, T. C. (1992) 'Neurexins: Synaptic cell surface proteins related to the α-latrotoxin receptor and laminin', *Science*, 257(5066), pp. 50–56. doi: 10.1126/science.1621094.

Vanessa, H., Wenshuo, W., Cornelia, D., Simon, W., Martin, T. and Wolfgang, P. (2018) 'Microwave-assisted one-step synthesis of white light-emitting carbon dot suspensions', *Optical Materials*. Elsevier, 80(March), pp. 110–119. doi: 10.1016/j.optmat.2018.04.039.

Venkatachalam, K. and Montell, C. (2007) 'TRP channels', *Annual Review of Biochemistry*, 76, pp. 387–417. doi: 10.4324/9781315152837-1.

Volynski, K. ., Silva, J. P., Lelianova, V. G., Rahman, M. A., Hopkins, C. and Ushkaryov, Y. A. (2004) 'Latrophilin fragments behave as independent proteins that associate and signal on binding of LTXN4C', *EMBO Journal*, 23(22), pp. 4423–4433. doi: 10.1038/sj.emboj.7600443.

Volynski, K. E., Capogna, M., Ashton, A. C., Thomson, D., Orlova, E. V., Manser, C. F., Ribchester, R. R. and Ushkaryov, Y. A. (2003) 'Mutant α-latrotoxin (LTXN4C) does not form pores and causes secretion by receptor stimulation. This action does not require neurexins', *Journal of Biological Chemistry*, 278(33), pp. 31058–31066. doi: 10.1074/jbc.M210395200.

Volynski, K. E., Meunier, F. A., Lelianova, V. G., Dudina, E. E., Volkova, T. M., Rahman, M. A., Manser, C., Grishin, E. V., Dolly, J. O., Ashley, R. H. and Ushkaryov, Y. A. (2000) 'Latrophilin, neurexin, and their signaling-deficient mutants facilitate -latrotoxin insertion into membranes but are not involved in pore formation', *Journal of Biological Chemistry*, 275, pp. 41175–41183. doi: 10.1074/jbc.M005857200.

Volynski, K., Silva, J.-P., Lelianova, V. G., Rahman, M. A., Hopkins, C. and Ushkaryov, Y. A. (2004) 'Latrophilin fragments behave as independent proteins that associate and signal on binding of LTX', *The EMBO Journal*, 23(7600443), pp. 4423–4433. doi: 10.1038/sj.emboj.7600443.

Wadel, K., Neher, E. and Sakaba, T. (2007) 'The Coupling between Synaptic Vesicles and Ca²⁺ Channels Determines Fast Neurotransmitter Release', *Neuron*, 53(4), pp. 563–575. doi: 10.1016/j.neuron.2007.01.021.

Van der Wal, J., Habets, R., Várnai, P., Balla, T. and Jalink, K. (2001) 'Monitoring Agonist-induced Phospholipase C Activation in Live Cells by Fluorescence Resonance Energy Transfer', *Journal of Biological Chemistry*, 276(18), pp. 15337–15344. doi: 10.1074/jbc.M007194200.

- Wheeler, D. B., Randall, A., Sather, W. A. and Tsien, R. W. (1995) 'Chapter 6 Neuronal calcium channels encoded by the $\alpha 1A$ subunit and their contribution to excitatory synaptic transmission in the CNS', *Progress in Brain Research*, 105(C), pp. 65–78. doi: 10.1016/S0079-6123(08)63284-7.
- Wheeler, G. L. and Brownlee, C. (2008) 'Ca²⁺ signalling in plants and green algae - changing channels', *Trends in Plant Science*, 13(9), pp. 506–514. doi: 10.1016/j.tplants.2008.06.004.
- White, G. R. M., Varley, J. M. and Heighway, J. (1998) 'Isolation and characterization of a human homologue of the latrophilin gene from a region of 1p31.1 implicated in breast cancer', *Oncogene*, 17(26), pp. 3513–3519. doi: 10.1038/sj.onc.1202487.
- White, G. R. M., Varley, J. M. and Heighway, J. (2000) 'Genomic structure and expression profile of LPHH1, a 7TM gene variably expressed in breast cancer cell lines 1', *Biochimica et Biophysica Acta*, 1491, pp. 75–92.
- Wu, X. S. and Wu, L. G. (2014) 'The yin and yang of calcium effects on synaptic vesicle endocytosis', *Journal of Neuroscience*, 34(7), pp. 2652–2659. doi: 10.1523/JNEUROSCI.3582-13.2014.
- Xing, Y., Nakamura, Y. and Rainey, W. E. (2009) 'G Protein-coupled receptor expression in adult and fetal adrenal glands.', *Molecular and Cellular Endocrinology*, 300((1-2)), pp. 43–50. doi: 10.1038/jid.2014.371.
- Yamagishi, S., Hampel, F., Hata, K., Del Toro, D., Schwark, M., Kvachnina, E., Bastmeyer, M., Yamashita, T., Tarabykin, V., Klein, R. and Egea, J. (2011) 'FLRT2 and FLRT3 act as repulsive guidance cues for Unc5-positive neurons', *EMBO Journal*, 30(14), pp. 2920–2933. doi: 10.1038/emboj.2011.189.
- Yamauchi, A., Kontani, K. and Kihara, M. (2006) 'Galectin-9, a Novel Prognostic Factor with Antimetastatic', *The breast journal*, 12, pp. 196–200. doi: 10.1111/j.1075-122X.2006.00334.x.
- Yasinska, I. M., Gibbs, B. F., Lall, G. S. and Sumbayev, V. V. (2014) 'The HIF-1 transcription complex is essential for translational control of myeloid hematopoietic cell function by maintaining mTOR phosphorylation', *Cellular and Molecular Life Sciences*, 71(4), pp. 699–710. doi: 10.1007/s00018-013-1421-2.
- Yasinska, I. M., Sakhnevych, S. S., Pavlova, L., Teo Hansen Selnø, A., Teuscher Abeleira, A. M., Benlaouer, O., Gonçalves Silva, I., Mosimann, M., Varani, L., Bardelli, M., Hussain, R., Siligardi, G., Cholewa, D., Berger, S. M., Gibbs, B. F., Ushkaryov, Y. A., Fasler-Kan, E., Klenova, E. and Sumbayev, V. V. (2019) 'The Tim-3-Galectin-9 Pathway and Its Regulatory Mechanisms in Human Breast Cancer', *Frontiers in Immunology*, 10(July), pp. 1–13. doi: 10.3389/fimmu.2019.01594.
- Zhang, S. L., Yu, Y., Roos, J., Kozak, J. A., Deerinck, T. J., Mark, H., Stauderman, K. A. and Cahalan, M. D. (2005) 'STIM1 is a Ca²⁺ sensor that activates CRAC channels and migrates from the Ca²⁺ store to the plasma membrane', *Nature*, 437(7060), pp. 902–905.
- Zhang, S., Liu, Y., Liu, Z., Zhang, C., Cao, H., Ye, Y. and Wang, S. (2014) 'Transcriptome Profiling of a Multiple Recurrent Muscle-Invasive Urothelial Carcinoma of the Bladder by Deep Sequencing', *PLOS ONE*, 9(3), pp. 1–14. doi: 10.1371/journal.pone.0091466.
- Zuko, A., Oguro-Ando, A., van Dijk, R., Gregorio-Jordan, S., van der Zwaag, B. and Burbach, J. P. H. (2016) 'Developmental role of the cell adhesion molecule Contactin-6 in the cerebral cortex and hippocampus', *Cell Adhesion and Migration*. Taylor & Francis, 10(4), pp. 378–392. doi: 10.1080/19336918.2016.1155018.